

RCA REVIEW

GEORGE M. K. BAKER
Manager

CHAS. C. FOSTER, JR.
Business Manager

SUBSCRIPTIONS:

United States, Canada, and Postal Union: One Year \$2.00, Two Years \$3.50, Three Years \$4.50
Other Countries: One Year \$2.40, Two Years \$4.30, Three Years \$5.70

SINGLE COPIES:

United States: \$.75 each. Other Countries: \$.85 each

Copyright, 1950, by Radio Corporation of America, RCA Laboratories Division

Published quarterly in March, June, September, and December by Radio Corporation of America, RCA Laboratories Division, 30 Rockefeller Plaza, New York 20, N. Y.

Editorial and General Offices: RCA Review, Radio Corporation of America,
RCA Laboratories Division, Princeton, New Jersey

Entered as second class matter April 3, 1946, at the Post Office at New York, New York, under the act of March 3, 1879

RADIO CORPORATION OF AMERICA

DAVID SARNOFF, *Chairman of the Board*

FRANK M. FOLSOM, *President*

LEWIS MACCONNACH, *Secretary*

ERNEST B. GORIN, *Treasurer*

PRINTED IN U.S.A.

RCA REVIEW

a technical journal

RADIO AND ELECTRONICS
RESEARCH • ENGINEERING

Published quarterly by

RADIO CORPORATION OF AMERICA
RCA LABORATORIES DIVISION

in cooperation with

RCA VICTOR DIVISION

RADIOMARINE CORPORATION OF AMERICA

RCA INTERNATIONAL DIVISION

RCA COMMUNICATIONS, INC.

NATIONAL BROADCASTING COMPANY, INC.

RCA INSTITUTES, INC.

VOLUME XI

MARCH 1950

NUMBER 1

CONTENTS

	PAGE
FOREWORD	3
Characteristics of High-Efficiency Deflection and High-Voltage Supply Systems for Kinescopes	5
O. H. SCHADE	
Adjustments for Obtaining Optimum Performance in Magnetic Recording	38
A. W. FRIEND	
Experimental Ultra-High-Frequency Television Station in the Bridgeport, Connecticut Area	55
R. F. GUY, J. L. SEIBERT and F. W. SMITH	
An Experimental Ultra-High-Frequency Television Tuner	68
T. MURAKAMI	
High-Efficiency Loud Speakers for Personal Radio Receivers.....	80
H. F. OLSON, J. C. BLEAZEY, J. PRESTON AND R. A. HACKLEY	
A Study of Cochannel and Adjacent-Channel Interference of Television Signals, Part I—Cochannel Studies	99
Resonant Frequencies and Characteristics of a Resonant Coupled Circuit	121
C. L. CUCCIA	
A Broadband Transition from Coaxial Line to Helix	133
C. O. LUND	
An Automatic Plotter for Electron Trajectories	143
DAVID B. LANGMUIR	
COLOR TELEVISION BIBLIOGRAPHY	4
RCA TECHNICAL PAPERS	155
AUTHORS	157

RCA Review is regularly abstracted and indexed by *Industrial Arts Index*, *Science Abstracts* (I.E.E.-Brit.), *Engineering Index*, *Electronic Engineering Master Index*, *Abstracts and References* (*Wireless Engineer*-Brit. and *Proc. I.R.E.*) and *Digest-Index Bulletin*.

RCA REVIEW

BOARD OF EDITORS

Chairman

C. B. JOLLIFFE

RCA Laboratories Division

M. C. BATSEL
RCA Victor Division

G. L. BEERS
RCA Victor Division

H. H. BEVERAGE
RCA Laboratories Division

I. F. BYRNES
Radiomarine Corporation of America

D. D. COLE
RCA Victor Division

O. E. DUNLAP, JR.
Radio Corporation of America

E. W. ENGSTROM
RCA Laboratories Division

A. N. GOLDSMITH
Consulting Engineer, RCA

O. B. HANSON
National Broadcasting Company, Inc.

E. A. LAPORT
RCA International Division

C. W. LATIMER
RCA Communications, Inc.

H. B. MARTIN
Radiomarine Corporation of America

H. F. OLSON
RCA Laboratories Division

D. F. SCHMIT
RCA Victor Division

S. W. SEELEY
RCA Laboratories Division

G. R. SHAW
RCA Victor Division

R. E. SHELBY
National Broadcasting Company, Inc.

S. M. THOMAS
RCA Communications, Inc.

G. L. VAN DEUSEN
RCA Institutes, Inc.

A. F. VAN DYCK
RCA Laboratories Division

I. WOLFF
RCA Laboratories Division

V. K. ZWORYKIN
RCA Laboratories Division

Secretary

GEORGE M. K. BAKER

RCA Laboratories Division

REPUBLICATION AND TRANSLATION

Original papers published herein may be referenced or abstracted without further authorization provided proper notation concerning authors and source is included. All rights of republication, including translation into foreign languages, are reserved by RCA Review. Requests for republication and translation privileges should be addressed to *The Manager*.

FOREWORD

THE RCA Technical Book Series currently consists of ten volumes. Three of the early volumes — Television, Volumes I and II, and Radio at Ultra-High Frequencies, Volume I — have been out of print for some time. Because of continual requests for these books, a second printing of each has been made, and they are now available.

Television, Volume V (1947-1949) is now being assembled, and should be ready for distribution about July 1, 1950. Further information thereon will be circulated at the appropriate time.

RCA Technical Papers — Index, Volume II(d) (1949) is being published this month and will be distributed shortly. Indexes now available include: Volume I (1919-1945); Volume II(a) (1946); Volume II(b) (1947); Volume II(c) (1948); Volume II(d) (1949).

Information concerning any of the above material may be obtained by writing to:

RCA Review
Radio Corporation of America
RCA Laboratories Division
Princeton, N.J.

March 15, 1950

The Manager, RCA Review

COLOR TELEVISION BIBLIOGRAPHY

Within the last four years the Radio Corporation of America has distributed a great deal of material on the subject of color television. This material has been in the form of published technical papers, exhibits submitted to the Federal Communications Commission, and various technical bulletins. For the convenience of those who are interested in the subject of color television, a list of the material distributed as of March 15, 1950 is given below:

"An Experimental Color Television System", R. D. Kell, G. L. Fredendall, A. C. Schroeder and R. C. Webb, <i>RCA Review</i> (June)	1946
"Simultaneous All Electronic Color Television", <i>RCA Review</i> (December)	1946
"Colorimetry in Television", W. H. Cherry, <i>RCA Review</i> (September)	1947
"An Experimental Simultaneous Color-Television System", "Part I—Introduction", R. D. Kell, "Part II—Pickup Equipment", G. C. Sziklai, R. C. Ballard and A. C. Schroeder, "Part III—Radio-Frequency and Reproducing Equipment", K. R. Wendt, G. L. Fredendall and A. C. Schroeder, <i>Proc. I.R.E.</i> (September)	1947
"Comments of Radio Corporation of America", C. B. Jolliffe (Letter to FCC, Exhibit 206) (August 25)	1949
"Engineering Statement Supplemental to Comments of Radio Corporation of America", E. W. Engstrom (Letter to FCC, Exhibit 207) (September 6)	1949
"A Six-Megacycle Compatible High-Definition Color Television System", (FCC Exhibit 209) (September 26)	1949
<i>RCA Review</i> (December)	1949
"A 15 by 20-inch Projection Receiver for the RCA Color Television System", Bulletin (October)	1949
"Synchronization for Color Dot Interlace in the RCA Color Television System", Bulletin (October)	1949
"A Two-Color Direct-View Receiver for the RCA Color Television System", Bulletin (November)	1949
"A Three-Color Direct-View Receiver for the RCA Color Television System", Bulletin (January)	1950
"An Experimental Determination of the Sideband Distribution in the RCA Color Television System", Bulletin (January) ...	1950
"A Study of Co-Channel and Adjacent Channel Interference of Television Signals", Part I, Bulletin (January)	1950
<i>RCA Review</i> (March)	1950
"A Study of Co-Channel and Adjacent Channel Interference of Television Signals", Part II, Bulletin (January)	1950
<i>RCA Review</i> (March)	1950
"Recent Developments in Color Synchronization in the RCA Color Television System", Bulletin (February)	1950
"Colorimetric Analysis of RCA Color Television System", Bulletin (February)	1950
"A Simplified Receiver for the RCA Color Television System", Bulletin (February)	1950

CHARACTERISTICS OF HIGH-EFFICIENCY DEFLECTION AND HIGH-VOLTAGE SUPPLY SYSTEMS FOR KINESCOPIES*

BY O. H. SCHADE

Tube Department, RCA Victor Division,
Harrison, N. J.

Summary—The energy required for cathode-ray beam deflection is determined as a function of kinescope constants and operating voltages. The total power input to the deflection-coil system can be reduced if circuit and tube losses are minimized. Because power and regulation in an associated pulse-operated high-voltage supply system are functions of the stored energy in the circuit, the kinescope screen brightness depends on the kinescope parameters and the circuit efficiency. It is shown that practical deflection systems having high efficiency and employing inexpensive tubes and components can be designed to provide satisfactory kinescope performance.

INTRODUCTION

IT IS of great value in the development of new cathode-ray tubes and deflection circuits to be able to predict the energy and power required by ideal and practical circuits for deflection of the cathode-ray beam. One likes to think that deflection of an electron beam requires, in principle, only energy, and that large field energies can be maintained in a tuned circuit by a small oscillator tube. What then is the cause for the large power loss in deflection circuits? The answer to this question lies in the fact that the deflection system in television cameras and receivers does not function like a simple tuned circuit but more like a motor generator where the output of the generator is connected for a full load test back to the power line to circulate real power and not volt-amperes. In a deflection system, the electron tubes must control and supply not only the power loss but also the total reactive power circulating through the system. It is, therefore, of interest to determine the power required for beam deflection, express this deflection power in terms of the kinescope parameters, and derive general relations for determining the required direct-current input power from the circulating power, circuit element losses, and tube losses.

The first two sections of this paper deal with fundamental functions and relations in deflection systems, while the third section illustrates the application of these principles to the problem of determining the

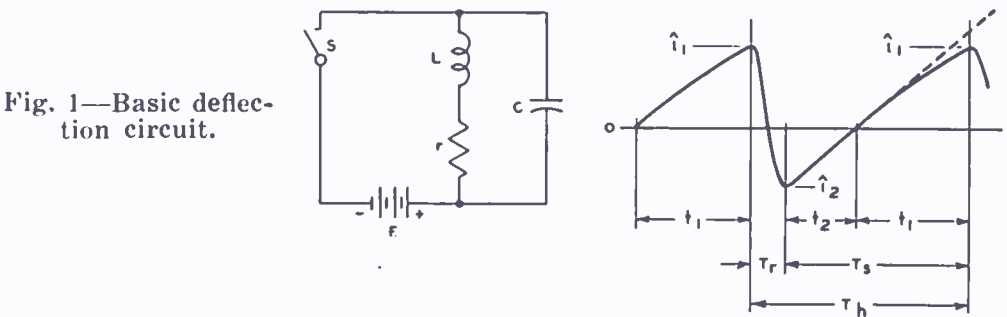
* Decimal Classification: R583.15.

circuit constants and the power loss distribution in practical deflection systems.

ENERGY AND POWER REQUIREMENTS FOR KINESCOPE BEAM DEFLECTION AND LIGHT OUTPUT

Energy and Circulating Power

The deflection cycle in the basic circuit given in Figure 1 is started by closing the switch S . Energy is built up in the magnetic field of the deflection coil L by the current i which increases exponentially during the time t_1 to a value \hat{i}_1 . The value of \hat{i}_1 is determined by the



required beam deflection angle α . At t_1 the switch is opened. The stored field energy,

$$W = 0.5L \hat{i}_1^2, \quad (1)$$

causes the tuned circuit LC to oscillate at its natural frequency f_o . Within one-half cycle of oscillation the current flow in L reverses and builds up to a negative peak value \hat{i}_2 the magnitude of which depends on the circuit losses as expressed by the effective Q -value of the tuned circuit:

$$\hat{i}_2 = -\hat{i}_1 e^{-1.65/Q}, \quad (2)$$

Current and field reversal in L cause, therefore, a rapid beam deflection in the opposite direction beyond the kinescope screen center over a total angle $\alpha_1 + \alpha_2$ within the retrace period. The retrace period T_r is expressed by*

$$T_r = 0.525/f_o. \quad (3)$$

At the end of the retrace period the switch is closed again. The current

* The retrace time is approximately 5 per cent longer than one half cycle as shown in Figure 2 of Reference (1). This relation furnishes the constants given in the exponents of Equations (2), (3), (5), (8), (9) and Table I.

in L decreases now approximately at the rate $di/dt = E/L$ from the negative value \hat{i}_2 to zero within the time t_2 thereby recharging the battery E and returning the beam to the center of the kinescope screen. After crossing the zero axis, the current increases again towards \hat{i}_1 and the switching operation is repeated.

In loss-free circuits ($Q = \infty$) the energy W stored in the magnetic field of the coil provides deflection over a total angle $\alpha_1 + \alpha_2 = 2\alpha$ and the peak-to-peak current is $\hat{i}_1 + \hat{i}_2 = 2\hat{i}_{1(\alpha)}$. The full deflection energy can then be recovered in the portion of the scanning period t_2 during which energy is returned to the power-supply system.

It is apparent that whatever the energy-control system (mechanical or electronic switches, transformers, etc.), it must handle the reactive energy W at the rate of the scanning frequency (f_h), i.e., 15,750 times in one second. The reactive power P_1 supplied to L during T_s is, hence,

$$P_1 = W f_h. \quad (4)$$

Because of circuit losses in practical systems, the current $\hat{i}_{1(\alpha)}$ must be increased by the factor

$$q = \hat{i}_1 / \hat{i}_{1(\alpha)} = 2 / (1 + \epsilon^{-1.65/q}) \quad (5)$$

to maintain full deflection over the angle 2α . Furthermore, a synchronizing margin of approximately 3 per cent requires a current increase by the margin factor

$$m = 1.03. \quad (6)$$

The reactive power supplied to L (including the factors q and m given in Equations (5) and (6)) is, therefore, given by

$$P_1 = q^2 \times 0.5L f_h (m \hat{i}_{1(\alpha)})^2 = q^2 P_o \quad (7)$$

where P_o is the reactive power required by a loss-free system and includes the synchronizing margin factor m . The fraction P_r of the power P_1 dissipated during the retrace time in the tuned circuit LC is given by

$$P_r = P_1 (1 - \epsilon^{-3.3/q}). \quad (8)$$

The power P_2 available for recirculation through the circuit is, therefore,

$$P_2 = P_1 \epsilon^{-3.3/Q}. \quad (9)$$

The decay functions in (2), (5), and (9) are given in Table I of the Appendix.

Kinescope Constants and Circulating Power

The current $\hat{i}_{1(\alpha)}$ is a function of the deflection angle α and the electron velocity in the beam, i.e., the anode potential E_a (in volts) of the kinescope, and the deflection-coil constants as expressed by the following equations:¹

$$\hat{i}_{1(\alpha)} = 2.65l (\sin \alpha) \sqrt{E_a}/\lambda'N \text{ amperes}, \quad (10)$$

and
$$L = 4\pi N^2 D \lambda' / (10^9) \text{ henries}, \quad (11)$$

where N = number of turns in deflecting coil L ,

l = length, in centimeters, of the magnetic flux lines in air, which is taken as the inside diameter of the iron shell of the coil,

λ' = effective field width, in centimeters, acting on the beam, i.e., the effective yoke length,

D = average field height or coil diameter, in centimeters, which corresponds closely to the kinescope neck diameter (outside diameter).

When Equations (10) and (11) are combined with (7) an expression for the reactive input power P_1 in terms of kinescope and coil constants is obtained.

$$P_1 = 4.4q^2 m^2 (\sin^2 \alpha) E_a D l f_h / \lambda' 10^8. \quad (12)$$

To minimize the power P_1 , the kinescope neck diameter D and the iron shell diameter l should be small and the effective field length λ' should be large (See Figure 2). The effective field length λ' is given by

$$\lambda' = r'^2 \sin \alpha / (1 - \cos \alpha), \quad (13)$$

(r' , in centimeters, defined in Figure 2), and can be eliminated from Equation (12), yielding

$$P_1/E_a = 8.8q^2 m^2 K D f_h \sin \alpha (1 - \cos \alpha) 10^{-5} \text{ watts per kilovolt} \quad (14)$$

with $K = l/2r'$ (dimensions in centimeters).

¹ O. H. Schade, "Magnetic-Deflection Circuits for Cathode-Ray Tubes", *RCA Review*, Vol. VIII, No. 3, p. 506, September, 1947.

The ratio $K = l/2r'$ can be regarded as a design constant for a given type of yoke design and has the value 1.66 for present kinescope yokes. It should be noted that r' and λ' are effective values (see Figure 2). For $2\alpha = 50-70$ degrees, r' is approximately 1.2 times the actual clearance radius r at the neckline, and λ' is approximately 1.2 times the physical "window" length λ of folded-yoke coils, because of the coil fringe fields. With the design values $K = 1.66$, $f_h = 15,750$ cycles

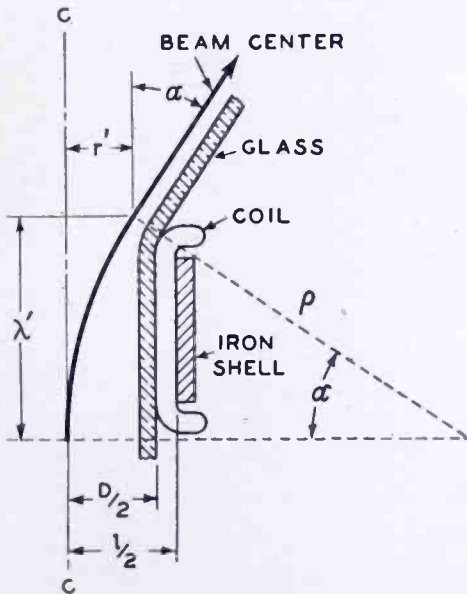


Fig. 2—Geometric relation of kinescope and deflection-coil dimensions to the beam-deflection angle α .

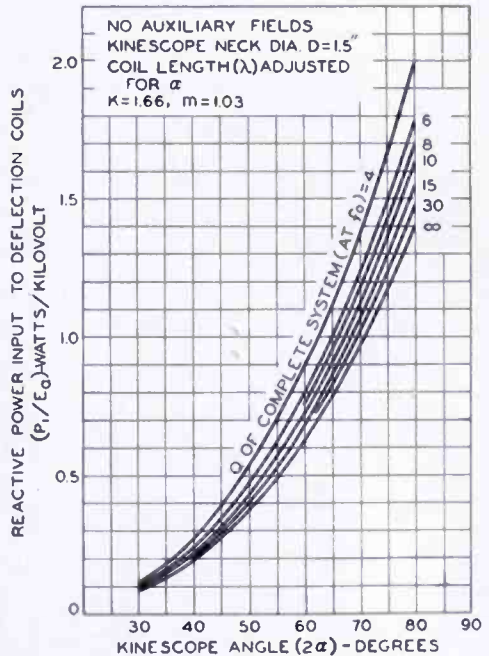


Fig. 3—Reactive power input to deflection coils as a function of kinescope angle 2α .

per second, $m = 1.03$, and $D = 3.8$ centimeters, the power input to the deflection coils per kilovolt of anode potential is expressed by

$$P_1/E_a = 9.33q^2 \sin \alpha (1 - \cos \alpha) \text{ watts per kilovolt.} \quad (15)$$

A plot of Equation (15) for full-diameter deflection (2α) is shown in Figure 3 for various values of Q .

Regulation and Reaction of an Associated High-Voltage Pulse Rectifier Circuit

A certain amount of power can be taken from the deflection power P_1 when a high-voltage pulse is generated in LC during the retrace period T_r . With the aid of a transformer and rectifier system, the pulse voltage can be adjusted to obtain the desired kinescope anode voltage E_a . Removal of power from P_1 during T_r reduces the initial

no-load value Q_0 of the system at its natural frequency f_0 to a lower full-load value Q_2 at the end of T_r and thus decreases the value of the negative peak current \hat{i}_2 . The beam current obtainable from the high-voltage supply circuit with a regulation of 10 per cent can be determined as follows. When 19 per cent of P_1 is taken out, the no-load peak anode voltage E_a is reduced to $\sqrt{0.81} E_a = 0.9E_a$ and the current \hat{i}_2 available for scanning at the end of T_r is reduced to $0.9 \hat{i}_2$. The effective deflection width on the kinescope screen remains, therefore, substantially constant. The 10 per cent change of the ratio \hat{i}_2/\hat{i}_1 does not seriously affect the deflection linearity. The pulse-voltage peak occurs at $0.5 T_r$, at which time, because of circuit losses, the available power has then decreased from P_1 to the lower value

$$P_{0.5T_r} = P_1 \epsilon^{-1.65/Q} \quad (16)$$

The anode current I_a at the 10 per cent regulation point $0.9E_a$ is, therefore,

$$I_a = 0.19P_{0.5T_r}/0.9E_a = 0.211 (P_1/E_a \epsilon^{-1.65/Q}) \text{ microamperes.} \quad (17)$$

The value given by Equation (17) is obtainable at $0.9E_a$ from the deflection-coil energy alone assuming an ideal transformer and rectifier system. Practical transformers increase the stored energy in the deflection coils by their own field energy, which for good design, is on the order of 10 to 20 per cent of the deflection energy. Practical high-voltage rectifier tubes and series reactance cause a voltage drop which more than cancels the current increase due to the transformer energy. The value of the available beam current is *independent of the anode voltage* for a given neck diameter and tube angle α because Equation (17) is derived for the condition that the voltage E_a is adjusted to obtain full deflection over the selected angle 2α . The current at 10 per cent regulation is substantially constant for $Q_0 \geq 4$ as shown by Figure 4.

High-Voltage Power and Light Output

The design of a satisfactory kinescope and deflection system has the primary objective of providing adequate picture brightness with good focus. The screen brightness, i.e., the light output per unit area of kinescope phosphors, is proportional to the average screen current per unit area but increases approximately as the square of the screen potential within the range of normal operation.

When the anode potential is limited, adequate screen brightness

may require operation with larger beam currents. Larger beam currents necessitate deflection systems in which the deflection field energy is supplemented by larger auxiliary fields in transformers or chokes to obtain the desired high-voltage power from a deflection pulse supply. In this case it may be advantageous to increase the deflection energy itself by selecting a shorter kinescope with a larger deflection angle.

It is, therefore, desirable to consider whether or not the high-voltage power available from an efficient deflection system with small auxiliary fields can provide adequate screen brightness.

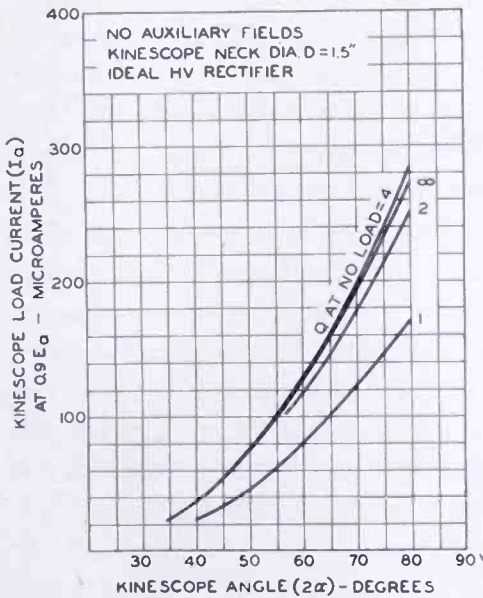


Fig. 4—Current obtained with 10 per cent regulation from ideal high-voltage-rectifier system supplied by the deflection-field energy.

of 300 to 400 microamperes, the published characteristics of the 10BP4, operated with an anode voltage of 9 kilovolts and with a 6×8 -inch focused raster, show a highlight brightness of 80 to 100 foot-lamberts. The highlight brightness is reduced to 58 to 73 foot-lamberts when a full screen raster of 7×9.35 inches is scanned. The brightness values obtainable with practical systems are from 10 to 20 per cent lower and can be considered adequate.

For the same brightness a 16-inch kinescope operated at 9 kilovolts would require that the current be increased by the ratio of the screen areas $16^2/10^2$, or 2.56. When the 16-inch kinescope is operated at an anode voltage of 12.6 kilovolts (0.9×14 kilovolts), the current ratio can be decreased to $(9/12.6)^2 \times 2.56 = 1.3$; i.e., the required average beam current is 100×1.3 or 130 microamperes. This current requires

The full deflection angle (2α) of a 10BP4 kinescope is 55 degrees. In a deflection system with a Q greater than 4, the beam current at $0.9E_a$ is, hence, 100 microamperes (Figure 4). This value represents the *average* beam current with picture modulation because the filter capacitance of the rectifier system can supply high peak currents without noticeable effect on the voltage stability. The ratio of peak to average current depends, obviously, on the picture content. For normal television images the peak beam currents which correspond to high-light brightness values are rarely less than 3 to 4 times the average beam current. For a peak current

a kinescope angle of 60 degrees. For better contrast in the presence of ambient light the use of a face plate made of a neutral filter glass with a transmission of 70 per cent requires that the beam current be increased to 186 microamperes for the same light output from a 16-inch tube. A short tube with a cone angle of 70 degrees provides theoretically 195 microamperes of beam current from an efficient deflection system and is, therefore, a more logical choice than a longer tube with a smaller angle operated with a deflection circuit of lower efficiency.

It is unfortunate that the performance of a television receiver is judged in some cases by the ability of the kinescope to light up the viewing room regardless of the fact that definition and picture quality are greatly reduced. It is of interest to describe what happens when a receiver with a 10-inch tube and limited high-voltage power is compared with one having unlimited high-voltage power. When the brightness test is made with a substantially "white" screen, as in certain test patterns, the pulse-operated, high-voltage supply will provide a maximum brightness in the order of 30 foot-lamberts; the brightness with a supply of unlimited power on the other hand, will remain at or even exceed 70 foot-lamberts. With normal television subjects on the screen, however, there will be very little difference between the two sets even when the kinescopes are over-driven because the average currents cannot exceed moderate values because the large peak signals cause rectification effects and overload in video and kinescope grid circuits.

CIRCUIT OPERATION AND CHARACTERISTICS

The Requirement for Linearity

The simple circuit shown in Figure 1 does not provide linear deflection current unless the circuit resistance is reduced to zero. Linearity is obtained during the scanning period T_s (switch closed) by inserting a negative resistance $-r$ in series with the switch, i.e., by inserting a power source generating the voltage $-ir$ to cancel the positive ir drop across the circuit resistance. This measure insures linearity of sawtooth current during T_s but does not compensate for the power loss in the retrace time.

A system compensated for series resistance in the inductive circuit L - S - E of Figure 1 by a "linearity control" generator but having a finite Q -value during T_r can, therefore, provide a linear deflection current within T_s . However, the power and the average current \bar{i}_1 furnished by the battery E to build up the field energy in L remain larger than the power and the average current \bar{i}_2 recovered after T_r to recharge the battery.

Circuit Q at No-load and Full-load

The no-load value of Q_o at the natural frequency, f_o , of a practical deflection circuit is determined largely by the power loss caused by eddy currents in copper and losses in the magnetic materials of the tuned-circuit inductances. The low loss of powdered (electrolytic) iron and particularly of ferrite cores has made it possible to obtain values of Q_o equal to or greater than 15 in circuits with inexpensive transformers. By use of these materials, the power dissipation during T_r in yoke and transformers has been reduced to less than 20 per cent of the reactive deflection power P_1 (Equation (7)). The Q_o of the circuit can be computed from the equivalent shunt resistance value R across the yoke and the associated transformer winding which, in parallel, have the inductance L ; $Q_o = R/\omega_o L$.

The total shunt resistance R is the parallel value of the shunt loss-resistances of yoke and transformer, and the reflected values of other resistance loads such as isolation or coupling resistors in high-voltage doubling circuits. Q_o and R are readily measured in a completed circuit by connecting a vacuum tube voltmeter across the yoke winding and exciting the circuit (scanning tubes not operating) at its natural frequency f_o (of the order of 70 kilocycles) by loose capacitive coupling with a signal generator. The frequency deviation Δf between the 0.707-voltage points on each side of f_o furnishes the value $Q_o = f_o/\Delta f$. The value of added shunt resistance which reduces the resonant voltage at f_o to one-half is equal to R thus giving also the inductance $L = R/\omega_o Q_o$.

The Q and the equivalent shunt resistance of the yoke can be found by tuning the yoke itself with a low-loss capacitor to f_o . These measurements furnish the distribution of the retrace-time power loss in the circuit elements which is proportional to the reciprocal value of their shunt resistances.

$$P_1 + P_2 + \dots + P_n = R (1/R_1 + 1/R_2 + \dots + 1/R_n) P_R. \quad (18)$$

Removal of power by the high-voltage supply system reduces the Q_o of the tuned circuit to an equivalent value Q_2 which would cause the same total power loss during the retrace period T_r . For example, a beam current with a 10 per cent regulation (see Equation (17)) causes a power loss of $0.19 P_1$ within T_r . This loss is equivalent to the loss in a circuit with $Q_1 \approx 15$ (Equation (8)). The equivalent Q of the circuit can then be computed from

$$1/Q_2 = 1/Q_o + 1/Q_1. \quad (19)$$

Q and Average Current Ratio

In circuits with electronic switch (Figure 5a), the bidirectional deflection current is carried by two electron tubes, V_1 and V_2 . The reactive current i is split into two components i_1 and i_2 joined at $i = 0$. This ideal "class B" operation is seldom realized in practical circuits. It is obvious, however, that this condition furnishes minimum average currents $I_{b1} = \bar{i}_1$ and $I_{b2} = \bar{i}_2$. These current values have a ratio equal to the triangular areas under the current waveforms i_1 and i_2 when the deflection current is linearized by proper control of V_1 and V_2 (see later). The ratio of the average currents is given by

$$\bar{i}_2 / \bar{i}_1 = \hat{i}_2^2 / \hat{i}_1^2 = \epsilon^{-3.3/Q_2} \tag{20}$$

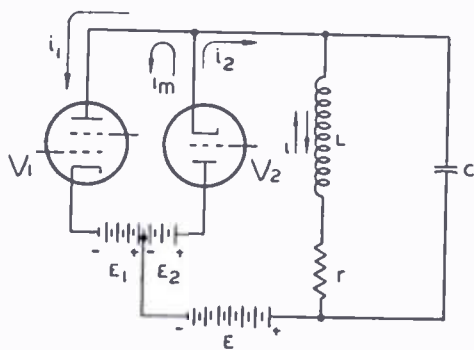


Fig. 5a — Basic deflection circuit with electronic switch.



Fig. 5c—Waveform distortion increasing the average value of i_{p2} .

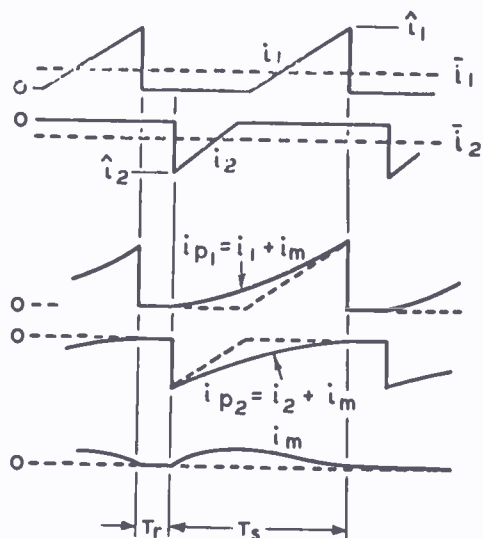


Fig. 5b — Current components in circuit of Figure 5a.

In practice the plate currents i_{p1} and i_{p2} may overlap in time as much as 100 per cent as indicated in Figure 5b. The "matching" current, $i_m = i_{p1} - i_1 = i_{p2} - i_2$, increases the average plate currents and the plate dissipation of V_1 and V_2 , but it cancels out in the common circuit branch $E-r-L$ of Figure 5a.

It is, therefore, not possible without the use of a transformer to obtain equal charge and discharge currents of the battery E with the condition that the inductive current i have a linear or symmetric* waveform. It is possible to equalize charge and discharge currents

* By symmetric is meant an S-shaped current such as a section of a sine wave extending equal angles below and above the sine-wave axis.

by distorting the current waveforms i_1 and i_2 as shown, for example, in Figure 5c, but the resultant current i is then non-linear or asymmetric.

Requirements for Series Power Feedback (Transformer Ratios)

The operating principle of circuits with series power feedback is readily understood when it is considered that equal charge and discharge currents of the battery E result in a total average current equal to zero and the battery E of Figure 5a, therefore, may be replaced with a capacitor C_b without disturbing the circuit operation. In order to start functioning, the circuit must have current waveforms giving initially a current ratio \bar{i}_2/\bar{i}_1 slightly greater than unity so that C_b can be charged gradually and the voltage E_{C_b} built up to the normal value E .

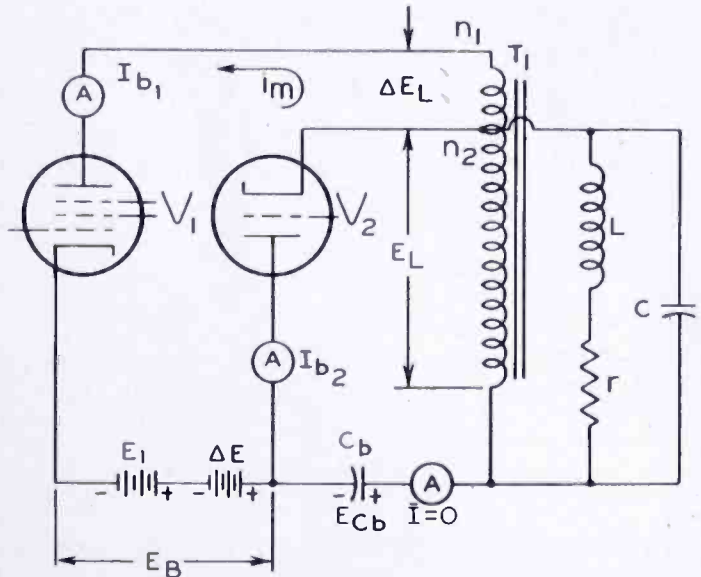


Fig. 6—Power feedback circuit with autotransformer.

Perfect linearity of deflection requires either an LC circuit with an infinite Q or the insertion of a transformer between the tubes V_1 and V_2 (Figure 6) to reduce the value of the larger current \bar{i}_1 so that $\bar{i}_1 = \bar{i}_2$.

Linearity of deflection current ($di/dt = \text{constant}$) results in constant reactive voltages on all of the transformer windings. The reactive power values are, therefore, equal to products of reactive voltages and average current values. The matching current, i_m , of V_1 and V_2 exists only in the section $n_1 - n_2$ of the transformer. (See Figure 6) The average current components in the common winding n_2 are, therefore, the values \bar{i}_1 and \bar{i}_2 of the ideal (triangular) class B currents, and the reactive powers with respect to this winding are $P_1 = \bar{i}_1 E_L$ and $P_2 = \bar{i}_2 E_L$, where $\bar{i}_1 > \bar{i}_2$. The power P_1 being supplied by V_1 is developed

actually in two windings; on n_1 by the current component \bar{i}'_1 , and on $(n_2 - n_1)$ by the full plate current I_{b1} , so that $P_1 = E_L \bar{i}'_1 + \Delta E_L I_{b1}$. When the turns ratio is adjusted so that $\bar{i}'_1 = \bar{i}_2$, it follows that $E_L \bar{i}'_1 = P_2$ and

$$\Delta E_L I_{b1} = P_1 - P_2 = P_r. \quad (21)$$

In practical circuits a fraction of P_2 is dissipated in the process of recharging C_b . Unless compensated, this power loss causes a reduction in the voltage E_{cb} to a value less than that of E_L , but the voltage loss has no effect on E_L or \bar{i}_2 which determine Equation (21). It may, however, be desirable to use a fraction of the feedback power P_2 to supply external load circuits with current from the "boosted" B -supply voltage $E_{BB} = E_B + E_{cb}$.

To supply this "bleeder" current from C_b , the charging current \bar{i}_2 must be increased by a current component equal to the bleeder current I_{BB} and a change is required in the transformer ratio to restore the power balance. The power loss P_r subtracted from the feedback power by the bleeder-current load is equal to $E_L I_{BB}$ and requires that Equation (21) be changed to

$$\Delta E_L I_{b1} = P_r + P_x. \quad (21a)$$

Substituting this expression into the voltage ratio $n_1/n_2 = (E_L + \Delta E_L)/E_L$, gives the equation

$$n_1/n_2 = 1 + (P_r + P_x)/I_{b1} E_L. \quad (22)$$

Equation (22) furnishes the required turns ratio n_1/n_2 between the V_1 and V_2 circuits. The ratio between V_1 and the deflection-coil connection can be left unchanged or may be given other values in practical circuits to adjust I_{b1} and E_L . For the general case, the voltage E_L in Equation (22) is the inductive voltage $E_{(n2)}$ across the transformer winding having n_2 turns and energizing the V_2 circuit. The substitution $E_{n2} = E_{n1} n_2/n_1$ results in the more useful form

$$n_2/n_1 = 1 - (P_r + P_x)/I_{b1} E_{n1} \quad (23)$$

where $P_x = I_{BB} E_{n1}$.

With respect to the plate circuit of the power tube the net "reactive" power load $I_{b1} (E_{n1} - E_{cb})$ has the characteristics of a "bucking battery" (square wave voltage drop). This load requires the increase, ΔE (Figure 6) in the supply voltage E_B but does not cause

any change in the plate dissipation of V_1 (See Part III). The reactive load $I_{n_1}(E_{n_1} - E_{Cb})$ does not contain the total copper loss or series resistance loss of the circuit. The V_1 plate circuit contains, therefore, also a series resistance load R_p (See next section).

Linearity Control Circuits and Functions

The action of the linearity control (tunable transformer T_2) in diode circuits (Figure 7) has been explained in detail in a previous article.¹ For the purpose of this discussion it is pointed out that the voltage generated across the diode winding of T_2 is equal and opposite to the resistive voltage drop in the diode circuit V_2-L-C_b and, in effect, cancels this circuit resistance, thereby providing linearity of deflection. The linearity transformer T_2 reflects, therefore, a series resistance into the plate circuit of V_1 in which the plate current i_{p1} develops a power output equal to the diode-circuit resistance loss. This action permits these conclusions for *circuits with controlled diode* (V_2):

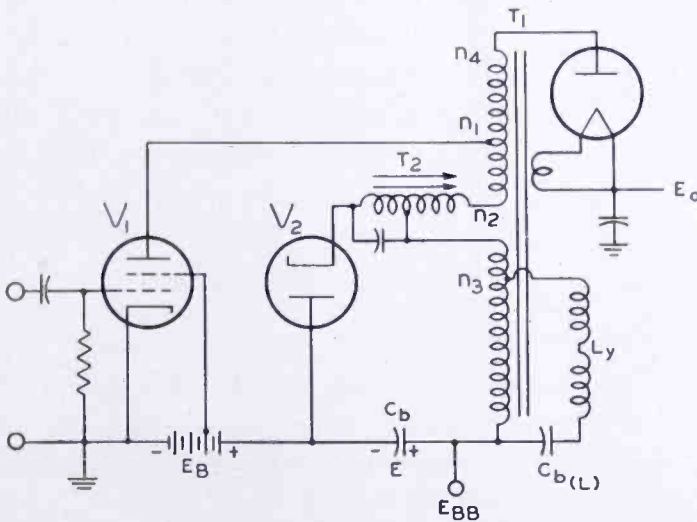


Fig. 7—Power feedback circuit with controlled diode and autotransformer supplying high-voltage rectifier.

1. The potential E_{Cb} developed across C_b (termed the "boost voltage") is exactly equal to the inductive voltage $E_{n_2} = L di/dt$ energizing the diode circuit which may be treated as a loss-free rectifier circuit. The reactive power load of V_1 is, therefore, $(P_r + P_x)$.
2. The power tube V_1 supplies *all* copper losses as well as the diode plate loss occurring in the deflection circuit during the scanning period T_s . These losses are reflected into the plate circuit of V_1 as a resistive load R_p .

When a triode rectifier (V_2) is used in place of the diode, the negative resistance (and hence linearity) is generated in the tube by

applying a suitable control-grid signal. In this case the resistive power loss in the V_2 circuit is supplied from the reactive power P_2 . Consequently, it may be concluded for *circuits with triode rectifier* (V_2):

1. The boost voltage E_{cb} is smaller than the inductive voltage and the reactive power tube load $I_{b1} (E_{n1} - E_{cb})$ containing resistive power losses is larger than in circuits with controlled diode.
2. The copper losses caused by the current components i_1 and i_{p1} only appear as a resistance load R_b in the plate circuit of the power tube V_1 . The reflected plate load R_p is, therefore, smaller than in circuits with controlled diode.

These characteristics must be considered when the total plate load of the power tube and the required B-power input are evaluated. The equivalent plate circuit of the power tube V_1 has, thus, the form shown

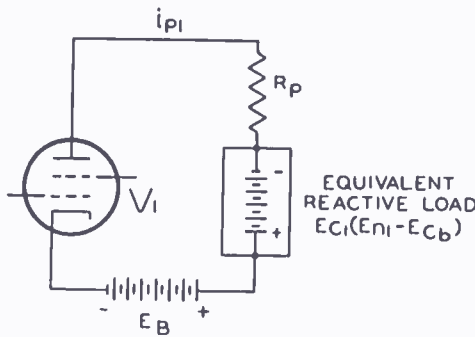


Fig. 8—Equivalent plate circuit of power tube V_1 .

in Figure 8 and will be discussed in Part III. It should be mentioned that constant velocity of the cathode-ray spot on a large-radius kinescope screen requires a reduction of the angular velocity (slightly S-shaped sawtooth current) for larger deflection angles. This velocity correction is controlled by adjusting the value of series capacitor $C_{b(L)}$ (Figure 7).

Pulse Voltage Step-up and Rectifier Circuits

The peak voltage \hat{e} built up across an LC circuit after $0.5 T_r$ can be expressed in terms of the circulating power $P_{0.5T_r}$ and the circuit capacitance; or in terms of current and the circuit impedance $\omega L = \sqrt{L/C}$. It follows from

$$P_{0.5T_r} = P_1 \epsilon^{-1.65/Q} = C \hat{e}^2 f_h / 2 \quad (25)$$

that
$$\hat{e} = \sqrt{2P_{0.5T_r} / C} f_h \quad (26)$$

Also:
$$\hat{e} = \hat{i}_1 \omega_0 L \epsilon^{-0.825/Q} \quad (27)$$

The voltage \hat{e} at the deflection-coil terminals of practical circuits ranges from 1.0 to 3.0 kilovolts. It is largest in direct-drive circuits (Figure 5a) where the capacitance C in Equation (25) is the sum of the capacitances of the deflection coils, the tubes V_1 and V_2 , and a filament isolation transformer for V_2 . This capacitance is equal to or greater than 150 micromicrofarads.

General requirements for generating voltages in the order of kine-scope operating potentials are indicated by Equation (26).

a. For a given power, the capacitance C at the input terminals of the high-voltage rectifier must be reduced considerably below the value in the deflection circuit (by a factor between 5^2 and 10^2). This impedance transformation is effected by connecting a step-up transformer with low winding capacitance parallel to the deflection coils. (Figure 7). The voltage step-up obtainable by this method is limited by the specified retrace time. The progressive increase in the diameter of the high-voltage coil causes larger layer capacitance and leakage inductance within the step-up coil.

Parasitic tuned circuits are formed by leakage inductance and coil capacitance. These circuits (Figure 9) absorb power from the system

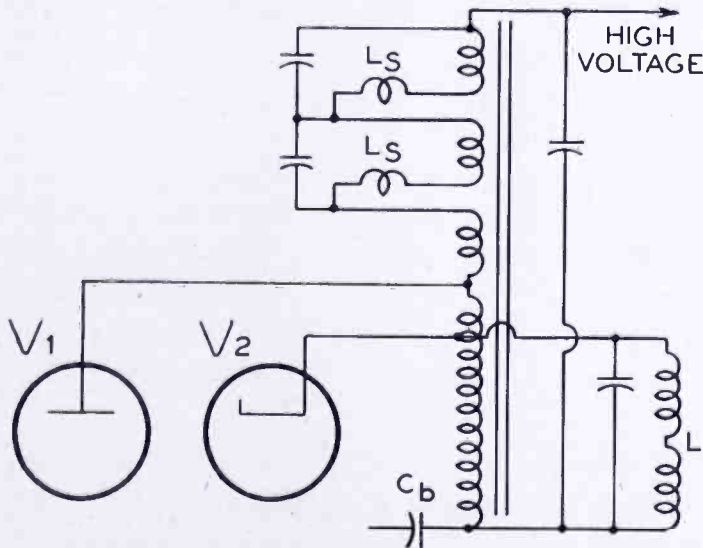


Fig. 9 — Tuned-circuit system formed by layer capacitance and leakage inductance of high-voltage winding.

particularly when their resonant frequencies approach the main resonant frequency f_o . Having no direct outlet into the V_2 circuit, the absorbed power is dissipated largely in the transformer winding. When limited by these difficulties the pulse voltage can be increased by raising the reactive power.

b. The circulating power in the circuit can be increased by connecting an auxiliary inductance in shunt or in series with the deflection-coil inductance. The shunt inductance of the transformer winding may, therefore, be reduced to serve this purpose, a lower limit being imposed by increasing core loss and saturation of the magnetic material.

A shunt inductance with a high Q does not disturb the general operation of the circuit because the additional circulating power is included in the power feedback. The increased plate currents, however, cause increased copper loss and plate loss in V_1 and V_2 . A sepa-

rate inductive shunt is used to advantage in deflection systems for projection tubes which require a large high-voltage power. Series inductance may be introduced into the plate circuit of V_1 in the form of a separate inductance or by leakage inductance (Figure 10) between the V_1 and V_2 windings of the transformer.

The series inductance L_s alter the system performance by introducing at least one new resonant system formed by L_s and associated capacitances C_s . This system has its own natural frequency f_s which is usually higher than f_o . The series circuit $L_s C_s$ is relatively undamped as it has no direct power outlet into the V_2 circuit and must, therefore, dissipate most of its power ($P_{1(s)}$) in the form of heat (partially in the plate resistance r_p of V_1). Coupling to the main circuit causes a trickle feed of oscillating current of frequency f_s into the main circuit and may produce "ripples" in the deflection current.

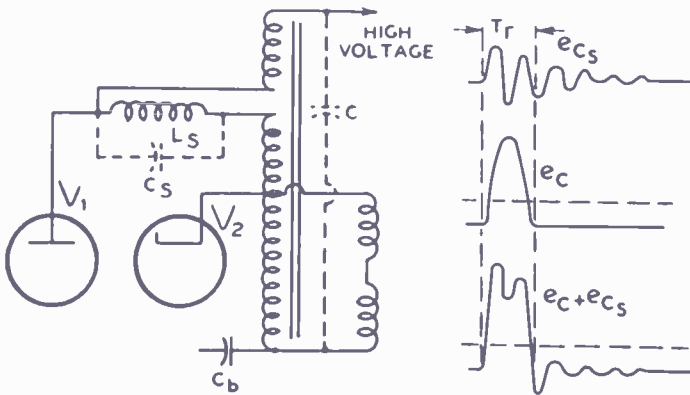
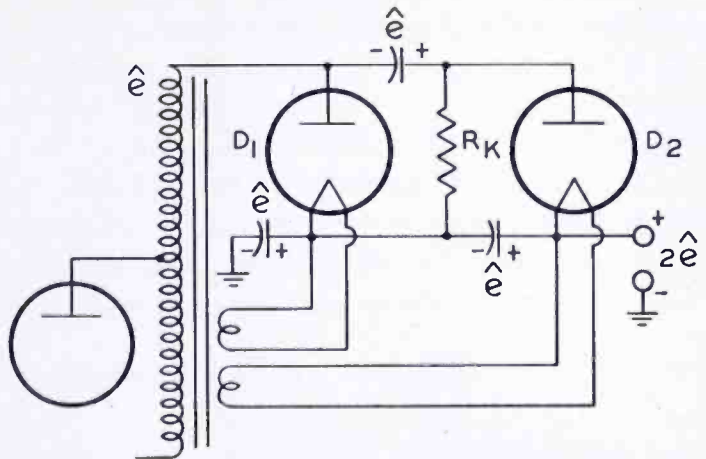


Fig. 10 — Deflection circuit with leakage inductance in plate lead of power tube causing negative plate-voltage swing.

Relatively small values of series inductance L_s cause an oscillating plate voltage (Figure 10) which becomes negative at the start of the scanning period T_s giving rise to high-frequency Barkhausen oscillations which may be picked up by the receiver on one or more channels. These oscillations can be shifted in frequency by changes in the power tube structure, usually at the expense of increased plate dissipation. Barkhausen oscillations do not occur when a plate voltage swing below the "knee" of the power tube plate characteristic is prevented.

c. High direct-current potentials can be obtained from a low pulse voltage by connecting two or more pulse rectifiers in cascade. The voltage-doubling circuit Figure 11 removes many of the difficulties which have caused low efficiency in deflection systems. Insulation problems are eased considerably because transformer and circuit components operate at one-half the direct-current output potential. The low tube voltages and high current efficiency are reflected in the design of single-ended low-cost rectifiers and power tubes permitting convenient sub-chassis mounting of the circuit components. The efficiency

Fig. 11—Voltage-doubling circuit with coupling resistor.



of the rectifier circuit can be increased still further by replacing the coupling resistor R_k in Figure 11 by a diode as shown in Figure 12. The coupling diode D_k removes alternating-current loading of the transformer circuit during T_r and eliminates the direct-current voltage drop on R_k caused by the kinescope current. For a moderate high-voltage power, a resistor R_k is satisfactory. It can be given a high value such as 3 megohms which causes a 300-volt drop for a 100 micro-ampere current and at a pulse voltage $\hat{e} = 5$ kilovolts ($E_a = 10$ kilovolts) represents a shunt power loss of approximately 0.75 watts. Replacement of R_k by a diode D_k eliminates the direct-current voltage drop and reduces alternating-current loading to the 0.25 watts required for heating the diode filament.

PRACTICAL CIRCUIT DESIGN

The usefulness of the relations derived in the first two sections is best illustrated by a description of the sequence of steps encountered in the design of a practical deflection system with high efficiency. For a numerical example consider a deflection circuit with auto-transformer having the circuit arrangement indicated by Figure 7 to operate a 70-degree kinescope at an anode voltage E_a of 14 kilovolts. Given are the scanning frequency $f_h = 15,750$ cycles per second, the retrace

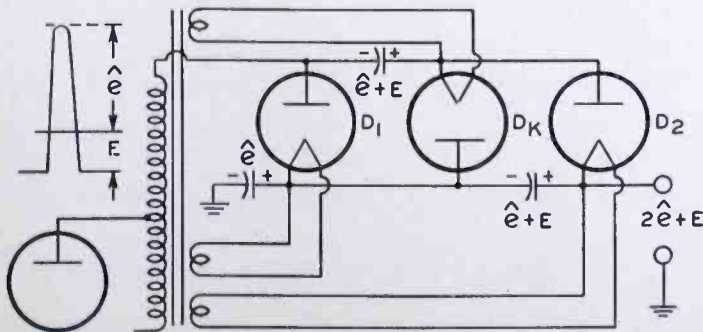


Fig. 12—Voltage-doubling circuit with coupling diode.

period $T_r = 7.5$ microseconds, and the scanning period $T_s = 56$ microseconds.

Yoke Inductance and Voltages

10 millihenries is chosen for the yoke inductance. This value can be readjusted later on if desirable. First, the voltages appearing on L_y are determined. It follows from Equation (7) that the peak current \hat{i}_1 is given by

$$\hat{i}_1 = 11.3 \sqrt{P_1/L} \text{ milliamperes} \quad (28)$$

for $f_h = 15,750$ cycles per second.

The inductive voltage during the 56-microsecond scanning period is constant and has a fixed value for a given peak-to-peak deflection current. It can, therefore, be computed from the reactive power P_o letting $Q = \infty$. With $E_L = L 2\hat{i}_1/T_s$ and Equation (28),

$$E_L = 404 \sqrt{P_o L}. \quad (29)$$

For $2\alpha = 70$ degrees, $E_a = 14$ kilovolts, and $Q = \infty$, from Figure 3 the value $P_1/E_a = 0.96$, hence, $P_o = 0.96 \times 14 \approx 13.5$ watts. With $L_y = 10$ millihenries, from Equation (29), $E_L = 148$ volts. The surge voltage \hat{e} can now be computed. For a normal waveshape and time ratios, Table II #4,

$$\hat{e} = 12.7 E_L \quad (30)$$

and the r-m-s value $|E| = 3.22 E_L$. (31)

The numerical values are, hence, $\hat{e}_y = 1.88$ kilovolts and $|E|_y = 476$ volts.

Transformer Inductance, Shunt-Loss Diagram, and Q

The transformer inductance L_3 in shunt with the deflection coil inductance L_y increases the reactive currents of the deflection system by the factor

$$s = (1 + L_y/L_3). \quad (32)$$

The reactive power is increased by the same factor (s) because the total inductance L is decreased to the smaller parallel value

$L = \frac{L_y L_3}{L_y + L_3}$. Large values of L_3 reduce the shunt power, but transformer windings with a large number of turns increase winding re-

sistances and leakage reactance, which in turn can cause a more serious power loss. Practical ratios L_3/L_y vary between 5 and 10 depending on the permeability and the flux density $B_{\max} = \hat{e} 10^8 / \omega_0 n A$ in the selected core cross section (A in square centimeters) and magnetic core material. If, for the example, the value $L_3 = 70$ millihenries, $s = 1.143$ and $L = 8.75$ millihenries. To compute power, currents, and turns ratios it is necessary to determine the losses of the system from a shunt resistance diagram such as shown in Figure 13.

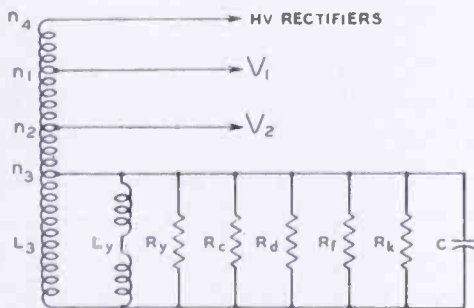


Fig. 13—Shunt-loss diagrams of deflection circuit.

Shunt Resistance (Megohms)	Representing Loss in
$R_y = 0.225$	Yoke with ferrite shell
$R_c = 2.$	Ferrite core of transformer
$R_d = 1.25$	Dielectric
$R_f = 0.302$	Rectifier filaments
$R_k = \infty$	Coupling resistors
<hr/>	
$R = 0.110$	Total Shunt
<hr/>	
$L_y = 10$ millihenries	
$L_3 = 70$ millihenries	
$L = 8.75$ millihenries	

The yoke loss resistance, $R_y = 225,000$ ohms, is measured by tuning the inductance L_y with an air capacitor to $f_0 = 70$ kilocycles as outlined previously. The transformer core loss R_c is determined as follows: A test coil wound on the transformer core with 10×38 Litz wire and having an inductance equal to that of L_3 is connected in shunt with the yoke. The value of the resistances R_y and R_c in parallel can then be measured and R_c calculated from this value. It will be observed that the shunt resistance values are substantially constant for flux densities below the saturation of the magnetic material and over a range of frequencies from 60 to 100 kilocycles. The value of f_0 , therefore, does not have to be known accurately. The Q , however, changes inversely with f_0 and requires an accurate frequency adjustment. It is pointed out that the saturation point of ferrites is also a function of temperature and that a relatively small core loss can cause a substantial temperature rise in materials having low thermal conductivity.

The shunt resistance R_d represents the dielectric loss in winding capacitances. It can be measured on the completed transformer and circuit or may be estimated by assuming a 0.3 per cent power factor for which $R_d = 330 / \omega_0 C = 330 \omega_0 L$.

The filament power P_f of high-voltage rectifier tubes is supplied by the transformer. The equivalent load resistance R_f reflected parallel to the yoke winding equals, therefore, E^2/P_f . The rectifier circuit selected for the example (Figure 12) contains 3 diodes and no coupling resistor ($R_k = \infty$).^{*} With the previously computed voltage $|E| = 476$ volts and the filament power $P_f = 0.75$ watts, we obtain the equivalent shunt resistance $R_f = 302,000$ ohms. The total shunt loss R of the circuit is, hence, 110,000 ohms and the value Q_o equals $R/\omega_o L$ for the circuit at f_o of 70 kilocycles and is, therefore, 26.

The retrace-power-loss distribution of the circuit, determined by Equation (18), is, hence, 110 $(1/225 + 1/2000 + 1/1250 + 1/302)P_R$. The power loss in the yoke represents 49 per cent, the transformer core loss 5.5 per cent, the dielectric loss 9 per cent, and the filament power 36.5 per cent of the power loss during retrace time. It should be mentioned that the low losses of yoke and transformer result from the use of ferrite cores operated with moderate flux densities. Should the transformer core loss prove too high, a higher inductance value L_3 is indicated because the shunt-loss resistance R_c is proportional to L_3 .

Retrace Power Loss, Reactive Power Input, and Recovered Power

The power loss occurring during T_r is readily computed from the shunt resistance $R = 110,000$ ohms and the r-m-s voltage during T_r (not the actual r-m-s value $|E|$ given by Equation (31)).

$$P_r = (\hat{e}^2/2R)T_r f_h. \quad (33)$$

$$\text{For normal time ratios } P_r = \hat{e}^2/16.9R. \quad (34)$$

For the values of the example, $P_r = 2.1$ watts. The reactive power input to the circuit inductance L is increased to $P_{1(L)} = sP_1$. For $Q = 26$, Equations (15) and (5) or Figure 3 furnish $P_{1(L)} \approx 16.5$ watts. The recovered power $P_{2(L)}$ computed from the decay function (Equation (9)) is $P_{2(L)} = 0.875P_{1(L)} = 14.4$ watts and $P_r = 0.125P_{1(L)} = 2.1$ watts, which checks with the previously computed value.

The values just computed are the "no load" values at zero beam current. The beam current I_a with a regulation of 10 per cent from an ideal transformer and high-voltage rectifier system is given by Equation (17) or Figure 4. Because of the increase in reactive power required by the transformer shunt field ($s = 1.143$), we obtain for

^{*} The small high-voltage winding of the voltage-doubling circuit avoids resonance effects in the transformer design permitting, therefore, a close check of computed values by measurement.

$2\alpha = 70$ degrees the theoretical value $I_a = 204s$ microamperes = 235 microamperes. Series resistance and leakage reactance in the high-voltage winding, however, reduce the rectification efficiency. Experience indicates that the current of practical circuits at 10 per cent regulation has a value between 50 and 70 per cent of the theoretical value sI_a taken from the curve $Q = \infty$ in Figure 4. For our example, a 10 per cent regulation is expected to occur at a current I_a between 110 and 155 microamperes. A current of 186 microamperes will hence occur with a regulation between 12 and 17 per cent and give a screen brightness from 4 to 14 per cent less than the theoretical values stated in the discussion of high-voltage power and light output.

At this point it is necessary to select an average value of kinescope current I_a at which perfect linearity of deflection current is to be obtained. For this example, the value of 120 microamperes is selected. The high-voltage power load for the example is approximately $P_{HV} = 0.95 E_{\max} I_a = 1.6$ watts. This value increases the power loss during retrace from 2.1 watts at zero beam current to 3.7 watts at a 120-microampere beam current. The recovered power is reduced from 14.4 watts at no load to 12.8 watts at 120-microamperes beam current. The various design constants are assembled in Table III of the Appendix for further reference.

Currents and Voltages

The peak current values are readily computed from Equation (28). The peak currents $s\hat{i}$ in the total inductance for the no-load condition $I_a = 0$ are obtained with the values $P_1 = 16.5$ watts and $P_2 = 14.4$ watts and $L = 8.75$ millihenries. Under load ($I_a = 120$ microamperes) the value $s\hat{i}_1$ remains the same but $s\hat{i}_2$ is decreased because of the reduced power value $P_{2(L)}$. The numerical values are listed in Table III as well as the peak currents in the yoke inductance L_Y , which are obtained by multiplication with the factor $1/s$. *The inductive voltage E_L* for the no-load condition is identical with the value computed by Equation (29) for $Q = \infty$. The voltage E_L decreases with load in proportion to the peak-to-peak current ($\hat{i}_1 + \hat{i}_2$) which has the previously computed full-load-to-no-load ratio 0.926/0.949.

The numerical values of E_L so obtained are also listed in Table III.

Calculation of the average plate current values I_{b_1} and I_{b_2} requires the selection of a representative current waveform. Evaluation of the average-to-peak current ratio I/\hat{i} (See Table II) indicates values from 0.23 to 0.44 for a linear intermittent sawtooth wave when the operating time is varied from the ideal class B case to a full class A sawtooth lasting over T_s . An inverted sine wave class A operation (#3 Table II)

furnishes the factor $I/\hat{i} = 0.32$. A good practical waveform factor is

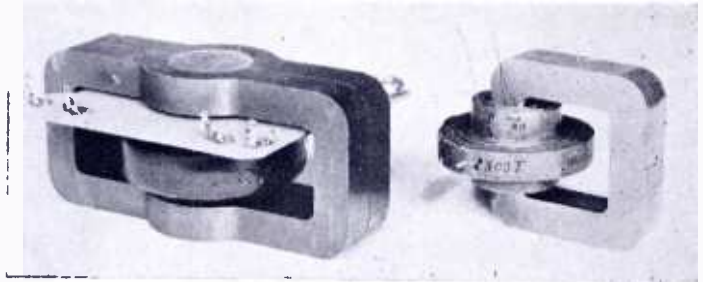
$$\hat{i}_p/I_b \approx 3. \quad (35)$$

The average plate current reflected into the transformer winding n_3 to which the yoke is connected is, therefore, $I_{b_1}' = 0.491/3 = 0.164$ amperes.

Transformer Turns Ratios

A general advantage of a transformer drive circuit is the flexibility available for adjusting the effective plate-circuit reactance by varying the transformation ratio n_3/n_1 between the deflection-coil terminals (n_3) and the power-tube plate circuit (n_1). With properly designed transformers the reflected plate-circuit inductance can be made considerably higher than the yoke inductance in direct-drive circuits for

Fig. 14—Autotransformer (right) has higher efficiency and smaller size than transformer with separate secondary winding (left). Both transformers have powdered-iron cores.



a specified retrace time. Auto-transformers are particularly suitable because the saving in winding space permits a considerable reduction in size (See Figure 14), reduces winding capacitances, and decreases leakage inductance values. The maximum plate inductance is limited by transformer and circuit capacitances and by the retrace time. Voltage-doubling circuits require only a small step-up coil to generate the required high voltage. Their small effective capacitance permits both a wider choice of transformation ratios and a higher operating efficiency than possible with single-stage high-voltage rectifier circuits.

Returning to the turns ratio n_3/n_1 between the deflection-coil circuit and V_1 suppose that V_1 is operated with a plate current value near 80 milliamperes and the ratio $n_1/n_3 = 2.1$. The peak and average plate currents and voltages \hat{i}_p , I_{b_1} , E_{n_1} and \hat{e}_{p_1} are readily computed by reflecting the yoke circuit values into the plate winding as listed in Table III. It is obvious that selection of a ratio n_3/n_1 giving lower plate currents will cause higher plate voltages. It also must be considered that high ratios increase leakage inductance as well as the surge voltage and that it may, therefore, be desirable to increase the ratio n_3/n_1 later on by adjustment of L_Y to the subsequently computed value n_2/n_1 .

The transformer ratio n_2/n_1 between V_2 and V_1 is determined by the reactive power input and the power loss of the system

$$n_2/n_1 = 1 - (P_r + P_x)/E_{n_1}I_{b_1}. \quad (23)$$

The reactive plate power ($E_{n_1}I_{b_1}$) and the retrace power loss (P_r) for a beam current of 120 microamperes have been determined and require the values of the bleeder current I_{BB} and external power load $P_x = E_{n_2}I_{BB}$ taken from the "boosted" voltage E_{BB} . The voltage E_{n_2} in the expression for P_x must be estimated at first for a trial value P_x . The true values P_x , E_{n_2} and n_2/n_1 are found by successive approximation. A bleeder current of 17 milliamperes will be drawn to operate the vertical deflection circuit from E_{BB} , thus, for the 120-microampere beam-current load,

$$n_2/n_1 = 0.69; E_{n_2} = (n_2/n_1)E_{n_1} = 210 \text{ volts}, P_x = 3.6 \text{ watts}.$$

A diode booster tube V_2 with linearity transformer (Figure 7) supplies, therefore, a "boost voltage" $E_{Cb} = E_{n_2} = 210$ volts. Other voltages and currents in the V_2 circuit are readily computed from the yoke circuit values as listed in Table III.

The high-voltage stepup n_4/n_3 required for obtaining an E_a of 14 kilovolts with the circuit of Figure 12 is theoretically $n_4/n_3 = E_a/(2\hat{e}_y + E_y)$. Table III furnishes the value $n_4/n_3 = 3.6$. A tap may be provided on the high-voltage winding at a ratio 10 per cent lower, because a correction for parasitic resonance effects may be necessary. A rectifier circuit with a single diode theoretically requires a step-up ratio $n_4/n_3 = 7.45$. Resonance effects in the high-voltage winding, however, can be effective in generating a higher voltage with a lower step-up ratio depending on the phase relation of the pulse voltage components. (Compare Figure 9). The power absorption increases the retrace power loss P_r , requiring, therefore, an increase of the ratio n_2/n_1 (Equation (23)).

r-m-s Currents, Transformer Windings, and Capacitances

The copper cross section of transformer and yoke windings should not be less than 500 circular mils per ampere of r-m-s current. The r-m-s value depends on waveshape (See Table II) and amplitude of the current. The current in the windings of the auto-transformer can be approximated closely by selecting waveforms representing normal efficient operating conditions.

The deflection coil current $|I|_y$ is a linear sawtooth current without direct-current component and is given accurately by:

$$|I|_y = 0.29 (\hat{i}_1 + \hat{i}_2). \quad (36)$$

The r-m-s plate current $|I|_{b_1}$ contains a matching current component. A practical plate current i_{p_1} has the shape of an inverted sine wave section (See Table II) which may have a slightly flattened peak (due to grid current). The r-m-s value is approximated with good accuracy by

$$|I|_{b_1} = 1.6 I_{b_1}. \quad (37)$$

This current value determines the wire size of the transformer winding $n_1 - n_2$ and part of the plate loss in V_1 (see later).

The r-m-s plate current $|I|_{b_2}$ can be computed from the diode peak current

$$\hat{i}_{p_2} = \left(\frac{n_3}{n_2} \right) s \hat{i}_2$$

and the relation $|I|_{b_2} = 0.41 \hat{i}_{p_2}$ (38)

which assumes a normal waveshape matching the selected plate current waveform.

The currents in the auto-transformer windings ($n_2 - n_3$) and n_3 consist of a number of components which have substantially ideal triangular class B waveshapes.

The current in $n_2 - n_3$ is the sum of the reflected current $(n_3/n_2) s i_2$, the component $(n_3/n_2) s i_1$ reduced by the ratio n_2/n_1 , and the small direct-current I_{BB} which can be neglected. Because of the triangular class B waveshape the r-m-s current is closely

$$|I|_{n_2 - n_3} \approx 0.41 \left(\frac{n_3}{n_2} \right) \left[\left(s \hat{i}_1 \frac{n_2}{n_1} \right)^2 + (s \hat{i}_2)^2 \right]^{1/2}. \quad (39)$$

The current in n_3 consists of the deflection-coil currents $i_1 + i_2$ minus the components $s i_1 (n_3/n_1)$ from V_1 and $s i_2 (n_3/n_2)$ from V_2 , and may be approximated by

$$|I|_{n_3} \approx 0.41 \left[\left(\hat{i}_1 - \frac{n_3}{n_1} s \hat{i}_1 \right)^2 + \left(\hat{i}_2 - \frac{n_3}{n_2} s \hat{i}_2 \right)^2 \right]^{1/2}. \quad (40)$$

The current values computed for the example (listed in Table III) determine the wire sizes and permit calculation of coil dimensions, winding resistances, and the copper loss (See Table IV).

It is beyond the scope of this paper to describe the design of the windings in detail. The number of turns per layer and the insulation thickness between layers and wires are varied to obtain a most favorable balance between leakage inductance and the winding capacitances which can be computed with good accuracy as the series value of layer capacitances. The computed winding capacitances of the transformer furnish the capacitance network shown for the example in Figure 15. Reflected into the yoke winding, the capacitances add up to a total of 434 micromicrofarads making $f_o = 81.5$ kilocycles. The desired retrace frequency $f_o = 70$ kilocycles requires, therefore, a padding capacitance $C = 116$ micromicrofarads across the yoke terminals. (A faster retrace increases the surge voltages.)

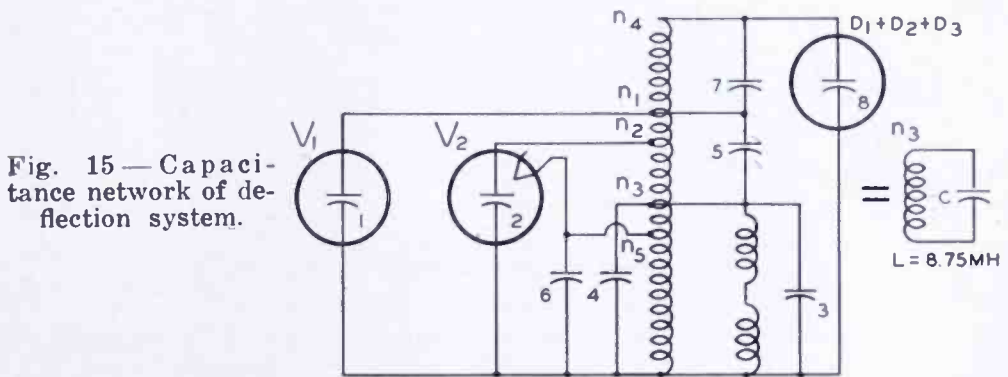


Fig. 15 — Capacitance network of deflection system.

C	micro-microfarads)	Description	C_{n_3} (micro-microfarads)
1	10	Plate V_1 and connection	44
2	15	Cathode V_2 and connection	32
3	80	Yoke and wiring	80
4	38	Winding n_3	38
5	40	Winding $n_2 - n_3$	48
6	260	Filament Winding (V_2)	60
7	8	Winding $n_4 - n_1$	54
8	6	High-voltage rectifier circuit	78
Total Capacitance $C = 434$			
$f_o = 81.5$ kilocycles			

Plate-Load Diagram, Power Loss Distribution, and Power Input

The effective load impedance in the plate circuit of the power tube (V_1) consists of a reactive load representing the power loss $I_{b_1} (E_{n_1} - E_{Cb}) = (P_r + P_x)$ and a resistive load R_p representing the diode plate loss and the copper losses of the circuit. (Compare Figure 8.) The equivalent plate-load diagram of V_1 is shown in Figure 16.

The power values for the reactive "square-wave voltage" section of the plate load have been computed except for P_s . Reactive loads of this

type do not contribute to the plate dissipation in V_1 and can, therefore, be assigned a direct-current to alternating-current conversion efficiency of 100 per cent. The net power which must be supplied by the B-supply for this load section is the sum of the retrace power loss P_r (containing the high-voltage power output), the direct-current power output P_x from the "boost" voltage, and the leakage- or series-inductance power loss P_s . The leakage inductance in the V_1 plate lead of the transformer is measured by shorting the yoke winding n_3 and measuring the inductance of the n_1 -winding. The transformer constructed according to our example has an inductance (L_s) of 2 millihenries. The inductive voltage drop developed by the plate current i_{p1} increases during T_s to the value

$$E_{L_s} = E_{n_1} L_s / L (n_1 / n_3)^2. \tag{41}$$

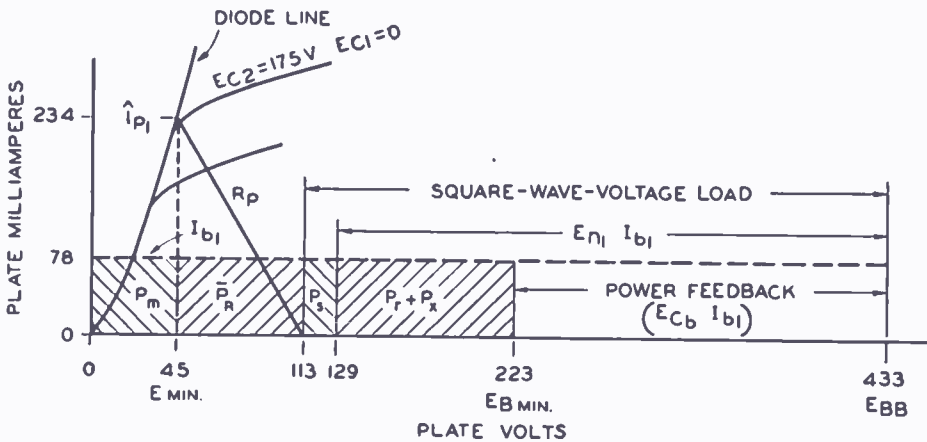


Fig. 16—Plate-load diagram of deflection power tube (V_1).

For the example, $E_{L_s} = 16$ volts and requires the B-power

$$P_s = E_{L_s} I_{b1}. \tag{42}$$

This power, $P_s = 1.25$ watts, is dissipated partly in the transformer and partly in the plate resistance of V_1 . The purely reactive power on L_s dissipated in the transformer equals

$$P_{sr} = 0.5 L_s \hat{i}_{p1}^2 f_h = 0.87 \text{ watt}, \tag{42a}$$

the remaining power (0.38 watt) is dissipated in V_1 during T_s .

The direct-current power input to the resistive load section (R_p) is obviously

$$\bar{P}_R = I_{b1} E_{R_p}.$$

The alternating-current power dissipated in R_p is given by

$$P_{Rp} = |I|_{b_1}^2 R_p = |I|_{b_1}^2 E_{Rp} / \hat{i}_{p_1}.$$

The conversion efficiency is, hence,

$$P_{Rp} / \bar{P}_R = |I|_{b_1}^2 / \hat{i}_p I_{b_1}. \quad (43a)$$

The conversion efficiency is controlled by the plate-current waveform which relates peak, r-m-s, and average values. Letting $|I|_{b_1} / \hat{i}_{p_1} = K_1$ and $I_{b_1} / \hat{i}_{p_1} = K_2$, Equation (43a) can be rewritten in the form

$$P_{Rp} / \bar{P}_R = K_1^2 / K_2. \quad (43b)$$

It is readily shown (See Table II) that the conversion efficiency varies from 0.625 for an inverted sine-wave current to 0.667 for a linear sawtooth current both of which may be continuous or intermittent. The value $P_{Rp} / \bar{P}_R = 0.645$ is a close approximation to all practical waveforms, and furnishes the value of direct-current input power to the R_p section:

$$\bar{P}_R = 1.55 P_{Rp}. \quad (44)$$

The power difference $\Delta P = 0.55 P_{Rp}$ is lost in the form of plate dissipation in V_1 in addition to the minimum plate power loss $P_m = E_{\min} \cdot I_{b_1}$ which is determined by the "diode line" or "knee" of the plate characteristic. *The power-tube plate dissipation* is, hence, with Equation (42),

$$P_{p_1} = E_{\min} I_{b_1} + 0.55 P_{Rp} + (P_s - P_{sr}). \quad (45)$$

The power loss P_{Rp} is the sum of all copper losses in the circuit including the diode (V_2) plate dissipation. The copper loss $P_{cu} = (|I|^2 \times r)$ in the transformer windings and the deflection coil is readily computed and totals 1.41 watts (The power losses are itemized in Table IV). The diode plate loss can be computed from the r-m-s diode current (Equation (38)) and the equivalent diode resistance

$$|r|_d = 1.06 \hat{e}_p / \hat{i}_p. \quad (46)$$

With Equation (38) *the diode plate loss* is expressed by

$$P_{p_2} = 0.18 \hat{i}_{p_2} \hat{e}_{p_2}. \quad (47)$$

for the example $\hat{i}_{p_2} = 0.3$ ampere. A 6W4-GT diode has a peak plate-voltage drop \hat{e}_{p_2} of 24 volts at this current. The diode plate dissipation P_{p_2} is, hence, 1.3 watts. To these losses must be added the copper loss in the linearity transformer T_2 , which will be estimated as 25 per cent of the power ($P_{p_2} + P_{cu}$) handled by T_2 ; i.e., 0.70 watt. The total copper and diode loss is equal to P_{Rp} and equals 3.41 watts.

The total power input to the deflection system is the sum of all losses:

$$P_B = E_{\min} I_{b_1} + 1.55 P_{Rp} + P_s + (P_r + P_a). \quad (48)$$

The power tube 6AU5-GT has a plate voltage drop $E_{\min} = 45$ volts at $\hat{i}_{p_1} = 0.234$ ampere. The minimum plate-power input P_B is, hence, 17.35 watts, and requires a minimum B-supply voltage

$$E_{B\min} = P_B / I_{b_1} = 223 \text{ volts.}$$

The power-tube plate dissipation P_{p_1} (Equation (45)) is 5.4 watts. The power losses in the remaining circuit elements are listed in Table IV. The plate load diagram, Figure 16, indicates clearly the power distribution and voltages in the deflection circuit during the scanning period T_s .

Discussion of Results

The lower section of Table IV shows that the power losses of the circuit components are well balanced. The largest loss (5.78 watts) occurs in the power tube V_1 ; but V_1 controls a total plate-power input of $0.078 \times 433 = 33.8$ watts, operating, therefore, with an efficiency of 83 per cent. Equation (45) shows that the plate dissipation of V_1 is increased by the copper losses, the V_2 plate loss and the leakage inductance loss. These losses should, therefore, be made as small as possible. (The values in the example are probably lower than in present deflection systems.)

The second largest item in Table IV is the power output of the system ($P.O. = 5.2$ watts) which is used for kinescope light output and to operate the vertical deflection tube from the augmented voltage $E_{BB} = 433$ volts. In view of the fact that the conversion efficiency with respect to the resistive load section in the power-tube characteristic is 100 per cent for these loads, this method of obtaining a higher B-voltage for vertical deflection is very efficient and particularly so for a system operating with a low B-voltage on the order of 250 volts. A further advantage of supplying the vertical deflection power from E_{BB} is the fact that the aspect ratio of the raster changes little with

high-voltage power output because E_{BB} decreases when the kinescope voltage drops due to regulation of the pulse rectifier system. The transformer operates with a power input of 30.3 watts, its power loss is 1.45 watts, and its efficiency has, therefore, the excellent value of 96 per cent. Similarly, we find the yoke efficiency to be 86 per cent and the efficiency of the diode 93.5 per cent.

A deflection system with voltage-doubling circuit was built according to the specifications in the example. The currents and voltages measured were within the accuracy of meter errors. The variation from the computed r-m-s values did not exceed 10 per cent in portions of the circuit where insertion of a meter caused small changes in the capacitance and resistance values.

For the minimum B-voltage $E_B = 223$ volts (See Figure 16) the screen-grid voltage of the 6AU5-GT was 178 volts and the screen current 8 milliamperes. At a B-voltage of 250 volts, the screen current dropped to 6 milliamperes. The measured high-voltage regulation is 10 per cent at a beam current of 130 microamperes.

The power load diagram, Figure 16, gives graphically the effect of circuit changes. If, for example, the coupling diode in the high-voltage rectifier were replaced by a 2-megohm resistor, the resistor would be reflected as a 154,000-ohm shunt across the winding n_3 and cause a power loss $|E|_v^2/154,000 \approx 1.5$ watts. When the diode filament power (0.25 watts) is removed, the power loss, P_r , is increased by 1.25 watts which requires an increase of E_B to 240 volts. Similarly, if the load $P_x = 3.5$ watts of the vertical deflection circuit is removed, the required B-voltage E_B would decrease to 170 volts. Removing the high-voltage rectifier system also would drop E_B to 146 volts. It is, of course, necessary to readjust the transformer ratio n_1/n_2 in each of these cases to comply with Equation (23).

Replacement of the voltage-doubling rectifier circuit by a single-diode high-voltage rectifier requires a re-evaluation of the circuit constants. Because of the larger step-up and capacitance of the high-voltage winding, it is necessary to decrease the transformer inductance, and increase the flux density in the transformer.

A system for deflecting a 70-degree kinescope and generating the voltage $E_a = 14$ kilovolts with a single high-voltage rectifier was computed and built for comparison with the voltage-doubling system. The plate-power input increased from 17.35 watts to 19.0 watts because, for the same value I_{b1} , the B-voltage had to be increased to $E_B = 250$ volts. The plate dissipation in the power tube and the plate loss of V_2 remained approximately the same but the transformer loss

increased from 1.45 to 3.0 watts (increased core loss and leakage resonance loss in the high-voltage winding).

Both systems were free of "ripples" in the deflection raster as well as negative "overshoots" in the plate voltage of V_1 .

CONCLUSIONS

The analysis of energy and power in reactive deflection systems with associated high-voltage supply has led to a relatively simple method of designing and examining practical deflection systems. The distribution of the power loss in tubes and circuit elements can be accurately determined from data on available materials for any chosen type of circuit. The plate load diagram of the power tube is readily established by measurement of a few circuit constants and current values. Its use can contribute much to the design of efficient deflection systems having trouble-free operation of electron tubes. It is shown that modern magnetic materials permit the design of efficient deflection coils and transformers with negligible power loss which make it possible to control large deflection energies with inexpensive electron tubes.

APPENDIX

Table I—Decay Functions and Q-Factors.

Q	$e^{-1.65/Q}$	$e^{-3.8/Q}$	q	q^2
50	0.968	0.936	1.0162	1.0326
40	0.960	0.921	1.0204	1.0412
30	0.946	0.895	1.0277	1.0561
25	0.936	0.876	1.0330	1.0670
20	0.921	0.848	1.0411	1.0838
15	0.896	0.802	1.0548	1.1126
12.5	0.876	0.768	1.0660	1.1363
10	0.848	0.718	1.0822	1.1711
9	0.832	0.693	1.0917	1.1918
8	0.813	0.662	1.1031	1.2168
7	0.790	0.624	1.1173	1.2483
6	0.760	0.577	1.1363	1.2911
5	0.718	0.516	1.1641	1.3551

Table II—Average and r-m-s Values of Deflection-Circuit Waveforms.

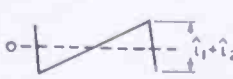

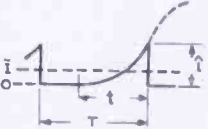
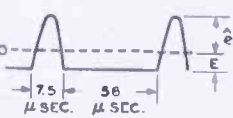
#	Wave Form	Average Value	r-m-s Value	
1		$\bar{i} = 0$	$ I = 0.29 (\hat{i}_1 + \hat{i}_2)$	sawtooth (alternating current only)
2		$\bar{i}/\hat{i} = 0.5 t/T$	$ I /\hat{i} = 0.577 \sqrt{t/T}$	intermittent sawtooth (alternating current + direct current)
3		$\bar{i}/\hat{i} = 0.363 t/T$	$ I /\hat{i} = 0.476 \sqrt{t/T}$	intermittent 90-degree sine wave section (alternating current + direct current)
4		$\bar{e}/E = 12.7$	$\hat{e}/ E = 3.94$	inductive voltage normal time ratios

Table III—Circuit Constants and Operating Conditions of a Deflection System (example).

	Symbol	Value No Load	Value at $I_a = 120$ microamperes
Circuit at 70 kilocycles	Q_0	26.	
Parallel value	L	0.00875 henries	
Shunt field factor	s	1.143	
Deflection power $Q = \infty$	P_0	13.5 watts	(Loss free circuit)
Reactive power Input	$P_{1(L)}$	16.5 watts	16.5 watts
Reactive power Output	$P_{2(L)}$	14.4 watts	12.8 watts
Retrace loss	P_r	2.1 watts	3.7 watts
High-voltage power output	P_{HV}	0	1.6 watts
Inductive voltage	$E_v = E_L$	148 volts	144 volts
Yoke peak voltage	$\hat{e}_L = \hat{e}_v$	1880 volts	Values for deflection coil circuit
Yoke r-m-s voltage	$ E _v = E _L$	476 volts	
Yoke peak current	\hat{i}_1	0.430 ampere	0.430 ampere
Yoke peak current	\hat{i}_2	0.400 ampere	0.380 ampere

Table III—(continued)

	Symbol	Value No Load	Value at $I_a = 120$ microamperes	
Peak current in L	$s\hat{i}_1$	0.491 ampere	0.491 ampere	
Peak current in L	$s\hat{i}_2$	0.458 ampere	0.435 ampere	
Equivalent average current	$I_{b'}$	0.164 ampere	0.164 ampere	
Peak-to-peak yoke current	$\hat{i}_1 + \hat{i}_2$	0.830 ampere	0.810 ampere	
Peak-to-peak current in L	$s(\hat{i}_1 + \hat{i}_2)$	0.949 ampere	0.926 ampere	
Peak plate voltage	\hat{e}_{p_1}	3950 volts + E_{BB}		Values for V_1
Peak plate current	\hat{i}_{p_1}	0.234 ampere		
Average plate current	I_{b_1}	0.078 ampere		
Yoke/ V_1	n_3/n_1	0.475		Transformer turns ratio
V_2/V_1	n_2/n_1	0.69		
Yoke/ V_2	n_3/n_2	0.687		
Inductive voltage	E_{n_1}	311 volts	303 volts	Transformer inductive voltages
Boost voltage	$E_{n_2} = E_{cb}$	214 volts	210 volts	
Reactive input power	$I_{b_1}E_{n_1}$	24.2 watts	23.6 watts	Power values (for $I_{BB} = .017$ ampere and $L_S = 0$)
Direct-current output power	P_s		3.6 watts	
Reactive power loss	$P_r + P_s$		7.3 watts	
Feedback power			16.3 watts	
Peak V_2 current	\hat{i}_{p_2}		0.30 ampere	V_2
Peak V_2 voltage	\hat{e}_{p_2}		—2720 volts	
V_1 current	$ I _{b_1} = I _{n_1-n_3}$		0.125 ampere	r-m-s cur- rent values
Transformer current	$ I _{n_2-n_3}$		0.155 ampere	
Transformer current	$ I _{n_3}$		0.052 ampere	
Yoke current	$ I _y$		0.235 ampere	
V_2 current	$ I _{b_2}$		0.123 ampere	

Table IV—Power-Loss Distribution in a Deflection System (example).

Description	Symbol		Power (Watts)	
Resistances and copper losses	r_y	19 ohms	1.050	Yoke
	$r_{n_1-n_2}$	10 ohms	0.155	Transformer
	$r_{n_2-n_3}$	6.5 ohms	0.156	Transformer
	r_{n_3}	17 ohms	0.046	Transformer
Total copper loss	P_{cu}		1.407	(During T_s)
V_2 plate loss	P_{p_2}		1.30	
Loss in linearity transformer	T_2		0.70	
Loss in R_p	P_{Rp}		3.41	Resistive losses during T_s
Loss in R_p load section	P_R		5.30	(P_{Rp} + conversion loss)
Minimum plate loss in V_1	P_m		3.50	($E_{min} I_{b_1}$)
Leakage reactance in V_1 plate circuit	P_s	($E_{L_s} = 16$ volts)	1.25	($E_{L_s} I_{b_1}$)
Reactive power loss	($P_r + P_s$)		7.30	(Loss during T_r and power output)
Total power input	P_B		17.35	
V_1 Plate loss	P_{p_1}		5.78	Equation (44)
V_2 Plate loss	P_{p_2}		1.3	During T_s
Total transformer loss	P_{T_1}		1.45	During T_s and T_r including P_r
Linearity transformer	P_{T_2}		0.70	
Total yoke loss	P_y	1.05 + 1.02	2.07	During T_s and T_r
Power output	$P.O.$	1.6 + 3.6	5.2	$P_{HV} + P_s$
Rectifier filaments	P_f		0.75	
Total	P_B		17.35	

ADJUSTMENTS FOR OBTAINING OPTIMUM PERFORMANCE IN MAGNETIC RECORDING*

BY

ALBERT W. FRIEND

Research Department, RCA Laboratories Division,
Princeton, N.J.

Summary—Theory indicates that in a perfectly adjusted magnetic recording and reproducing system the record medium should produce no even harmonics of a single sine wave magnetizing signal which is applied to the medium, if the recording medium is initially in a completely neutral magnetic condition. Quite simple and inexpensive means are described for control and adjustment of a magnetic recording system to approach this ideal performance. It is recognized that additional limits of performance are imposed by the quality and adjustment of the audio frequency amplifiers and the other components of the system.

Numerous curves are provided to indicate the optimum operating conditions of a particular recording system, using "Scotch" brand, No. 111, magnetic record tape (red iron oxide on a cellulose acetate base) as manufactured by the Minnesota Mining and Manufacturing Company. The erasing, recording and reproducing heads are of a precisely designed and adjusted type (P-4) developed and constructed by the RCA Laboratories Division. It is found that particularly excellent performance may be attained by this system when all of the indicated adjustments have been made and when the operating conditions are within the prescribed limits.

INTRODUCTION

EARLY magnetic record systems were made to function with an essentially linear relationship between the recorded and the reproduced signals, by the application of a fixed or direct-current magnetic "bias" to the medium, either before or during the recording process.¹ This direct-current bias caused the applied signal to act along the residual magnetization characteristic of the medium in a region of the characteristic which was essentially free from the large nonlinear effects which are observed near the point of zero residual magnetization.

The reason for this method of recording is revealed more clearly by reference to Figures 1 and 2. Figure 1 is a plot of the residual magnetic flux density, B_r , versus the magnetizing excitation, H , for a typical recording medium, as drawn by Camras.¹ Figure 2, from the

* Decimal Classification: R 365.35.

¹Marvin Camras, "Graphical Analysis of Linear Magnetic Recording Using High-Frequency Excitation," *Proc. I.R.E.*, Vol. 37, No. 5, pp. 569-573, May, 1949.

same source,¹ and as shown elsewhere in the literature,^{2,3} illustrates the distortion which is produced when a recording is made upon an unmagnetized medium with no bias applied. If a fixed or direct-current magnetic polarization is applied to move the working point from the origin to point *P* of Figure 1, the resultant output wave is distorted much less, as is indicated in Figure 3. It is noteworthy, however, that the amplitude must be restricted quite severely to minimize distortion, when operating with the "direct-current bias" or "offset zero" recording method.

There are *at least* two important disadvantages of this direct-current bias operational arrangement in comparison with more modern procedures. First, the useful operating range is restricted to only a single sign of magnetic polarity; and, second, the linearity of the transfer characteristic is not as perfect as one may desire to attain.

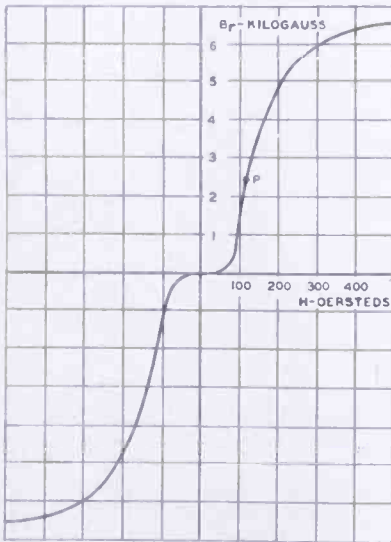


Fig. 1—Retained flux density versus applied field for a typical magnetic recording medium.

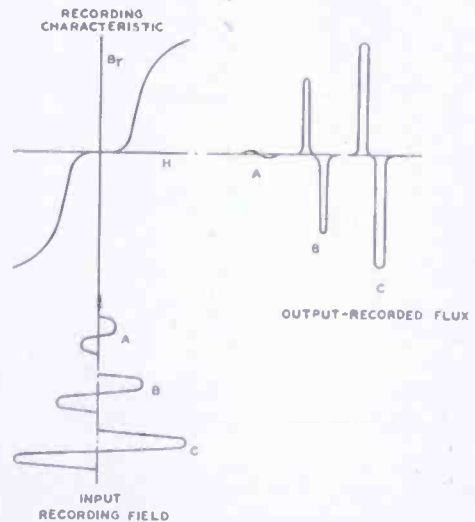


Fig. 2—Distortion caused by attempt to record directly on a demagnetized record medium.

In 1921, W. L. Carlson and G. W. Carpenter,⁴ then of the General Electric Company, disclosed a very ingenious method for avoiding these difficulties. This new system utilized a high frequency "bias" signal, which was added to the desired signal during recording. The method was applied before and during the last war in several laboratories in

²S. J. Begun, "Magnetic Recording," *Scientific Monthly*, Vol. 69, No. 3, pp. 192-197, September 1949.

³S. J. Begun, *MAGNETIC RECORDING*, Murray Hill Books, Inc., New York, N. Y., 1949.

⁴W. L. Carlson and G. W. Carpenter, U.S. Patent No. 1,640,881, Application filed March 26, 1921, patent issued Aug. 30, 1927.

this country^{3,5,6,7} and abroad,⁸ and it has since been used by most other participants in this field of sound recording.

If the high frequency bias is of symmetrical wave form, and if other signals are absent, it is simply recorded upon the medium, in the manner indicated in Figure 2. The frequency of this bias signal is usually arranged to be quite high (5 to 10 times) with respect to the frequencies of the desired signals, so its recorded wavelength upon the medium is exceedingly short. This causes the internal demagnetizing effect in the medium to be very pronounced, so that the net recorded bias signal is almost negligible. An average residual magnetization is practically all that remains of the recorded bias signal.

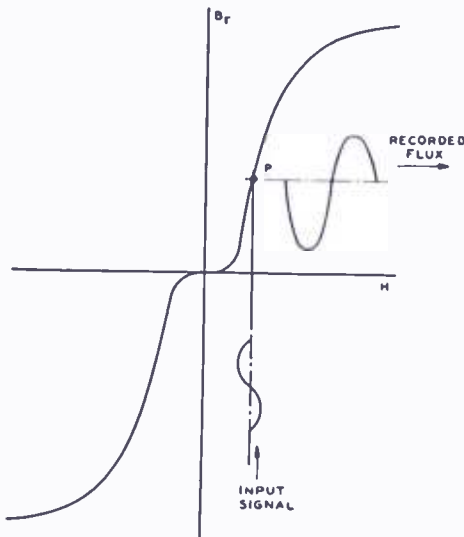


Fig. 3—Recording with direct-current bias or offset zero.

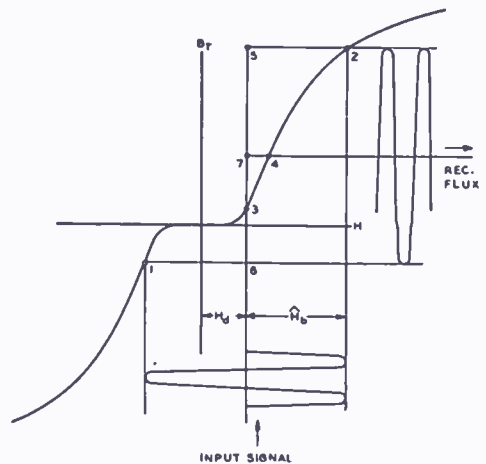


Fig. 4—Average retained flux for a displaced high-frequency signal.

Therefore, if a bias signal which has a symmetrical wave-form is applied to the recording medium, this medium returns essentially to its original demagnetized condition.

If a symmetrical bias signal is applied with its zero axis displaced from the origin, as indicated in Figure 4, it is apparent that the residual magnetization B_{r1} becomes greater than the opposite residual magnetization B_{r2} , so that their mean value $B_{rm} = (B_{r1} + B_{r2})/2$ is no longer zero. This effect may be produced in a number of ways. During the recording process, the applied signals of lower frequency produce an analogous effect by the displacing action of their instantaneous

⁵D. E. Wooldridge, U.S. Patent No. 2,235,132 (1940).

⁶D. E. Wooldridge, "Signal and Noise Levels in Magnetic Tape Recording," *Elec. Eng.*, Vol. 65, No. 6, pp. 343-352, June, 1946.

⁷Marvin Camras, U.S. Patent No. 2,351,004.

⁸Publication No. 60899, Office of Technical Services, Department of Commerce, Washington, D.C.

values of amplitude. This is the method of operation which is employed in the high frequency bias recording process, as first described by Carlson and Carpenter,⁴ and later by Wooldridge,^{5,6} and as outlined by Camras,^{1,7} whose simple form of graphical analysis is followed here in Figures 5, 6 and 7.

The dashed curve (B_r) of Figure 5 is replotted from Figure 1. When the bias signal of peak recording amplitude \hat{H}_b is applied symmetrically about the dashed curve of residual magnetization, as indicated, their peaks trace out curves of the residual magnetization (B_{r1} and B_{r2}), which is left in the medium by each positive or negative alternation of any symmetrical bias excitation wave which acts about the various points along the original residual magnetization (B_r) curve. The mean values of residual magnetization, which correspond to the various points upon the B_{r1} and B_{r2} curves, yield new values of

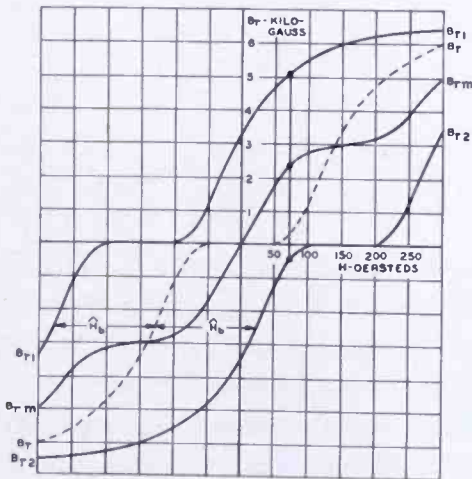


Fig. 5—Graphical construction of recording characteristic B_{rm} .

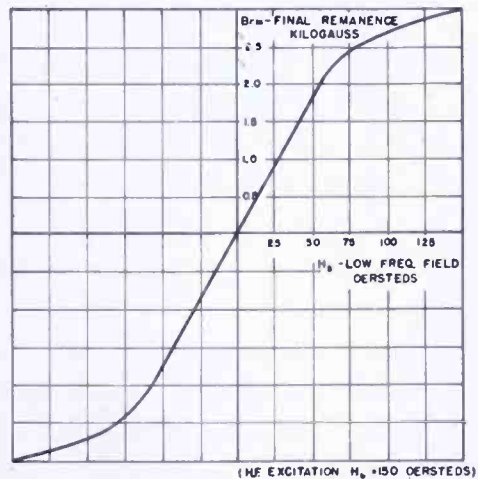


Fig. 6—Linear recording characteristic obtained by the addition of high-frequency excitation.

mean residual magnetization (B_{rm}), which are plotted to yield the corresponding curve of B_{rm} of Figure 5. This is the magnetic recording characteristic of the medium. It is replotted alone, for clarity, in Figure 6.

It is evident, from the construction of the B_{rm} curve of Figures 5 and 6, that the bias wave (and hence the mean residual magnetization) may be displaced from the zero axis by *any* lower frequency signal, including direct current. Likewise, it is evident that if the applied bias wave contains either any even harmonic or direct-current component, or both, so that its opposite peaks are not displaced equally about the axis of $H = 0$, a corresponding resultant value of residual magnetization will be recorded in the medium.

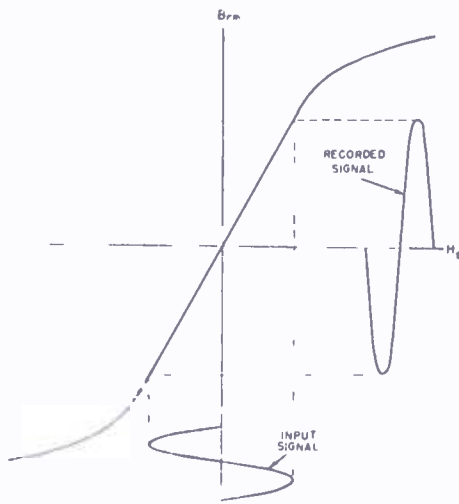


Fig. 7—Recording of sine wave signal by characteristic of Figure 6.

in accordance with the symmetrical nature of the recording transfer characteristic (Figure 6). The precise record which results when a sine wave signal (H_s) is recorded upon a medium which possesses the recording characteristic of Figure 6 is indicated by the graphical construction of Figure 7.

The object of the present investigation has been to develop means for minimizing the noise and the even harmonic distortion in the reproduced signal, and to determine experimentally the operational characteristics of a widely used magnetic record tape in combination with a set of precisely adjusted magnetic erasing, recording and reproducing heads in a magnetic recording and reproducing system which utilizes the developed modifications.

CIRCUIT MODIFICATIONS

A simple circuit arrangement which may be employed for the magnetic recording of signals is illustrated in Figure 8. If the magnetic core of the recording head (L_R) becomes slightly magnetized by exposure to external magnetic fields, by the switching of applied high-level recording or bias signals, or by any other means, the fixed residual magnetization will act upon the recording medium as a direct-current bias to displace, from its neutral position, the zero axis of the mag-

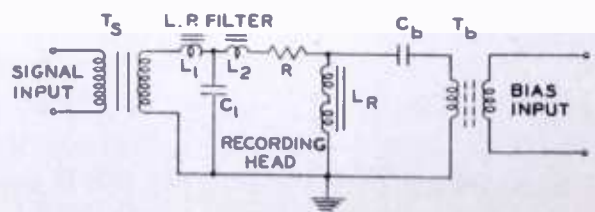


Fig. 8—A common type of magnetic recording circuit.

netization which is produced in the medium by the high frequency bias signal, as in Figure 4, so that a net direct-current magnetization signal is applied to the record. It is found that the recording of this useless direct-current magnetization signal produces an increase in the ambient noise of the record, just as an applied useful signal produces a modulation noise. It seems that the two effects are identical in every respect. In addition, the displacement of the zero axis of the alternating-current recording magnetization from the neutral magnetic axis of the medium, by the applied direct-current field, causes the recording characteristic to be asymmetric to the desired applied recording signal, so that *even*-harmonic components of that signal are recorded upon the tape. The even harmonic output increases essentially linearly with the amount of applied direct-current magnetic polarization (see Figure 14). A second effect which causes the same result is produced by the application of a "high-frequency" alternating-current bias signal (actually about 40 to 120 kilocycles) which has an asymmetric wave-shape, and which therefore contains *even* harmonics of its fundamental frequency. In this instance, the medium attains a direct-current polarization in accordance with the averaging process indicated in Figure 5, where

$$B_{rm} = (B_{r1} + B_{r2})/2, \quad (1)$$

simply from the asymmetry of the bias current wave, which produces different amplitudes of the oppositely polarized residual flux densities B_{r1} and B_{r2} of successive alternations of the bias magnetization wave.

It is apparent that pre-polarization of the recording medium by direct-current or by asymmetrical erasing signals, or by any other means, will likewise produce the same direct-current recording effects upon the completed record, and so cause an increase in the noise level, over that which occurs with no input signal, and in the factors which introduce even harmonics of any input signal into the record.

It seems clear that all these effects produce the same result, so it is equally clear that all of them may be annulled, in a single stroke, by the addition to the recording signal of a direct-current component whose magnitude and polarity may be adjusted and controlled at will. The very simple circuit modification from that of Figure 8 to Figure 9 is all that is required to produce the desired result. It is assumed that a small current (0 to 1.0 milliampere) may be obtained from a direct-current power source (1 to 6 volts) which is already available in the recorder, so this modification only requires the addition of a quite inexpensive center-tapped potentiometer, or its equivalent, as indicated in Figure 9 by R_n , the "harmonic-null" potentiometer. A possible

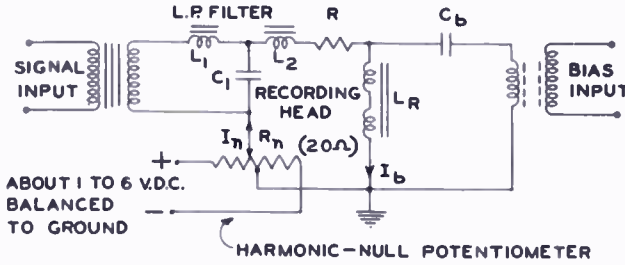


Fig. 9—Modified magnetic recording circuit.

variation of this arrangement, as shown in Figure 10, is adapted for use with a high resistance potentiometer which is connected to a source of higher voltage. In this case the direct-current power dissipation of the circuit is increased in comparison to the arrangement of Figure 9, but the performance is essentially identical. Various other minor modifications may be made to adapt the same arrangements for application to circuits wherein the high-frequency bias is inserted in series with the signal channel, instead of by the indicated shunt arrangement of Figures 9 and 10.

MEASUREMENTS AND OPERATIONAL TESTS

Details of the Test System

It was thought desirable to choose a well known standard commercial magnetic record medium for tests of the harmonic-null circuit of Figure 9. The No. 111 red iron oxide (Fe_3O_4) coated tape (.0005-inch coating thickness) with a cellulose acetate base (.002 inch thick), as manufactured by the Minnesota Mining and Manufacturing Company (3 M Co.) of Saint Paul, Minnesota, was chosen for these tests. A tape speed of 15.6 inches per second was used throughout the tests.

The heads were of a special, highly precise variety, type P-4 developed and constructed in these laboratories.

A standard recording frequency of 700 cycles was chosen as an important frequency which produced approximately the maximum distortion effect. The magnetic erasing and biasing processes were operated at a constant frequency of 100 kilocycles. This signal was derived from an oscillator (Model 200C), manufactured by the Hewlett-Packard

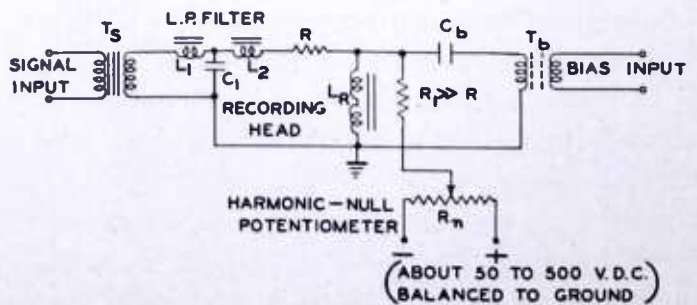


Fig. 10—Variation of modified magnetic recording circuit.

Company, of Palo Alto, California. This particular instrument produced second and third harmonic output signals of less than one per cent at the maximum output setting. When this source of bias and erase signal was used to drive a special power-amplifier system, with a push-pull output stage, to provide the erase and bias currents for a laboratory test system, the harmonic output levels were as indicated in Figure 11. It is apparent that the second harmonic output was excessive at all values of bias current greater than about 30 milliamperes, but systems with considerably greater harmonic distortion of the bias signal were tested during the course of these measurements.

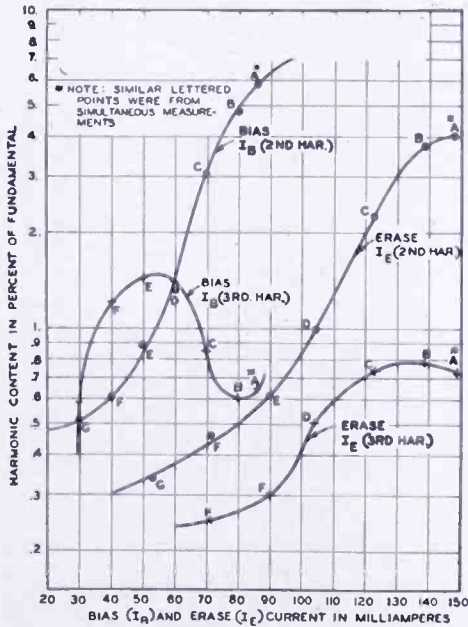


Fig. 11—Harmonic content of bias and erase currents. $f_1 = 100$ kilocycles from modified RCA Victor MI-4288-J amplifier driven by Hewlett-Packard Co., No. 200-C, oscillator (maximum gain setting).

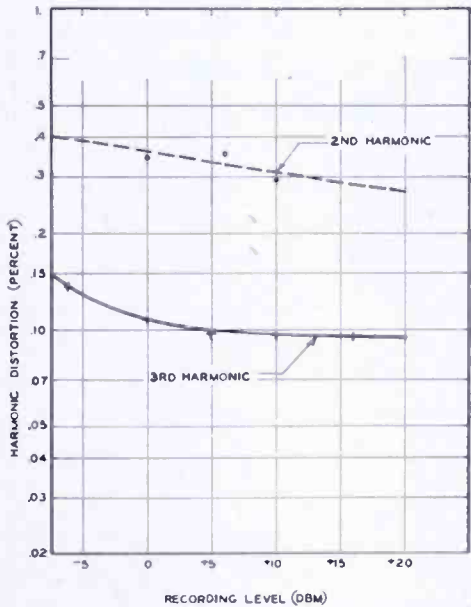


Fig. 12—Harmonic distortion of 700-cycle signal output of Hewlett-Packard, No. 205-AG signal generator (with output meter set at about 29 dbm).

The recording signal was derived from a standard signal generator (Model 205-AG), which was also manufactured by the Hewlett-Packard Company. The second and third harmonic contents of the output signal from this generator are plotted in Figure 12. When these signals were passed through an RCA Victor type BA-3C recording amplifier, the magnetic recording circuits and components, a BA-1A preamplifier and a BA-4C monitor amplifier, the resultant harmonic distortion was as indicated in Figure 13. The sharp null in the third harmonic was produced by a particular phasing-cancellation effect between the various third harmonic components of the signal generator and of the system apparatus. It is apparent that the harmonic distortion produced by the

signal generator and the apparatus was quite small, especially the third harmonic. A Hewlett-Packard, Model 300A, Harmonic Wave Analyzer was used for making all measurements of harmonic voltage amplitudes.

The schematic diagram of Figure 9 illustrates the recording arrangement used for these tests. A zero center (1-0-1 milliamperes) milliammeter was inserted at point I_n (Figure 9) to read the "harmonic-null" current, which is the direct-current component in the recording head circuit. A 1.00 ohm non-inductive resistor at the point

I_b was used for sampling the bias current, which was indicated by a Ballantine Electronic Voltmeter, Model 300.

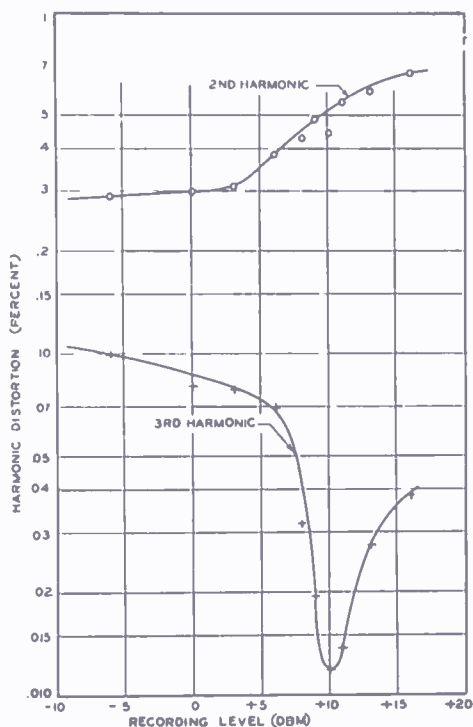


Fig. 13—Harmonic distortion of 700-cycle signal output of magnetic recording and reproducing equipment with Hewlett-Packard No. 205-AG signal generator input at 700 cycles.

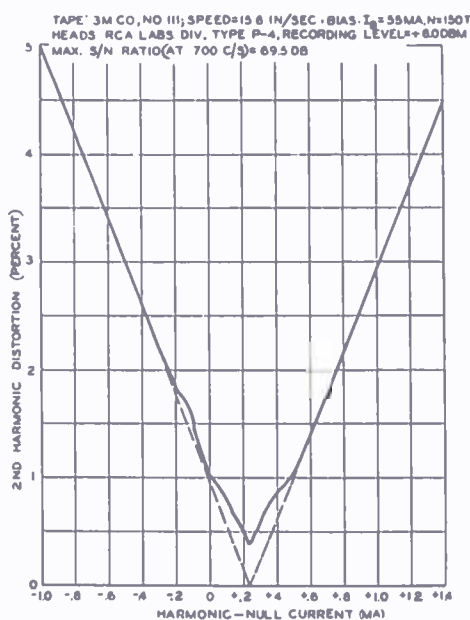


Fig. 14—Null effect of direct-current recording component upon the reproduced second harmonic output.

Measurements

It was soon found that an indicated bias current of 55 milliamperes was approximately the optimum value for use in the 150-turn recording head. When this value was used, with a recording level of +6.0 dbm,* the third harmonic output was about 1.83 per cent of the fundamental, when the system was corrected to yield uniform reproduction as a function of frequency.

Figure 14 illustrates the performance of the harmonic-null system

* Decibels referred to a zero level of 1 milliwatt in 600 ohms.

as a function of the direct-current component of the recording current. At the time of this test, the well balanced, unmodified system (zero direct current) produced slightly more than 1.0 per cent second harmonic output. Values up to at least 3.0 per cent are not unusual under these conditions, when no correction is applied. It will be noticed that extrapolation of the upper portions of the V-curve of second harmonic output toward zero distortion, along the dashed lines, leads to an intersection at essentially the zero value. The deviation from a complete null results from inclusion in the readings of the second harmonic components generated in the signal source and the apparatus. The addition of the several second harmonic components, in varying phase relationships, leads to the irregular solid-line curve, of actual measured values, which is plotted within the lower portion of the "V" curve. Comparison of Figure 14 with Figure 13 reveals that it is possible to reduce the second harmonic output of the reproduced signal to a value approximately the same as that produced by the apparatus alone (without the recording medium). In some instances, fortuitous phase relationships have made possible the attainment of even somewhat lower values, on account of partial cancellation of apparatus distortion by the remaining oppositely phased medium distortion. It seems clear, however, that a satisfactory minimization of second harmonic distortion is made easily attainable by this method. Other measurements indicated that, when the second harmonic null adjustment was made, the *very small* fourth harmonic component was also minimized, within the limitations of relative phase combinations.

It is possible to detect the second harmonic null value, in operational applications, by selecting a specific test frequency and adding a simple tuned filter to eliminate all but the second harmonic output from the input to a standard signal level meter (VU meter)⁹⁻¹², which should be a part of any broadcast transcription recording apparatus. A simple adjustment of the harmonic-null control to minimize the second harmonic output before each recording period, should produce entirely adequate second harmonic reduction. It will be shown that the third harmonic may be controlled by selection of the correct operating bias current and recording level.

⁹ F. E. Terman, RADIO ENGINEER'S HANDBOOK, p. 939, McGraw-Hill Book Co., Inc., New York, N. Y., 1943.

¹⁰ H. A. Affel, H. A. Chinn and R. M. Morris, "New Standard Volume Indicator and Reference Level," *Electronics*, Vol. 12, p. 28, February, 1939.

¹¹ H. A. Chinn, D. K. Gannett and R. M. Morris, "A New Standard Volume Indicator and Reference Level," *Proc. I.R.E.*, Vol. 28, p. 1, January, 1940.

¹² Leo L. Beranek, ACOUSTICAL MEASUREMENTS, pp. 504-506, John Wiley and Sons, Inc., New York, N. Y., 1949.

It is also found that if the above second harmonic indication device is either undesirable or economically unjustified in a particular application, one may simply adjust the harmonic-null control to minimize the noise produced by the medium. This may be done with greatest accuracy by observation of the noise level reading on a standard VU meter, but entirely satisfactory results may be achieved by simply listening to the noise output of a monitoring circuit and adjusting the harmonic-null control for minimum noise output. In cases where the hum level is nearly equal to, or greater than, the medium noise level, it is found that the aural adjustment may be somewhat superior to that attained by reading the noise indication on the VU meter, unless a high-pass hum elimination filter is available for insertion in the meter circuit.

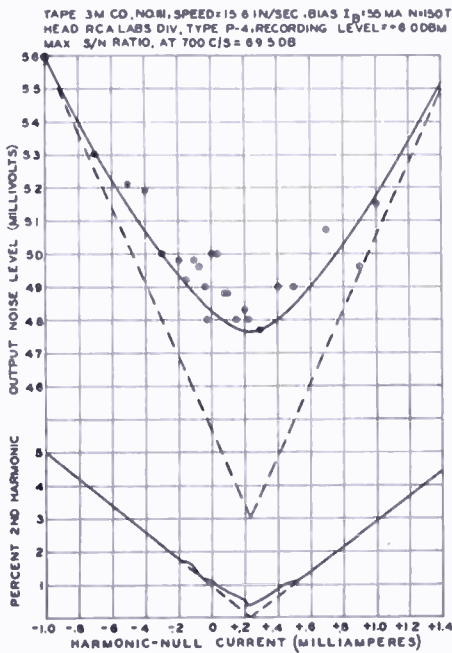


Fig. 15—Null effects of direct-current recording component upon the reproduced second harmonic and noise voltages.

The plot of Figure 15 illustrates the results attained by measurements of the noise output with a Ballantine voltmeter as the harmonic-null current was varied. Similar results are attained when the measurements are made with a VU meter. The linear voltage scale was desired for this plot, so that the dashed curve could be extrapolated by straight lines from the higher values of noise level. The null of this extrapolated curve coincides essentially with the broader null plotted from the actual measurement of minimum noise output, and likewise with the second harmonic null of the lower curve of Figure 15, which was replotted from Figure 14 for comparison. It is most fortunate and noteworthy that these two null currents are the same, as predicted from theoretical studies.

A series of measurements was made in order to indicate the magnitudes of the second, third, fourth and fifth harmonics of all useful levels of bias current and recording level. Within the desirable ranges of operating parameters, the amplitudes of the fourth and fifth harmonic voltages were always less than 0.20 per cent of that of the reproduced fundamental signal, so they were not plotted. Figures 16, 17, 18 and 19 indicate the percentages of the second harmonic (null

value), and the third harmonic voltages, and the required recording levels, as functions of bias current or bias ampere-turns, for conditions which yield constant output values of the 700-cycle fundamental signal of 100, 200, 300 and 400 microvolts across the type P-4 reproducing head. This head is wound with a total of 150 turns (hum bucking) to yield an inductance of 5.90 millihenries at 1000 cycles. The equivalent

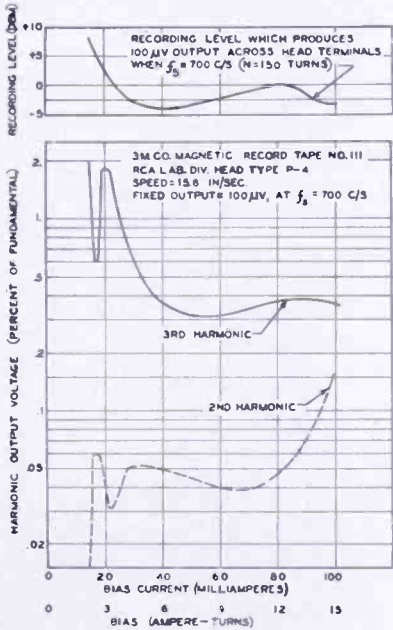


Fig. 16

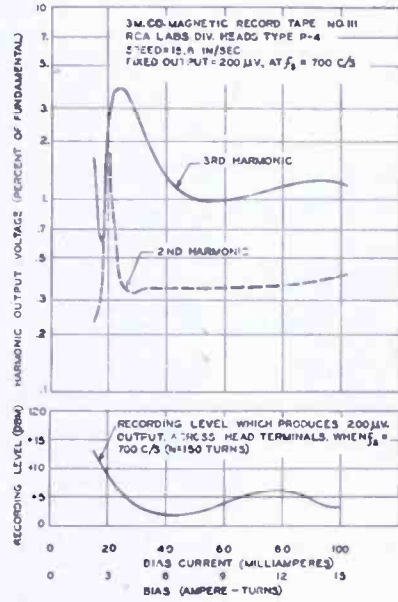


Fig. 17

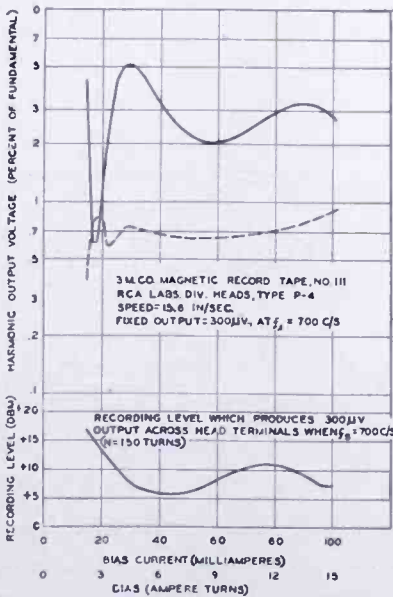


Fig. 18

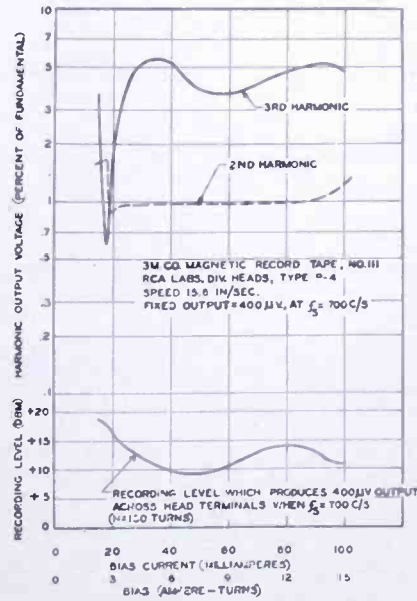


Fig. 19

Figs. 16-19—Harmonic distortion and recording levels with specified operating conditions.

gap spacing is .00035 inch, as measured from the lowest null-frequency of the reproduced signal at a very low tape speed.

Figure 18 shows that 2.0 per cent distortion is produced with 58 milliamperes bias current and a recording level of +7.5 dbm. This is a recording level 1.5 decibels greater than that required to produce the same output (300 microvolts) from the reproducing head at the value of bias (43 milliamperes) which produces maximum sensitivity at this output level.

These plots may be combined in different ways, as shown in Figures 20 and 21, to yield an improved concept of the operating conditions. In Figure 20, the family of constant output voltage curves, as function of recording level and bias excitation, show a definite locus of the *mini-*

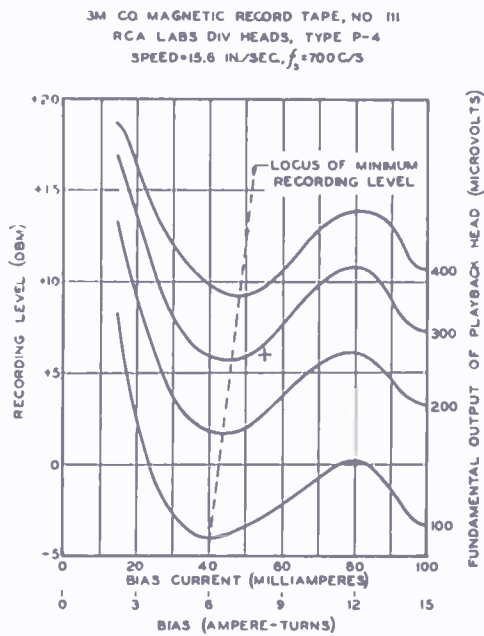


Fig. 20—Reproduced signal level as a function of recording level and bias current.

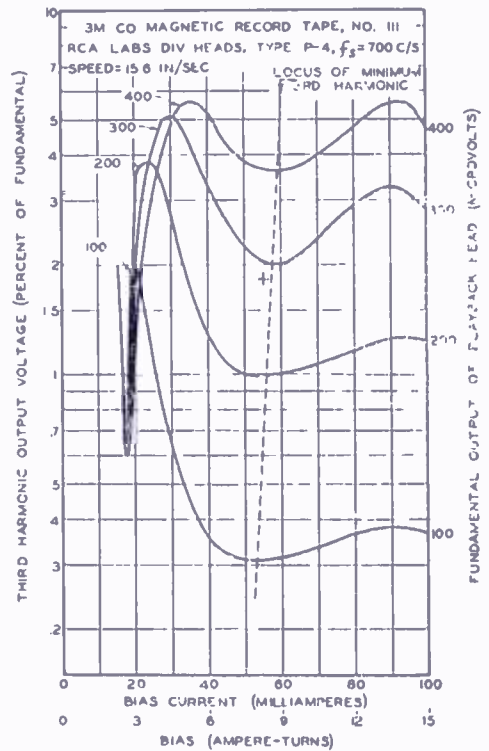


Fig. 21—Reproduced third harmonic distortion as a function of reproducing level and bias current.

imum required recording level, as indicated by the dashed line, in the range of bias currents between 40 and 50 milliamperes. In Figure 21, the family of constant output voltage curves, as functions of the equalized response third harmonic output and the bias excitation, indicate a definite locus of *minimum third harmonic* distortion. This is marked by the dashed line, in the range of bias current between 52 and 60 milliamperes. A comparison of the position of loci of optimum performance, in Figures 20 and 21, leads to the observation that they specify only slightly different values of current, and that the broad

regions of nearly optimum performance allow one to specify an excellent compromise value of bias current.

The limitation of the maximum third harmonic distortion is a matter of considerably greater importance than the limitation of the required recording level, so it is desirable to specify more nearly the optimum value of bias which will produce minimum distortion at the maximum allowable recording level, and which produces a relatively constant value of distortion as a function of small variations in the setting of the high-frequency bias current control. Reference to Figure 21 leads to specification of a bias current of 55 milliamperes, or 8.25 ampere-turns excitation, for optimum performance of the test system with RCA Laboratories Division type P-4 heads and Minnesota Mining and Manufacturing Company, No. 111 magnetic record tape. This leads to a practical minimum of distortion over most of the range of recording levels. At the same time, it leads to only slightly more than the minimum required recording level at the highest allowable output levels. The bias may be specified as a numerical value of current, or as that value of current which is sufficiently *greater than the value which produces maximum recording sensitivity* to cause a recording level of +6.0 dbm to produce 1.5 ± 0.5 decibels less than the maximum reproduced output signal.

This operating condition is indicated by the cross (+) on Figures 20 and 21. It is a sufficiently conservative value of limiting operating condition to allow for occasional excessive peak recording levels, which may not be anticipated, and to allow for the usual variations in the tape characteristics. At the same time, it does not penalize the operational characteristics by excessively cautious reduction of the recording level.

A plot of third harmonic distortion versus recording level, for the condition of second harmonic null adjustment, is given in Figure 22. One may set his own desired operating level of distortion by reference to this figure. Figure 23 shows the same data plus the corresponding values of output level, by a plot of relative fundamental output level versus the recording level (dbm). The third harmonic distortion scale is marked along the transfer characteristic for convenience in estimating the desired operating region.

An indication of a representative degree of improvement which may be attained when the harmonic-null adjustment is applied to a system which is already well designed and adjusted for best laboratory performance, is available by reconsideration of the data of Figures 14 and 15. With 55 milliamperes bias current the second harmonic content of the bias and erase signals was 1.07 and 0.36 per cent, respectively. Application of the second harmonic null system reduced the second

harmonic output from 1.05 to 0.38 per cent. The noise level (at the output of the monitor amplifier) was reduced from a fluctuating range of 48 to 50 millivolts to the more stable and lower range of 47.7 to 48.3 millivolts. *Equally low null values of second harmonic distortion and noise level have been attained with the same system, when the initial second harmonic distortion and noise levels were 4.0 per cent and 55 to 60 millivolts, respectively.* This latter sort of performance was found to be typical of operation with up to 5 per cent second harmonic content in the bias current, or after failure to carefully demagnetize

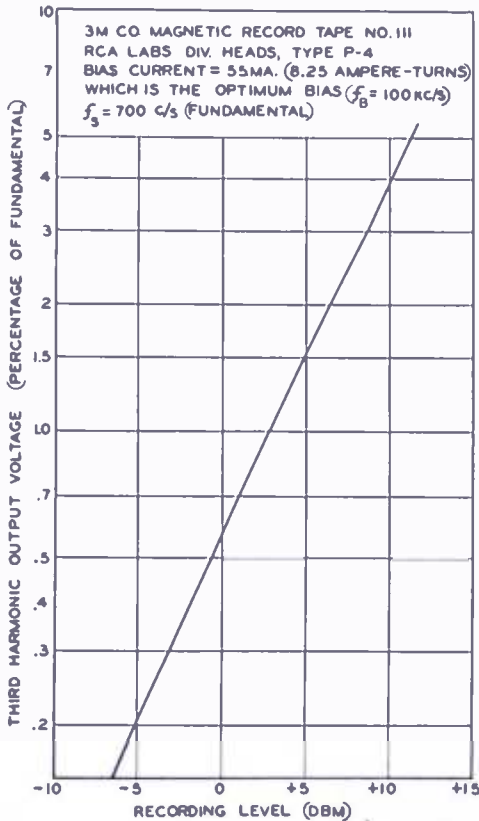


Fig. 22—Third Harmonic Distortion versus recording level (dbm).

the various heads after exposure to magnetized objects, to high peak surges of recording signal or to the abrupt switching of erase, bias or high level signal currents. The second harmonic null adjustment has been found capable of correction of all difficulties which have been encountered from these sources.

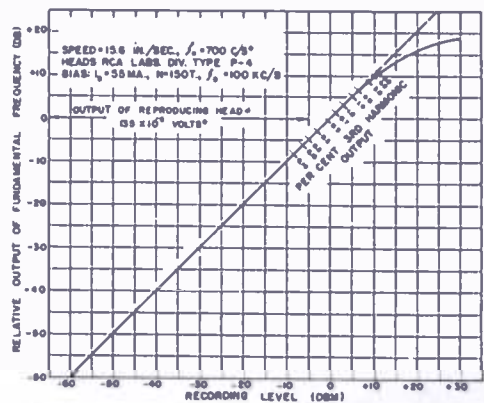


Fig. 23—Signal transfer characteristic, Minnesota Mining and Manufacturing Company, No. 111, magnetic record tape.

A set of curves is plotted in Figures 24 and 25 to exhibit the performance characteristics of a relatively good magnetic recording system before and after application of the harmonic-null potentiometer adjustment. The *original* characteristics are indicated in Figure 24. The *improved operation* is as shown by the curves of Figure 25. It is noteworthy that the null in the original second harmonic curve (Figure 24) was caused by the *opposition* of the effects of the residual magnetism of the recording head and the asymmetry (even harmonic) effect of the bias current. Had these two effects been *additive*, the *minimum* second harmonic distortion should have been greater than

3 per cent at *any* bias current adjustment. This could have been reduced to an acceptable value only by sacrificing recording level, and hence causing a degraded signal-to-noise ratio, or by using the harmonic-null system.

An additional factor which may be of importance in choosing the precise value of bias excitation, is the effect of the bias value upon the reproducing response at the higher signal frequencies. Figure 26 has been plotted to indicate the performance in this respect. A family of curves which was recorded within the frequency range between 0.100 and 15.00 kilocycles is plotted with the relative reproducing level (decibels) versus the bias current, with the amplitude spectral re-

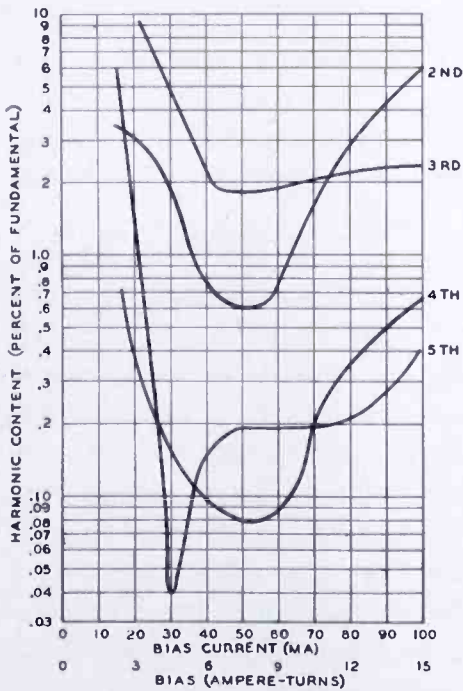


Fig. 24—Harmonic distortion produced by a particular magnetic record system.

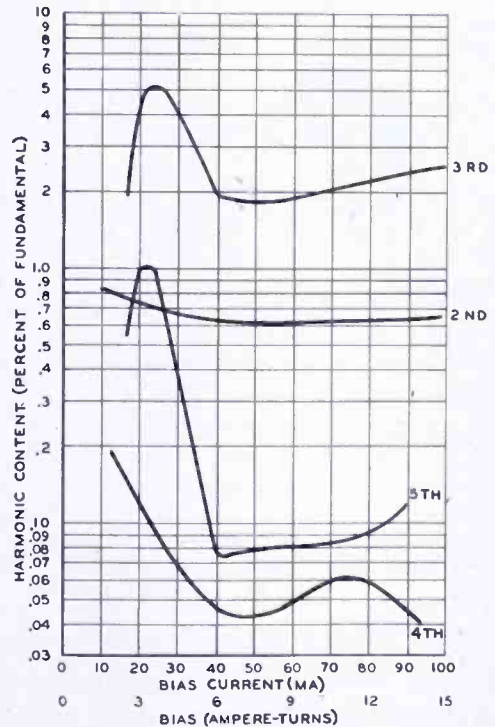


Fig. 25—Typical reduction of even harmonic distortion by application of harmonic-null principle to system of Figure 24.

sponse of the system equalized at a bias of 55 milliamperes. It is obvious that a precise value of bias setting must be maintained to assure maintenance of a specified high frequency response characteristic; but there seems to be no necessity for specifying any particular value of bias, from this viewpoint, provided only that the signal-to-noise ratio at the highest frequency is maintained sufficiently large. If the output level at 15 kilocycles must be maintained within ± 3 decibels of that produced at 1 kilocycle, for instance, it is apparent from Figure 26 that the bias current must be maintained constant within ± 5 milliamperes or about

± 9 per cent. Means for maintenance of this accuracy must be built into the recording unit. A gas-discharge type of voltage regulator tube should prove adequate for stabilizing the power supply, and hence the bias output, against power line voltage variations. An accurate bias-current meter is recommended for adjustment of the equipment to the desired value of bias current.

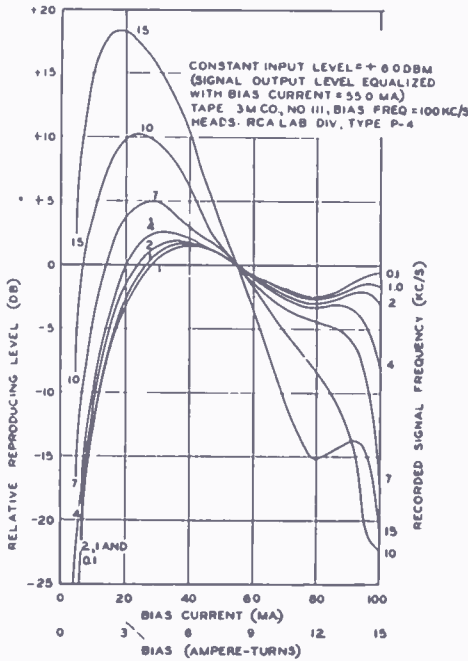


Fig. 26—Relative output signal level as a function of bias current.

tape passing through the recorder, with no input signal, and adjusting this output noise to a minimum audible value. When the harmonic phase and amplitude relations are optimum, it is sometimes found that the reproduced second harmonic output may be reduced to a level which is actually *less* than the second harmonic output of the amplifying and recording system alone, without the magnetic record.

Numerous curves are provided to indicate the optimum operating conditions of a particular recording system, using "Scotch" brand, No. 111, magnetic record tape (red iron oxide on a cellulose acetate base) as manufactured by the Minnesota Mining and Manufacturing Company of St. Paul, Minnesota. The precisely adjusted type P-4 erasing, recording and reproducing heads used in these tests were developed and constructed by the RCA Laboratories Division. It is found that particularly excellent performance may be attained by this system when all of the indicated adjustments have been made and when the operating conditions are within the prescribed limits.

CONCLUSIONS

An unusually simple solution has been found for attaining the objective. Most magnetic recording systems may be converted so that a convenient null adjustment for minimum second harmonic and minimum noise output may be made by the addition of only one simple adjustable potentiometer of standard design.

A number of simple and convenient methods are indicated for detecting the approximate null of either the reproduced second harmonic, or the noise output signal. A quite satisfactory adjustment may be made by simply listening to the noise output reproduced from a

EXPERIMENTAL ULTRA-HIGH-FREQUENCY TELEVISION STATION IN THE BRIDGEPORT, CONNECTICUT AREA*

BY

RAYMOND F. GUY, JOHN L. SEIBERT AND FREDERICK W. SMITH

Radio and Allocations Engineering, National Broadcasting Company, Inc.,
New York, N. Y.

Editor's Note: This paper constitutes the first in a series of reports on the NBC UHF field tests at Bridgeport, Connecticut. The second of the series—"An Experimental Ultra-High-Frequency Television Tuner"—appears on pages 68-79 of this issue.

It is currently planned to include the following two papers in the June 1950 issue of RCA Review:

"A New Ultra-High-Frequency Transmitter"

"Ultra-High-Frequency Antenna and System for Television Transmission"

Subsequent papers will include reports on propagation studies, service area surveys, service operating characteristics of equipment, and subsequent equipment and other technical developments.

Summary—The engineering considerations involved in the construction and operation of an experimental television broadcast station in the ultra-high-frequency band are presented. The transmitter, KC2XAK, is located in the Bridgeport, Connecticut area and operates in a standard bandwidth of six megacycles from 529 to 535 megacycles with a newly developed transmitter and high-gain antenna. Programs are picked up directly from Station WNBT in New York on Channel 4 and are demodulated, processed and retransmitted on the ultra-high-frequency band.

INTRODUCTION

AS World War II drew to its close, it became apparent that great expansion in radio service was imminent, particularly in the very-high-frequency (VHF) and ultra-high-frequency (UHF) spectrums. It was also evident that the whole field of frequency allocations in these spectrums should be reviewed in preparation for these new and extensive services of the future. One of the most important of the new services under consideration for the postwar period was television broadcasting. Accordingly, the Federal Communications Commission (FCC) held a public hearing which began on September 28, 1944, with the purpose of reviewing existing allocations in the light of future needs. As a result of this hearing and subsequent developments, commercial television is now assigned twelve channels in the VHF band on which there are currently in operation approximately one hundred stations. But it has been apparent that twelve

* Decimal Classification: R588×R310.

channels do not permit adequate television service for a truly nationwide system.

For future use the FCC set aside a block of ultra-high frequencies in the 475-890 megacycle band for television. Insufficient information was available with which to adopt standards and allocate frequencies at that time. The need for this information has been most apparent and both government and the industry have undertaken to obtain such information. It is necessary to determine whether or not the television transmitter standards presently used for VHF could be adopted for UHF service. It is also necessary to determine the propagation characteristics of the ultra-high frequencies. These two generalized fields require a large amount of data which must be obtained and integrated. The areas which could be served by UHF television transmitters with practicable radiated powers and antenna heights must be determined. Moreover, the propagation characteristics which determine the minimum separation which can be tolerated between cochannel stations, and the characteristics of transmitting and receiving apparatus and the propagation characteristics which determine the minimum separation necessary between adjacent-channel stations must be known.

During the last several years, much has been learned from work done in the development of apparatus and the studies of propagation undertaken by various government and private laboratories and by manufacturing and operating companies.

Radio Corporation of America has conducted, concurrently, a number of projects^{1,2} to determine the propagation characteristics and the television service potential of the ultra-high frequencies, particularly in the band from 475 to 890 megacycles, and has made this information available to the FCC and the industry at large.

Upon completion of the tests described in Reference (2), it was decided that an experimental ultra-high-frequency television transmitting station should be erected in a representative city which was not adequately served by a local VHF transmitter. It was felt that such a station should be a full scale custom built prototype of future commercial installations in the UHF band so that the results obtained would be truly indicative of the practical possibilities of ultra-high-frequency broadcasting in the type of community in which many of these stations would be operated. Accordingly, such a project was initiated.

¹ G. H. Brown, J. Epstein and D. W. Peterson, "Comparative Propagation Measurements; Television Transmitters at 67.25, 288, 510 and 910 Megacycles", *RCA Review*, Vol. 9, No. 2, p. 177, June 1948.

² G. H. Brown, "Field Test of Ultra-High-Frequency Television in the Washington Area", *RCA Review*, Vol. 9, No. 4, p. 565, December 1948.

SELECTION OF THE SITE

After considerable investigation, an area having Bridgeport, Connecticut as its approximate center was selected for the station site. Application for a construction permit for an experimental television station, to transmit in the band from 529 to 535 megacycles and specifying Bridgeport as the general location, was made to the FCC on February 8, 1949. The permit was granted May 4, 1949, assigning the call KC2XAK.

The city of Bridgeport is located on Long Island Sound (see Figures 1 and 2) at the mouth of the Poquonock River and has a popula-



Fig. 1—Map of general area surrounding Bridgeport transmitter location.

Courtesy Esso Standard Oil Company (Copyrighted by General Drafting Company, Inc., New York.)

tion, for the metropolitan district, of approximately 216,600 according to the 1940 census. While fringe reception of television stations in New York and New Haven is obtained in this area, there is no locally originated television service.

As can be seen from Figure 2, the city is ringed with a series of hills all of which are about 200 feet high. Of these, Success Hill, in Stratford, Connecticut, which is north-northeast of the center of Bridgeport and just outside the city limits, was chosen after extensive surveys as the most suitable site for the installation of a television transmitter. From the standpoint of covering not only Bridgeport, but



Fig. 2—Topographic map of Bridgeport and immediate vicinity.

(Geological Survey, United States Department of the Interior.)

Fig. 3—Transmitter Building (front view).

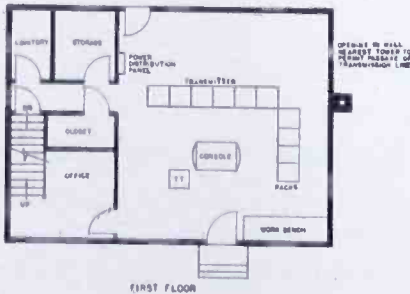


also neighboring communities such as Stratford, Devon and Milford adequately, Success Hill appeared to be the most attractive location.

Application was thereupon made to the FCC, modifying the Construction Permit to show Success Hill as the exact location of the transmitter site. This modification was granted by the FCC on October 12, 1949, with a proviso that construction should start on or about December 12, 1949, and be complete on or before June 12, 1950.

TRANSMITTER BUILDING

The transmitter building resembles a conventional Cape Cod cottage from the exterior, as shown in Figure 3. The floor plans of this structure are shown in Figure 4. The useful floor area of the apparatus rooms is 1164 square feet.



The peak power requirement of the installation was initially estimated as 50 to 60 kilovolt-amperes at 240-120 volts alternating current and it was therefore necessary to provide a 400-ampere service in order to achieve adequate regulation. Ventilation of the transmitting equipment is secured by means of vents located in the first floor ceiling which are arranged to accept the air exhausted from the transmitter racks. The attic in turn is ventilated by a pair of two speed 24-inch exhaust fans which are operated whenever it is undesirable to retain the equipment heat within the building. The construction of

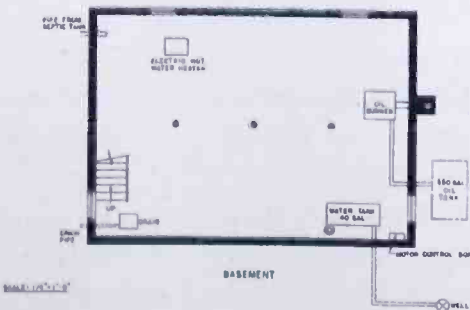


Fig. 4—Floor plans of transmitter building.

the transmitter building started on September 22, 1949 and was completed on November 15, 1949.

As a supporting structure for the transmitting antenna, a steel tower 210 feet in height with a base 24 feet square was erected next to the transmitter building as shown in Figure 3. In order to adequately ground the tower as protection against lightning discharges, copper straps six inches wide were attached to three of the four tower legs and these were separately bonded to the well casing. A considerable reduction in cost of the tower lighting system was effected by employing a newly developed weatherproof cable, Simplex Anhydrex, for the lighting cable runs, rather than conventional cable in conduit. These cables were secured to the tower ladder risers by means of worm-type hose clamps and this arrangement permitted installation of the tower wiring in a fraction of the time normally required.

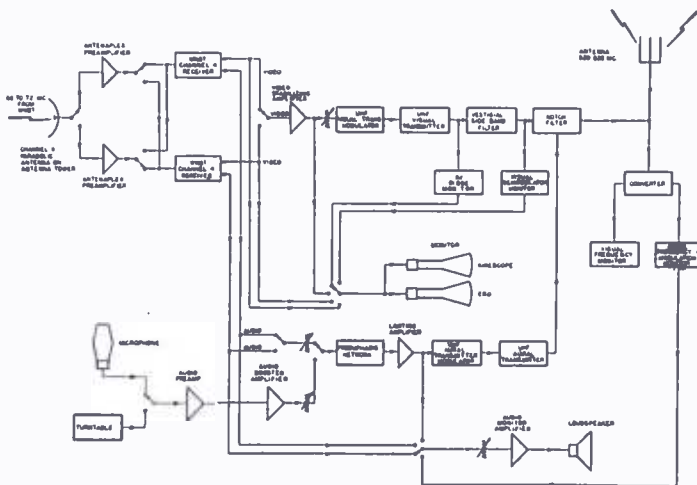


Fig. 5—Block diagram of transmitting system.

An efficient ground system for the radio transmitting equipment installed in the building was secured by situating all equipment racks on a continuous copper sheet placed over the flooring. This sheet was grounded to the well casing in the manner described above. Erection of the tower was started on November 17 and completed on November 24.

TRANSMITTING SYSTEM

The transmitting system employed at Station KC2XAK is outlined in the overall system block diagram shown in Figure 5. The transmitter is arranged to operate as a satellite of the VHF television station WNBT in that the visual and aural program signals are picked up directly from WNBT and retransmitted on the UHF band. While provisions are incorporated for local aural station identification, none are included for local origination of test pattern or other video signal.

The manner in which this system of satellite operation is accom-

plished may be seen from Figure 5. The signal from WNBT is picked up directly from the transmitter located atop the Empire State Building in New York City at a distance of approximately 54 miles by means of a parabolic antenna located on the antenna tower. The signal is then fed to a preamplifier located in the station building which in turn provides the radio-frequency signal for two specially constructed receivers tuned to Channel 4.

The video signal is taken from the receiver through a built-in isolation amplifier and is then processed by a stabilizing amplifier which improves the quality of the signal and corrects any degradation which may have occurred in the synchronizing information. The video signal is then applied to the UHF visual transmitter modulator and final power amplifier. The output of the visual transmitter is filtered by a vestigial sideband filter to attenuate the lower sideband in accordance with the television transmission standards established by the FCC.

The demodulated audio signal from the receiver is taken from the audio output stage of the receiver, pre-emphasized, and fed into a limiting amplifier which prevents over-modulation of the transmitter by audio surges. In the event that a local station identification is to be made, the output of either a microphone or a turntable may be introduced into the system at this point as indicated in Figure 5.

The output of the limiting amplifier is then applied directly to the frequency-modulation exciter which constitutes the UHF aural transmitter modulator. The outputs of the UHF aural and visual transmitters are combined in a notch type cross coupling filter and the resultant signal is used to excite a newly developed high gain UHF television transmitting antenna through a coaxial transmission line. Thus, programs originating from Station WNBT on the present VHF band are received, demodulated, processed and retransmitted on the UHF band.

In addition to the facilities just described, monitoring equipment has been provided which permits observation of either picture or sound quality anywhere within the system as indicated by Figure 5. Also, frequency monitoring equipment has been installed which makes it possible to hold the frequency of the visual and aural carriers well within the tolerances set for standard television broadcasting.

INPUT EQUIPMENT FEATURES

Although certain components in the overall transmitting system are standard units, most contain innovations which are of technical interest and will therefore be described.

The parabolic receiving antenna is located on a platform on the

160-foot level of the antenna tower as shown in Figure 6. It consists of a dipole which is mounted in the focus of a circular, parabolic screen 10 feet in diameter. The parabola has a focal length of $29\frac{1}{2}$ inches and provides an antenna gain of 3.5 decibels as compared to a simple dipole. The receiving antenna transmission line consists of an ATV-225 balanced shielded pair which has a nominal characteristic impedance of 225 ohms and a loss of 2.3 decibels per hundred feet at 50 megacycles. Although the line loss incurred with this cable is greater, the use of shielded transmission line affords a degree of noise immunity not possible with the standard unshielded 300-ohm line.



Fig. 6—Transmitter building (side view) and antenna tower. The Channel 4 parabolic receiving antenna can be seen at the 160 foot level of the tower.

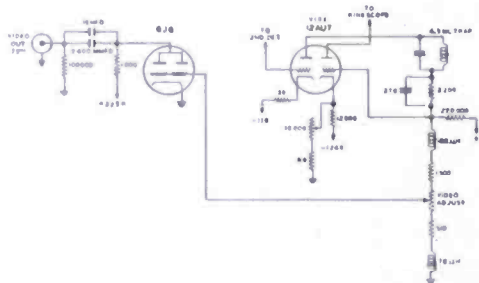


Fig. 7a—Revised video output circuit of Channel 4 receivers.

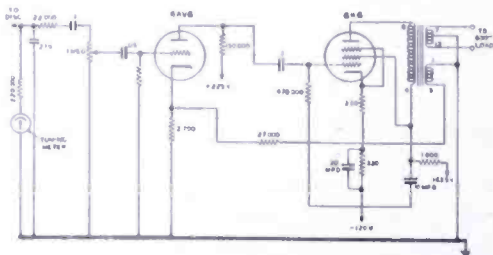


Fig. 7b—Revised audio amplifier circuit of Channel 4 receivers.

The preamplifiers which precede the Channel 4 receivers are fixed tuned amplifiers and are identical with the type SX9A amplifier normally furnished as part of the RCA Antenaplex television distributing system. The amplifier consists of two 6J6 push-pull cross-neutralized amplifier stages in cascade which provide a gain of approximately 20 decibels, as well as an improvement in the signal to noise ratio. The output stages of these amplifiers are equipped with isolation pads which permit a signal to be fed to one or both of the 300-ohm receiver inputs without undesirable interaction.

The Channel 4 receivers used for the actual detection of the Channel 4 signal are standard RCA 9T246 receivers with 10-inch screens which have been specially modified for this particular application. The

major changes made in this receiver are modifications of the audio and video output circuits and these are illustrated in Figures 7a and 7b.

The revised video output circuit is shown in Figure 7a. The normal plate load of the first half of the 12AU7 video amplifier has been divided in such a way that the input of the 6J6 isolation amplifier may be shunted across a portion of it without undesirably affecting normal operation of the receiver video circuits. This isolation amplifier will provide an output signal of 2 volts peak to peak at an output impedance of 75 ohms when the "video adjust" and receiver automatic gain controls are properly adjusted.

Figure 7b indicates the modifications made in the receiver audio amplifier. The power amplifier has been altered to provide a standard audio output impedance of 600 ohms and the overall distortion characteristics of the amplifier have been improved by the addition of an inverse feedback loop from a separate winding on the output transformer to the cathode of the penultimate audio amplifier stage. In addition, a tuning meter has been connected across the output of the discriminator which permits adjustment of the fine tuning control of the receiver for minimum audio distortion, which point is indicated by a zero indication on the meter. By this means an audio output of +5 dbm* with but .4 per cent second harmonic distortion can be obtained. The receivers have also been completely shielded, housed in a manner suitable for rack mounting, and have been aligned for optimum reception on Channel 4.

The video stabilizing amplifier employed in the system is a type ND-329 Clamp and Sync Amplifier. It incorporates clamp circuits which stabilize the video signal and contains provisions for the independent adjustment and restoration of sync pulse amplitude so that the video signal fed to the visual modulator will at all times meet FCC standards. The remaining input equipment consists mainly of standard commercial audio amplifiers.

UHF TRANSMITTER

The television transmitter, which constitutes the major link in the transmitting system, is an RCA type TTU-1A. The TTU-1A, which operates in the UHF band, meets the FCC standards for VHF television broadcast transmitters.

The transmitter is housed in six racks, as is shown in Figure 8, the left hand 3 racks containing the aural portion of the transmitter and the right hand 3 racks containing the visual portion. The transmitter includes, as an integral part, a slightly modified RCA type

* Decibels referred to a zero level of 1 milliwatt in 600 ohms.

TT-500B television transmitter which comprises the center two racks in Figure 8.

In the visual section of the transmitter, the radio-frequency output of the 4X150A's in the final stage of the TT-500B is used to drive a tripler employing eight type 4X150A tubes in parallel in a single cavity. The output of the tripler in turn drives a power amplifier containing eight additional 4X150A tubes and employing a cavity design similar to the tripler. These cavities can be seen in the second rack from the right in Figure 8. The video modulator circuits of the TT-500B have been modified to drive a direct-coupled cathode follower stage, consisting of eight 6L6 tubes, which serves as a modulator for the UHF power amplifier.

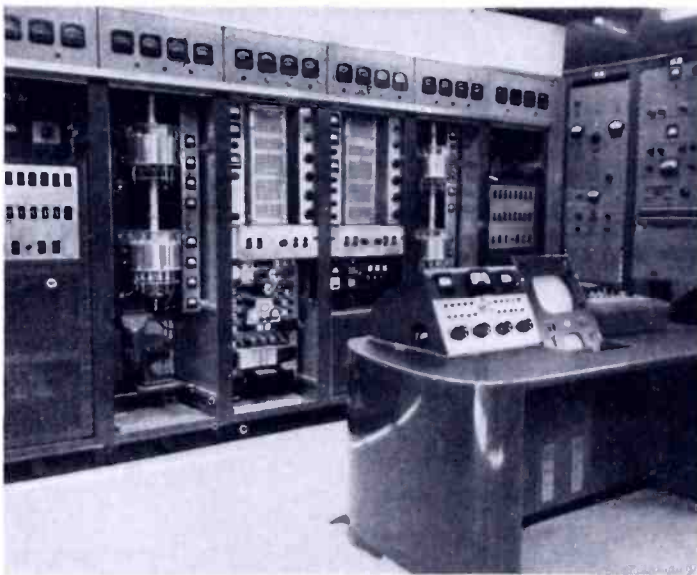


Fig. 8—The RCA TTU-1A transmitter, input and monitoring racks and control console.

In the aural section of the transmitter the arrangement of tripler and power amplifier cavities is identical to that just described, and these are located in the second rack from the left in Figure 8. Modulation, of course, takes place in the frequency modulation exciter which is located in the TT-500B.

The transmitter operates in a standard six-megacycle band, 529 to 535 megacycles, the visual and aural carrier frequencies being 530.25 and 534.75 megacycles respectively. This requires that the TT-500B output stages which drive the UHF triplers operate at 176.75 and 178.25 megacycles. An overall frequency multiplication of 108 occurs between the oscillator and the final frequency in both the visual and aural transmitters. The visual carrier is held within ± 0.002 per cent of the assigned operating frequency and the sound carrier is automatically maintained 4.5 megacycles above the visual by means of a

novel system of frequency control which eliminates relative drift between the visual and aural carriers. This arrangement makes it unnecessary to hold transmitter carrier frequency stability closer than the present FCC requirements for carrier frequency stability in the UHF band even though the intercarrier sound reception feature may be incorporated in future UHF television receivers.

Each of the transmitter sections is designed to work into a 51.5-ohm, $1\frac{5}{8}$ -inch transmission line, and will deliver normal power outputs of .5 kilowatt aural and 1.0 kilowatt peak visual.

FREQUENCY MONITORING EQUIPMENT

The arrangement of frequency and aural modulation monitoring equipment used in conjunction with the UHF transmitter is illustrated in Figure 9. As can be seen, the method used to monitor the transmitter is to convert the transmitter signal frequencies to 45.25 megacycles for the picture carrier and 49.75 megacycles for the sound carrier and then monitor at these frequencies with a standard RCA WF-49A and WF-50A visual frequency monitor and General Radio type 1170-AT FM aural monitor. The converter heterodyning signal is supplied by a standard frequency crystal oscillator at 30.3 megacycles and a multiplying chain. The crystal used in this oscillator is of a special design that has a long term stability of better than 2 parts per million per 30 days. In order to check the actual amount of frequency drift, means have been provided for the calibration of the oscillator against WWV. For this purpose, a 250-kilocycle oscillator is used as a secondary frequency standard and is calibrated against WWV at 5 or 10 megacycles by the use of an external communications receiver. The 250-kilocycle signal frequency is then multiplied and the resultant signal frequency compared to that of the heterodyning signal so that the heterodyne signal can be set to exact zero beat.

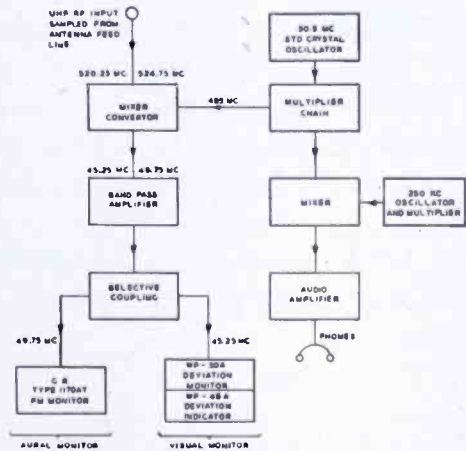


Fig. 9—Block diagram of transmitter monitoring equipment.

OUTPUT NETWORK, TRANSMISSION LINE AND ANTENNA

The coaxial vestigial sideband filter and notch filter indicated in the block diagram of the system (Figure 5) are located behind the

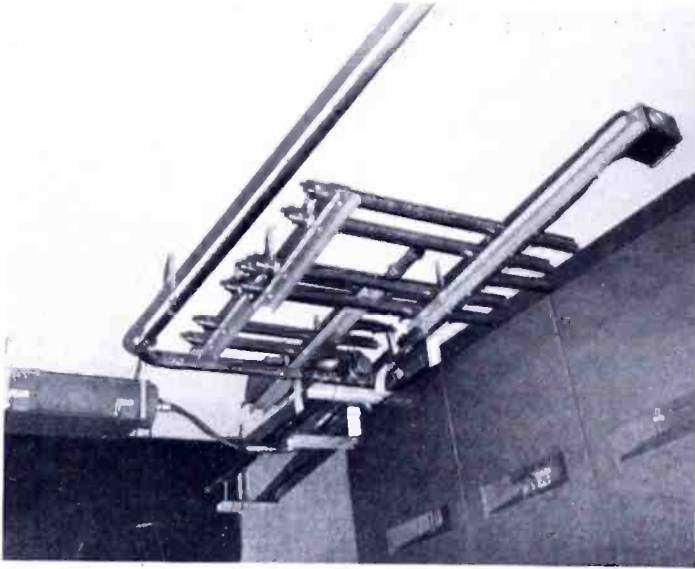


Fig. 10 — Coaxial vestigial sideband filter and diplexer suspended on ceiling behind the transmitter.

transmitting equipment in the station building as shown in Figure 10. The output of these networks is fed to the antenna by means of special $3\frac{1}{8}$ -inch UHF transmission line pressurized with nitrogen, similar to that employed in the UHF transmission tests in the Washington area.^{2,3}

The antenna itself is an RCA type TFU-20A. It is similar in structure to the standard pylon antenna (See Figure 11) but is operated as a slot antenna. The slot radiators are covered by polyethylene covers which are the protrusions which appear on the antenna pole in Figure 11.

The antenna has gain of 17, a diameter of $10\frac{3}{4}$ inches and an overall height of forty feet above the pole socket in which it mounts. Because of the nature of the antenna structure, efficient operation requires that ice formation over the slot radiators be prevented. A thermostatically controlled de-icing system consisting of a hot air

Fig. 11—The RCA TFU-20A UHF antenna in test position before erection on tower.



³ D. W. Peterson, "Notes on a Coaxial Line Bead", *Proc. I.R.E.*, Vol. 37, No. 11, p. 1294, November, 1949.

blower has therefore been installed to prevent icing conditions and losses due to extreme humidity. The output of the blower is forced into the antenna at the base of the antenna pole and is exhausted at the top of the antenna just below the beacon. The electrical power input to the blower heaters can be increased to as much as 14 kilowatts if conditions demand. The overall height above ground of the antenna and antenna tower is 250 feet and the overall height above mean sea level is 440 feet. The height of the antenna radiation center above average terrain is 330 feet.

SYSTEM EFFICIENCY

The overall system efficiency from the transmitter to the antenna is approximately 80 per cent. With an antenna gain of 17 and a visual transmitter power output (peak) of one kilowatt, the effective radiated power of the system will be roughly 13.9 kilowatts peak visual. It is estimated that the power costs for the entire system for 16 hours per day, 7 days per week operation would be roughly \$4000 per year.

Additional developments are under way to increase the efficiency of the various UHF system components and raise the antenna gains. It would be possible, for example, to employ wave guide operating in the $TE_{0,1}$ mode for the antenna feed system. Such a wave guide would have dimensions of roughly $15 \times 9\frac{1}{2}$ inches and would have an efficiency of about 92 to 93 per cent for the length of guide necessary.

FIELD TESTS

Experimental television station KC2XAK went on the air with full power and full modulation on December 29, 1949. A number of television receivers and converters designed to receive KC2XAK are being installed in homes in the Bridgeport area. Field tests will include observations in homes throughout the service area, at distances and under conditions which will determine the extent of coverage of the station. Various types of receiving antenna will be tested, shadow areas and multipath problems investigated and extensive field intensity measurements will be made.

Such measurements will be taken at representative receiver locations and will include actual voltages obtained at receiver terminals. In addition, measurements will be conducted along various radials and an investigation made of field intensity versus receiving antenna height under various conditions. Upon completion of the surveys, the results obtained will be disclosed to the FCC and the industry in subsequent papers.

AN EXPERIMENTAL ULTRA-HIGH-FREQUENCY TELEVISION TUNER*

BY

T. MURAKAMI

Home Instrument Department, RCA Victor Division,
Camden, N. J.

Summary—This paper describes an ultra-high-frequency television tuner developed for use in field tests of the experimental television station, KC2XAK, located in Bridgeport, Connecticut. A compact tuning system utilizing modified transmission lines is used in this tuner which covers a frequency range of 500 to 700 megacycles. Each tuning element consists of two strips of copper foil mounted on a thin cylindrical coil form, tuned by means of a copper or brass core. A double heterodyne system is used to convert the ultra-high-frequency signals to the 21-27 megacycle intermediate frequency of the conventional television receiver, with a switching arrangement provided to change from the very-high-frequency to the ultra-high-frequency head end.

INTRODUCTION

THE experimental ultra-high-frequency (UHF) television station KC2XAK† in Bridgeport, Connecticut operates in the channel from 529 to 535 megacycles (Mc). This is near the low frequency end of the UHF band; therefore, it has been possible to obtain satisfactory performance using conventional tubes in this particular tuner, which covers the range from 500 to 700 Mc. A tuner which is to perform satisfactorily in the region above 700 Mc would probably require a different tube complement, and other design changes. For this reason, the tuner described here is not intended to represent a finished commercial design, but rather is an experimental model to be used on a limited basis to acquire further technical information pertinent to UHF television transmission and reception.

The particular type of UHF tuned circuit used in this tuner was originally developed for a converter built for reception of the experimental UHF television transmitter in Washington, D.C., which operated during the fall of 1948 in the channel from 504 to 510 Mc. The converter used in the Washington tests tuned from 500 to 600 Mc using the same tube complement as the present model for the radio-frequency

* Decimal Classification: R583.5.

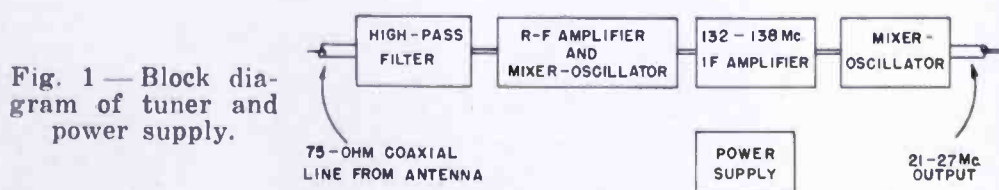
† R. F. Guy, J. L. Seibert and F. W. Smith, "Experimental Ultra-High-Frequency Television Station in the Bridgeport, Connecticut Area", pp. 55-67 of this issue.

(r-f) amplifier and the mixer-oscillator. These tests indicated that the tuning system was satisfactory; therefore, a similar type was adapted for the tuner described here.

The amplified output signal of the tuner is fed to the intermediate-frequency (i-f) amplifier of any conventional television receiver; in this way either very-high frequencies (VHF) or UHF may be received by switching the output of the head ends. Both the tuner and its power supply may be mounted directly on the television receiver chassis or operated as a separate unit.

GENERAL CONSIDERATIONS

As shown in the block diagram of Figure 1, the tuner consists of an input high-pass filter cutting off at 500 Mc, an r-f amplifier, a first mixer-oscillator, a 132-138 Mc first i-f amplifier, a second mixer-oscillator, the output of which is at 21-27 Mc and low impedance. The UHF amplifier and oscillator tuning elements are designed to cover the signal range of 500 to 700 Mc.



The first i-f has been chosen high enough to provide satisfactory image rejection with two UHF tuned circuits, but low enough so that reasonable i-f gain and noise factor can be realized with conventional tubes. If the sound and picture i-f in the VHF receiver were redesigned for higher frequencies, a single superheterodyne system might be more satisfactory.

DESCRIPTION OF CIRCUIT

A circuit diagram of the tuner and its power supply is shown in Figure 2. The high-pass input filter reduces (1) the image response, (2) the direct i-f response, (3) the oscillator radiation, because in this double superheterodyne receiver the first local oscillator is below the signal frequency. This filter, shown schematically in Figure 2, is a "printed" circuit, as shown in Figures 3 and 4. The "printing" is accomplished by photoengraving a 1.5 mil copper sheet bonded to a paper-base bakelite sheet. A high-pass filter was used since it was less critical to variations in photoengraving than the band-pass type. The filter and the r-f amplifier are designed to operate with 75-ohm coaxial antenna transmission line. The insertion loss of the high-pass filter is

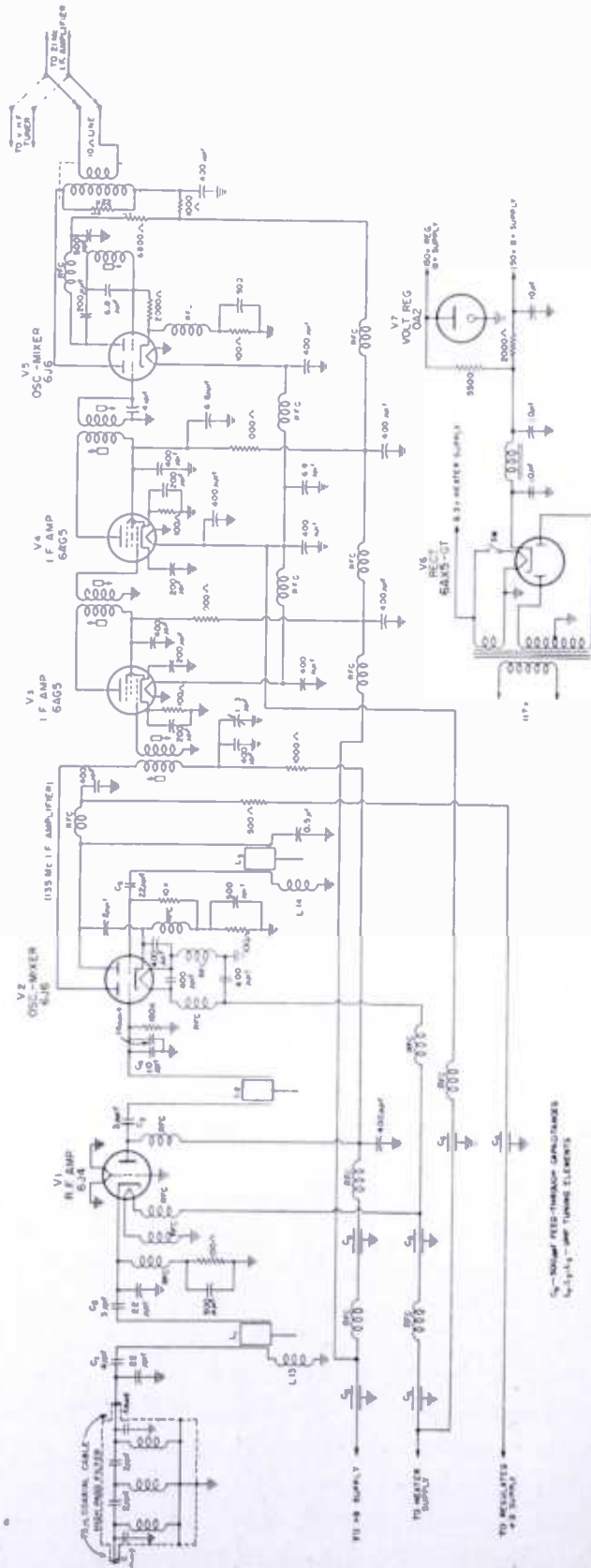
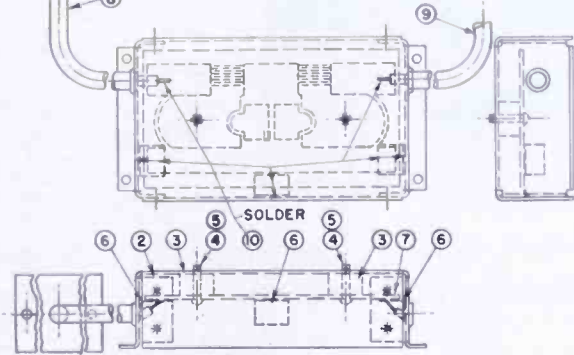


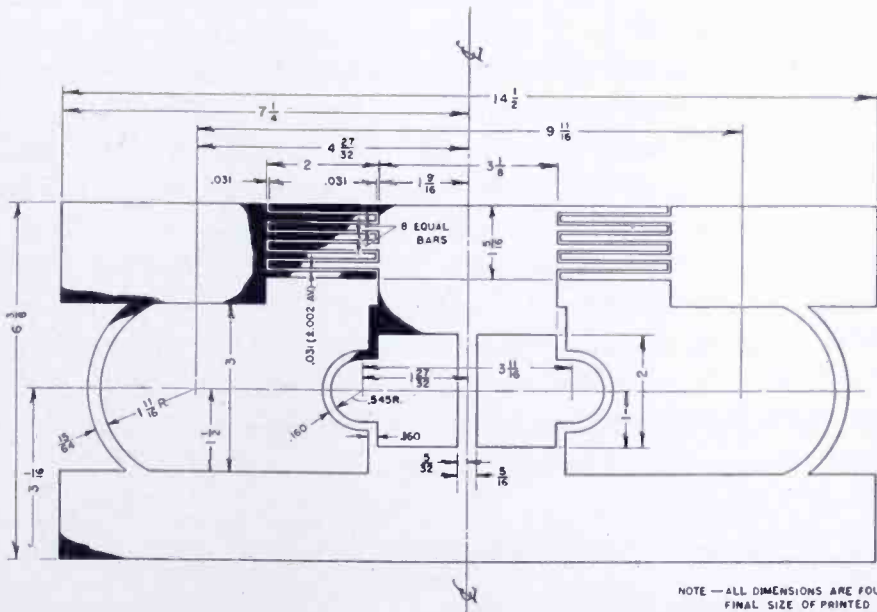
Fig. 2—Circuit diagram of UHF tuner and power supply.

shown in Figure 5. In the transmission range, the insertion loss is approximately 2 decibels. To prevent excessive loading by the transmission line and the amplifier cathode on the tuned input circuit, capacitive impedance transformations have been used as shown in Figure 2.

SPREAD BRAIDING ON PLATE & SOLDER TOGETHER



LIST OF PARTS	
ITEM	DESCRIPTION
1	ASSEMBLY
2	SHIELD
3	SPACER
4	SCREW-FILL HD - 4-40x1/2 LG
5	LOCK WASHER
6	STRAPS
7	HIGH-PASS FILTER
8	CABLE
9	CABLE
10	SOLDER
11	PLATE



1 LAYOUT FOR BLACK & WHITE REPRODUCTION DRAWING.

NOTE — ALL DIMENSIONS ARE FOUR TIMES FINAL SIZE OF PRINTED CIRCUIT FILTER, THE BLACK AND WHITE DRAWING TO BE PHOTOGRAPHED TO ACTUAL SIZE.

Figs. 3a (above) and 3b (below)—Construction details of “printed” circuit filter.

A 6J4 triode is used as a grounded-grid r-f amplifier, and a single 6J6 tube for the first oscillator-mixer, with cathode injection of the oscillator voltage. The 132-138 Mc first i-f amplifier consists of two stages of 6AG5 tubes with three double-tuned circuits. Two stages are necessary to sufficiently isolate harmonics of the second oscillator from

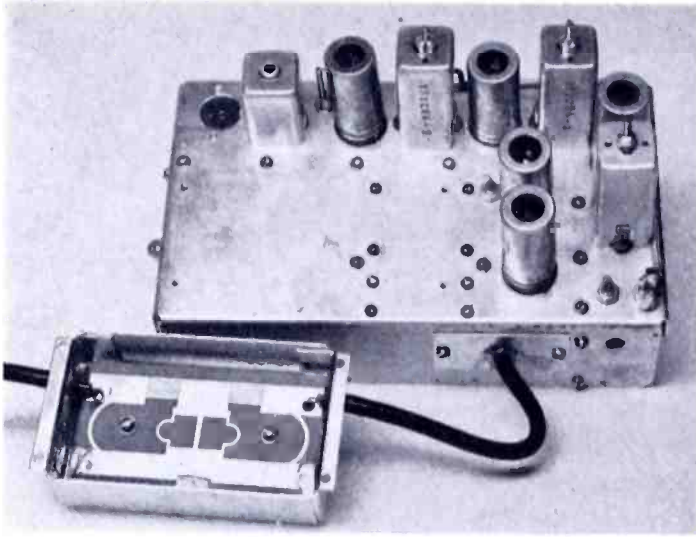


Fig. 4—Photograph of tuner, showing high-pass filter.

the first mixer. Automatic gain control is not applied to this amplifier because of the effect of varying transconductance on the selectivity curve shape.

A 6J6 tube is also used as the second oscillator-mixer to heterodyne the 132-138 Mc signal to 21-27 Mc. The output from the tuner is linked-coupled to the first picture i-f amplifier of a standard VHF television receiver through a low-impedance line. 110-ohm shielded twin line is used. If the tuner is to be used with a receiver which has an i-f of other than 21-27 Mc, it is only necessary to retune the fixed oscillator to the appropriate frequency and redesign the output i-f transformer. Switching between the UHF tuner and the conventional VHF tuner (which is normally an integral part of the television receiver) is made in the low-impedance link circuit. In some television receivers it may be necessary to modify either this switching arrangement or the 21-27 Mc i-f amplifier, since the link circuit may alter the band-pass characteristics of the amplifier.

UHF TUNING ELEMENTS

The tuning elements used in the r-f and oscillator circuits are shown in Figure 6. These elements consist of strips of 2.5-mil copper foil mounted with a low loss cement on natural paper base bakelite tubing with an inside diameter of 0.251 inch and a 10-mil wall thickness. The input and interstage elements

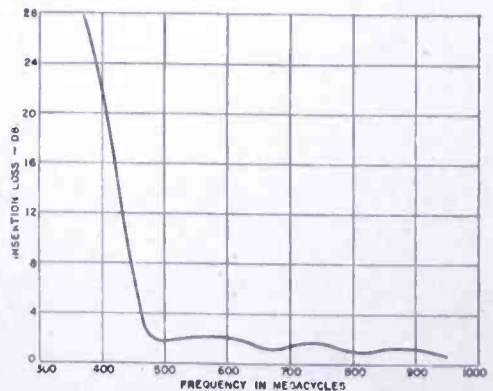


Fig. 5—Insertion loss of high-pass filter.

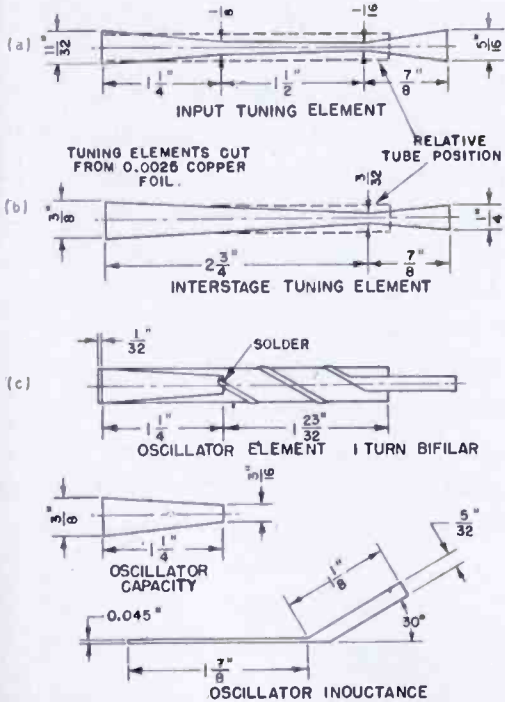


Fig. 6—Tuning elements used in r-f and oscillator circuits.

are shown in Figures 6-a and 6-b. The copper foil in these elements has been tapered to obtain a desirable tuning curve and proper tracking of the r-f and oscillator circuits. The copper foil at the ends of these elements has been flared to reduce the lead inductance. The oscillator element consists of a bifilar winding terminating in a split capacitor section. The bifilar winding increases the inductance of the oscillator tuning element so that the oscillator will operate 135 Mc below the signal frequency for this particular tuner. Oscillator radiation is also reduced by use of the bifilar winding in the oscillator circuit since the fields produced in the tuned circuit partially cancel. All three elements are tuned by means

of copper or brass cores, shown in Figure 7, moved inside the bakelite tubing. These cores are mounted on kovar wire which is broken in several places with glass bead supports. The use of kovar wire minimizes oscillator drift due to thermal expansion. It is necessary to break the wire into small segments to decouple the cores from the surrounding metal and avoid spurious "suck-outs." In the oscillator element excessive oscillator radiation is prevented by use of the broken wire segments. A 500 to 700 Mc tuning range is covered with a core movement of approximately $1\frac{3}{8}$ inches.

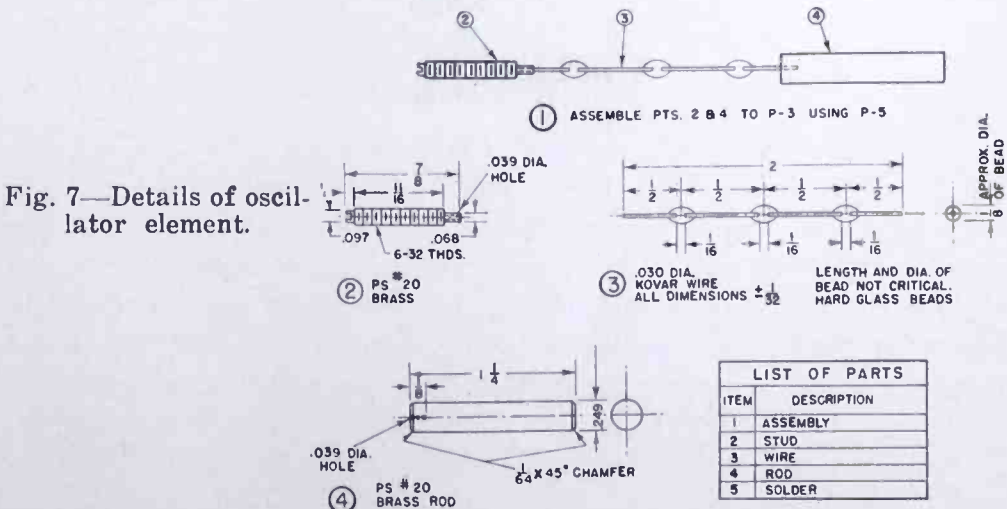


Fig. 7—Details of oscillator element.

When the metal core is moved in the tube, both the effective length of the line and the capacitive reactance terminating the line are varied. The tuning range of a particular unit can be changed by varying the maximum and minimum amount of the capacitive and inductive reactance of the line. This can be most readily done by changing the diameter of the thin-walled tubing and the size of the foil strips. If the diameter of the tube is increased, the tuning range, in general, will increase. If the length of the line is increased, the open-ended line extending beyond the core may become a quarter wave length at some frequency in the tuning range. This may cause the impedance of the line to fall below a usable value depending upon the core position when this critical frequency is reached. However, the length of line will determine the highest frequency which can be obtained with the core in the extreme "in" position due to the capacity loading effect of the overhanging end of the line.

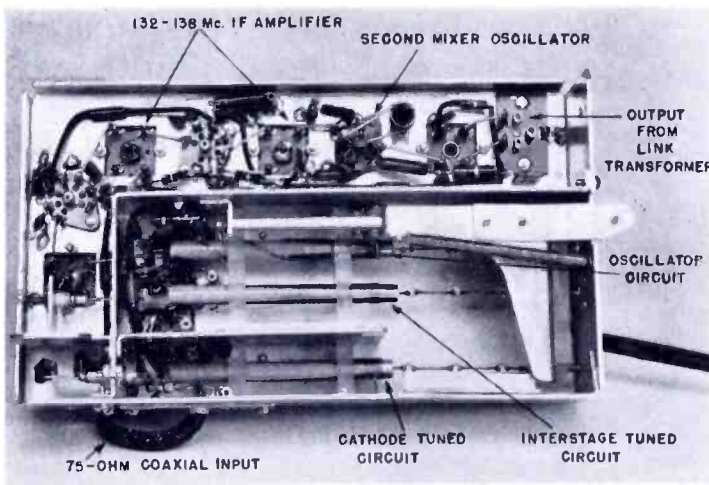


Fig. 8—Bottom view of tuner.

The unloaded Q of the tapered transmission line tuning elements measures between 100 and 200 in the 500 to 700 Mc frequency range. The effective operating Q of these tuning elements is approximately 25 at 500 Mc and the overall bandwidth of the input and interstage circuits is about 12 Mc at 500 Mc.

Figure 8 shows a bottom view of the tuner with the r-f and oscillator tuning elements in place. The 75-ohm coaxial cable and the high-pass filter can be seen to come in to the tuned circuit in the cathode of the grounded-grid stage. The tuning element between the plate of the grounded-grid amplifier and the mixer grid is shown in the center next to the oscillator tuning element. The 132-138 Mc i-f amplifier is placed near the edge of the chassis with the second mixer oscillator. The output terminals from the link transformer can be seen in the upper right hand corner.

PERFORMANCE

Sensitivity

The sensitivity of the tuner is defined as the input signal required to give a 10 to 1 ratio between peak to peak modulation and peak to peak noise. The modulation on the carrier is 400 cycles at 30 per cent. The measurements shown in Table I were made with the carrier at the top of the picture i-f selectivity curve.

Table I

Frequency in Mc	Sensitivity (Microvolts)
500	140
600	200
700	220

Noise Factor

The noise factor of the UHF tuner was measured using the signal generator method. The receiver and the signal generator used in this measurement were an RCA 9T246 and a Measurements Corporation Model 84. The fixed bias applied to the receiver i-f amplifier was such that 1.0 volts direct current of rectified noise was developed across the second detector load resistor with the tuner coupled to the receiver. The detector was checked to insure operation in the linear portion of the detector characteristic. With the Model 84 matched to the input of the tuner with an M-255 pad (50-72 ohms, 6-decibel voltage attenuation), enough carrier was fed into the tuner so that 1.41 volts direct current of carrier plus noise was read at the second detector. In Equation (1) below, e_o is the open circuit voltage of the signal generator. The signal generator is calibrated in terms of the voltage developed across a load resistor equal to the impedance of the generator; therefore, to find e_o the output reading of the generator was multiplied by the factor 2. With the M-255 matching pad, e_o was equal to the output reading of the signal generator.

$$F = \frac{e_o^2}{4KT\Delta fR_a}, \quad (1)$$

where $R_a = 72$ ohms, $\Delta f = 3.4$ Mc, $T = 290$ degrees Kelvin, $K = 1.38 \times 10^{-23}$ joules per degree (Boltzmann's constant).

Expressing the noise factor in decibels

$$F_{db} = 10 \log (0.254e_o^2), e_o \text{ in microvolts.}$$

The noise factor measurements for a representative tuning unit are shown in Table II.

Table II

Frequency (Mc)	500	530	550	600	650	700
e_o (Microvolts)	8	8	9	13	15	15
Noise factor (decibels) without high-pass filter	12	12	13	16	17.5	17.5
e_o (Microvolts)	10	10	11	16	17	16
Noise factor (decibels) with high-pass filter	14	14	15	18	18.5	18

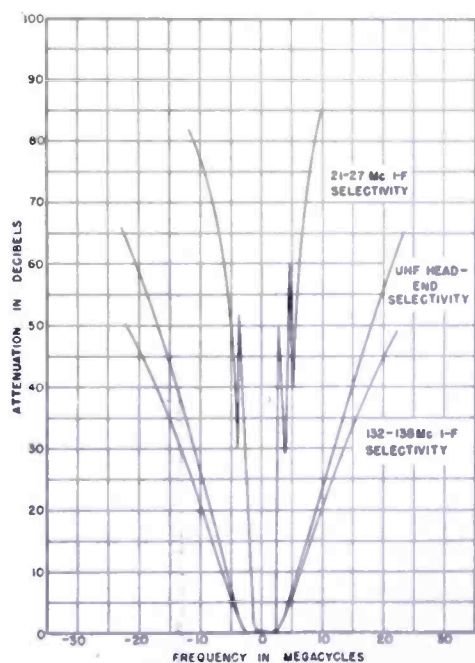


Fig. 9—Tuner selectivity curves.

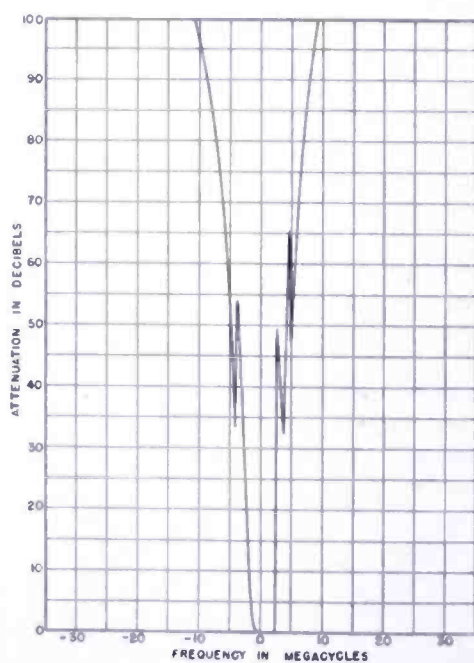


Fig. 10—Overall tuner selectivity curves.

Gain

The voltage gain of the tuner is 49 decibels at 500 Mc, 48 decibels at 600 Mc and 46 decibels at 700 Mc.

Selectivity

Curves in Figure 9 show the 132-138 Mc i-f selectivity, UHF head-end selectivity (including 135 Mc i-f) at 500 Mc, and the 21-27 Mc i-f selectivity of the 9T246 receiver. The overall selectivity curve for the UHF tuner and receiver, with the UHF head end tuned to 500 Mc is shown in Figure 10.

Oscillator Stability

The UHF tuner operates with the heaters of the tubes on at all times. Regulation of the plate voltage for the UHF oscillator is used to prevent frequency change due to variations in supply voltage. The oscillator drift at 500 Mc with preheated heaters is 150 kilocycles from the frequency measured $\frac{1}{2}$ minute after the time B plus is turned on. All of the drift occurs in less than $2\frac{1}{2}$ minutes, the oscillator stabilizing after that time. At 600 and 700 Mc the drift characteristics are very similar to those at 500 Mc.

Oscillator Radiation

The power measured across 75 ohms at the antenna terminals is less than 0.2 microwatt over the tuning range of 500 to 700 Mc.

Spurious Responses

A table of spurious responses with their attenuation relative to the desired signal is given in Table III. These values were obtained using the constant output method of measurement; in this case sufficient signal at the spurious response frequency was fed into the tuner to give the same output as would a given amount of desired signal. The undesired signal in each case was set at approximately 0.1 volt to the UHF unit. Since some spurious response ratios depend on signal level, 0.1 volt was chosen as representative of a reasonably strong interfering signal. It is also a value that can be obtained from available signal generators.

Table III

Signal frequency (megacycles)	Image (decibels)	Half i-f (decibels)	2nd harmonic of oscillator heterodyning with undesired signal to give 135 Mc (decibels)
500	78	78	42
550	73	73	42
600	66	66	58
650	67	67	59
700	70	70	—

The i-f response is more than 80 decibels down from the desired signal frequency response when the high-pass filter is used in the input circuit. To suppress spurious responses caused by harmonics of the fixed oscillator it is necessary to isolate this circuit from the UHF circuits. In addition to the mechanical shielding attained by careful

placement of components, it is necessary to decouple thoroughly the B-plus and heater-supply leads.

There is a spurious response caused by the fourth harmonic of the fixed oscillator (158 Mc) feeding back to the r-f circuits at 632 Mc. The 6.8-micromicrofarad capacitor in the B-plus supply line and the 1-3 micromicrofarad trimmer in the low side of the primary winding of the first 132-138 Mc transformer are used to suppress this 632-Mc harmonic. This response can be further reduced with a 632-Mc trap circuit inductively coupled to the fixed oscillator.

TUNING CHARACTERISTIC AND TRACKING

The tuning curve for the tuner is shown in Figure 11. The tuning curve consists very nearly of two linear sections, from 500 to 600 Mc and 600 to 700 Mc. The tuning elements for the r-f and oscillator circuits track within 1/16 inch of core movement; this tracking error, which corresponds to 7 to 10 Mc in frequency, does not appreciably degrade the sensitivity.

Tracking is accomplished first by adjusting the lead length of the UHF oscillator capacitance C_5 (Figure 2) with the oscillator core in its low-frequency position so that the frequency is about 365 Mc. Concurrently, the UHF tuned circuits are tuned to 498 Mc with their cores in the low-frequency position by adjustment of the lead lengths of capacitances C_1 to C_4 in Figure 2. If the tuning cores are made too loose in the coil forms, the values of the capacitors C_1 - C_5 may have to be increased. The tracking is further improved over the band by adjustment of the relative positions of the cores.

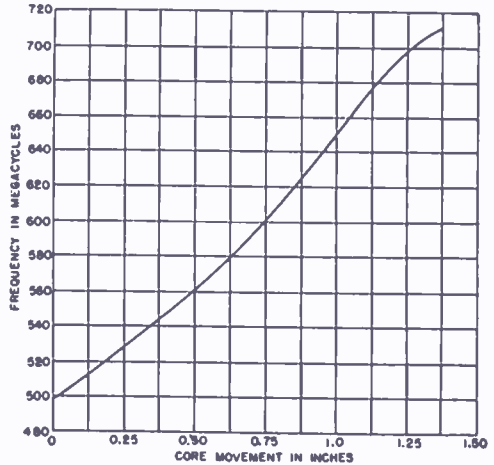


Fig. 11—Tuning curve.

UHF-VHF RECEIVER

The tuner chassis does not include its power supply, which is on a separate small chassis. One method of mounting the tuner and its power supply is shown in Figure 12, where the tuner is mounted directly above the regular VHF tuner, and the power supply is mounted in front of the horizontal deflection high voltage compartment. Figure 13 shows a view of the UHF-VHF receiver with the UHF tuning dial and directly below it the UHF-VHF switch.

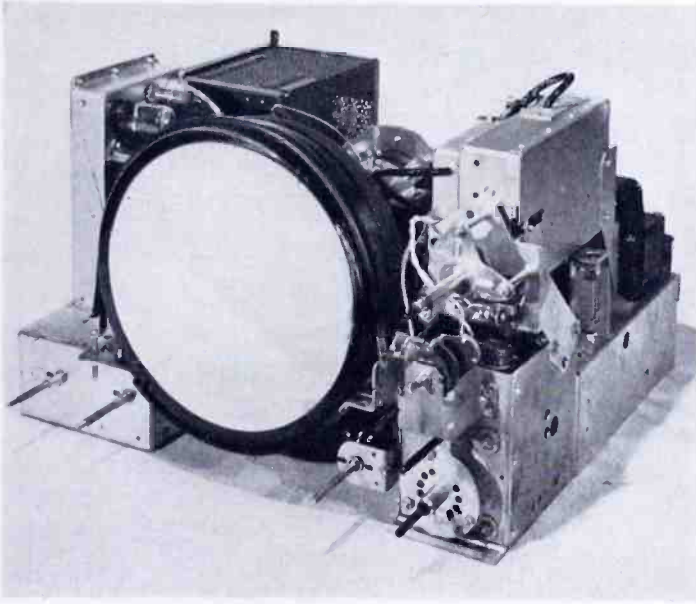


Fig. 12—Standard VHF chassis with UHF tuner added.



Fig. 13—Standard VHF receiver with UHF tuner added. UHF controls are to the right of the kinescope.

ACKNOWLEDGMENTS

The author wishes to acknowledge the valuable work contributed by S. Klein and the suggestions given by W. R. Koch and Wm. F. Sands of the Home Instrument Advanced Development Section in the development of this tuner. The design of the tuning mechanism is credited to E. D. Dawson.

HIGH-EFFICIENCY LOUD SPEAKERS FOR PERSONAL RADIO RECEIVERS*

BY

H. F. OLSON, J. C. BLEAZEY, J. PRESTON AND R. A. HACKLEY

Research Department, RCA Laboratories Division,
Princeton, N. J.

Summary—The term *personal radio receiver* is used to designate a complete radio receiver with self-contained power supply, and of such physical dimensions that it can be easily carried by hand or in the pocket. The performance and compactness of personal radio receivers are limited by the efficiency with which electrical power is converted into sound power by the loud speaker. Since the electrical power output is limited in the personal receiver, the efficiency of the loud speaker is an important factor. A number of loud speaker systems have been investigated, both theoretically and experimentally, as follows: direct radiator, combination direct radiator and phase inverter, horn, and combination horn and phase inverter. An efficiency of 25 per cent has been obtained with the combination horn and phase inverter. This loud speaker system has been incorporated in a complete four-tube radio receiver, having a content of 25 cubic inches.

INTRODUCTION

THE term personal radio receiver is used to designate a complete radio receiver with self-contained power supply, and of such physical dimensions that it can be easily carried in the hand or in the pocket. The performance and compactness of personal radio receivers are limited by the efficiency with which electrical power supplied by the output stage is converted into sound power by the loud speaker. Regardless of size, the efficiency of direct radiator loud speakers is inherently low because of the small ratio of the radiation acoustical impedance to the acoustical reactance of the air load, diaphragm, and coil. The outstanding advantage of the dynamically driven direct radiator loud speaker resides in the fact that, in a mass controlled system operating in the frequency range below the ultimate resistance, the efficiency is independent of the frequency. Therefore, it is a simple task to obtain a uniform response frequency characteristic. When there are no power limitations as, for example, in socket-powered receivers, the efficiency of the loud speaker is a minor consideration compared to smooth response. Since the electrical power output is limited in the personal receiver, the efficiency of the loud speaker is an important factor. Obviously, an increase in efficiency

* Decimal Classification: R365.21.

requires an improvement in the ratio of acoustical radiation resistance to acoustical reactance in the loud speaker system.

One of the simplest means for increasing this ratio is by the use of a horn. However, small physical dimensions and adequate low frequency response are incompatible in a horn system. Therefore, for a horn with dimensions which are tolerable in a personal type radio receiver, the region of high efficiency is confined to a relatively high frequency range. The acoustical phase inverter is another means for increasing the ratio of radiation acoustical resistance to acoustical reactance. The useful frequency range of an acoustical phase inverter is about one octave. Furthermore, high efficiency in the phase inverter is usually confined to a relatively low frequency. From the foregoing, it appears that the combination of a horn and phase inverter would provide a system with the characteristics of high efficiency and a relatively wide frequency range. It is the purpose of this paper to describe the efficiency limitations of direct radiator loud speakers and a high efficiency combination horn and phase inverter loud speaker having dimensions suitable for personal type radio receivers.

CONVENTIONAL BACK ENCLOSED LOUD SPEAKER¹

The conventional loud speaker system used in personal radio receivers consists of a small direct radiator loud speaker with the back of the loud speaker diaphragm coupled to an enclosed case, and with the front of the diaphragm radiating directly into the air.

Top and sectional views of the basic loud speaker mechanism used in these experiments are shown in Figure 1. The case dimensions of the personal radio receiver used in these experiments are shown in the perspective view of Figure 2. These are the minimum dimensions for housing a superheterodyne radio receiver employing four sub-miniature tubes and the complementary components. The batteries were selected to give what is considered a commercially tolerable life. A sectional view and the mechanical circuit of the vibrating system are also shown in Figure 2. The mechanical impedance frequency characteristics of the loud speaker and case volume are shown in Figure 3.

The efficiency, in per cent, of this loud speaker is given by

$$\mu = \frac{(Bl)^2 r_{MA} \times 100}{(Bl)^2 (r_{MS} + r_{MA}) + r_{EC} [(r_{MS} + r_{MA})^2 + (x_{MA} + x_{MC} - x_{MS} - x_{MV})^2]} \quad (1)$$

¹H. F. Olson, ELEMENTS OF ACOUSTICAL ENGINEERING. Second Edition, D. Van Nostrand Company, New York, N. Y., 1947.

where

B = flux density in the air gap, in gaussses,

l = length of the voice coil conductor, in centimeters,

r_{MS} = mechanical resistance of the suspension system, in mechanical ohms,

r_{MA} = mechanical resistance due to radiation, in mechanical ohms,

r_{EC} = electrical resistance of the voice coil, in abohms,

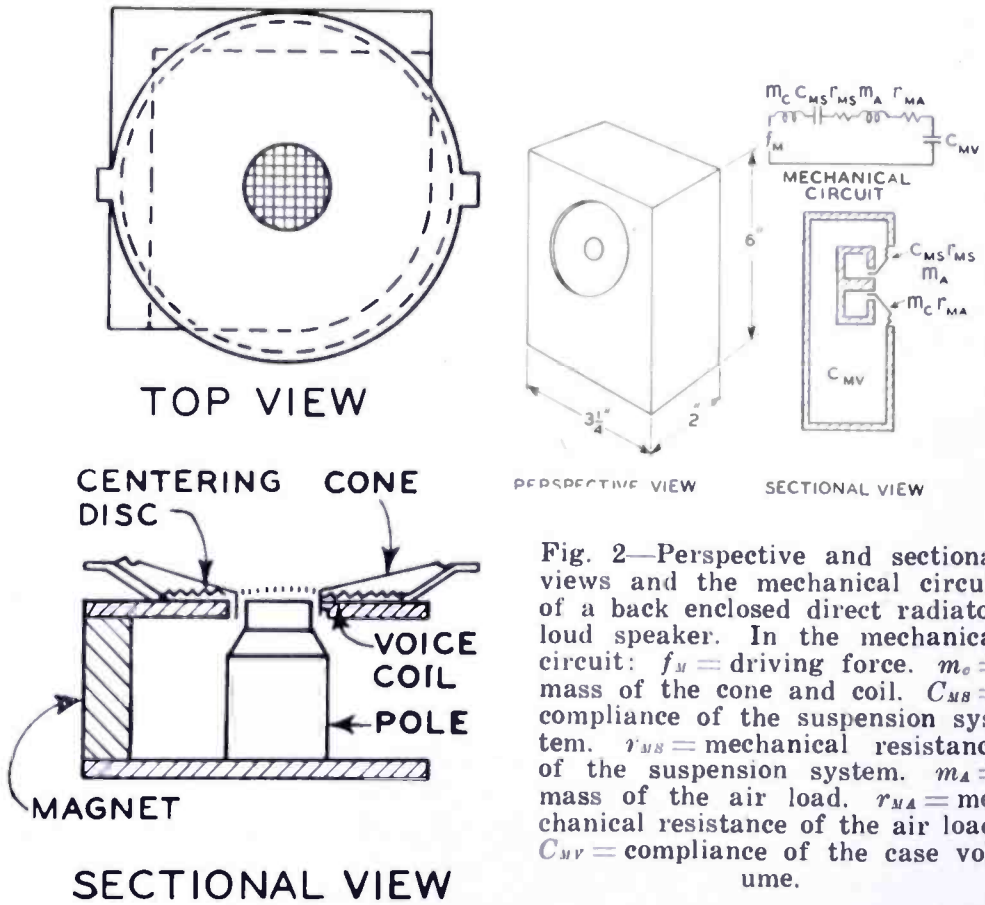


Fig. 2—Perspective and sectional views and the mechanical circuit of a back enclosed direct radiator loud speaker. In the mechanical circuit: f_M = driving force. m_o = mass of the cone and coil. C_{MB} = compliance of the suspension system. r_{MS} = mechanical resistance of the suspension system. m_A = mass of the air load. r_{MA} = mechanical resistance of the air load. C_{MV} = compliance of the case volume.

Fig. 1—Front and sectional views of the loud speaker mechanism.

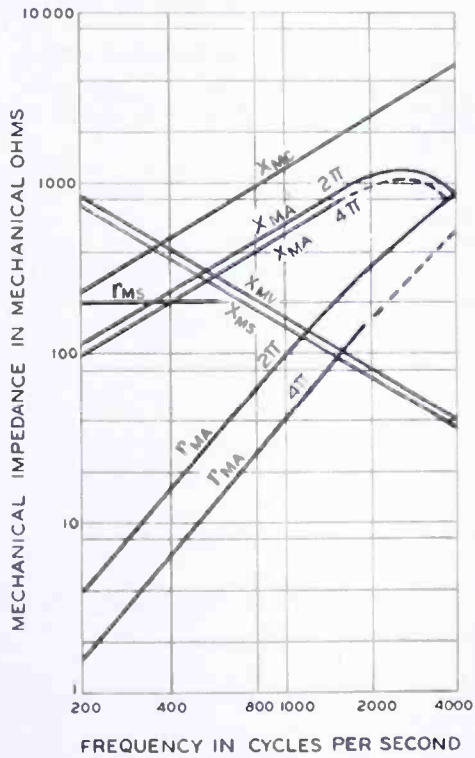
Table of Constants of the Loud Speaker Mechanism

Mechanism	Cone Dia.	Cone Mass	Coil Mass	Coil Mat.	Add. Mass	Gap Flux
A	2"	.085 gm	.083 gm	cu.	.040 gm	10,000
B	2"	.085 gm	.083 gm	cu.	.040 gm	21,000
C	2"	.085 gm	.083 gm	al.	.040 gm	21,000

- x_{MC} = mechanical reactance of the cone and voice coil, in mechanical ohms,
- x_{MA} = mechanical reactance of the air load, in mechanical ohms,
- x_{MS} = mechanical reactance of the suspension system, in mechanical ohms, and
- x_{MV} = mechanical reactance of the case volume, in mechanical ohms.

Personal radio receivers are operated in two ways, namely, on a table and in the hand. In the first case the sound radiation angle is 2π steradians, while in the latter case it is 4π steradians. When the

Fig. 3—Mechanical impedance frequency characteristics of the elements in the vibrating system of the loud speaker. x_{MC} = mechanical reactance due to the mass of the cone and coil. x_{MA} = mechanical reactance due to the air load. x_{MV} = mechanical reactance due to the volume of the case. x_{MS} = mechanical reactance of the suspension system. r_{MA} = mechanical resistance of the air load. r_{MS} = mechanical resistance of the suspension system.



diameter of the diaphragm is less than a wavelength, the radiation mechanical resistance differs for these two examples as follows: For 2π steradians, the mechanical resistance, in mechanical ohms, due to sound radiation is

$$r_{MA} = \frac{1}{2} \rho c k^2 R^4, \tag{2}$$

where ρ = density of air, in grams per cubic centimeter,
 c = velocity of sound, in centimeters per second,

$$k = 2\pi/\lambda,$$

λ = wavelength, in centimeters, and

R = radius of the diaphragm, in centimeters.

For a solid angle of 4π steradians, the mechanical resistance, in mechanical ohms, due to radiation is

$$r_{MA} = \frac{1}{4} \rho c k^2 R^4. \quad (3)$$

In the following discussion the latter type of radiation will be used for efficiency considerations. It will be about 3 decibels lower than the radiation into 2π steradians.

For 2π steradians the mass, in grams, of the air load on the two sides of the cone is

$$m_A = 1.72\pi\rho R^3. \quad (4)$$

For 4π steradians the mass, in grams, of the air load on the two sides of the cone is

$$m_A = 1.47\pi\rho R^3. \quad (5)$$

The mechanical reactance, in mechanical ohms, due to the air load is

$$x_{MA} = \omega m_A. \quad (6)$$

The mechanical reactance, in mechanical ohms, due to the mass of the cone and voice coil is

$$x_{MO} = \omega m_C, \quad (7)$$

where m_C = mass of the cone and coil, in grams.

The mechanical reactance due to the suspension system is given by

$$x_{MS} = \frac{1}{\omega C_M}, \quad (8)$$

where C_M = compliance of the suspension system.

The compliance of the suspension system is given by

$$C_M = \frac{x}{f_M} \quad (9)$$

where x = deflection, in centimeters, and

f_M = applied force in grams.

The compliance of the suspension system was experimentally determined from Equation (9).

The mechanical reactance of the case volume is given by

$$x_{MV} = \frac{S_c^2 \rho c^2}{\omega V}, \quad (10)$$

where S_c = area of the cone, in square centimeters,

ρ = density of air, in grams per cubic centimeter,

c = velocity of sound, in centimeters per second, and

V = volume of the case, in cubic centimeters.

The mechanical resistance due to loss in the suspension system was obtained from motional impedance measurements in a vacuum. The motional electrical impedance of the mechanism, in abohms, is

$$z_{EM} = \frac{(Bl)^2}{z_{MT}}, \quad (11)$$

where $z_{MT} = r_{MO} + r_{MA} + j(x_{MA} + x_{MO} - x_{MS})$.

If the unit is operated at the resonant frequency in a vacuum,

$$z_{MT} = r_{MS}. \quad (12)$$

The mechanical resistance of the suspension system, r_{MS} , for the mechanism of Figure 1 as used in these tests, was 200 mechanical ohms.

The acoustical output of the system shown in Figure 2, in ergs per second, is

$$P_A = \frac{1}{\rho c} \int \int p^2 dS, \quad (13)$$

where p = pressure, in dynes per square centimeter, over the element of area dS , and

dS = element of area on the spherical surface, in square centimeters.

The electrical input, in ergs per second, is

$$P_E = r_E i^2, \quad (14)$$

where r_E = electrical resistance of the loud speaker, in abohms,
and

i = current in the voice coil, in abamperes.

The efficiency, in per cent, is

$$\mu = \frac{P_A}{P_E} \times 100. \quad (15)$$

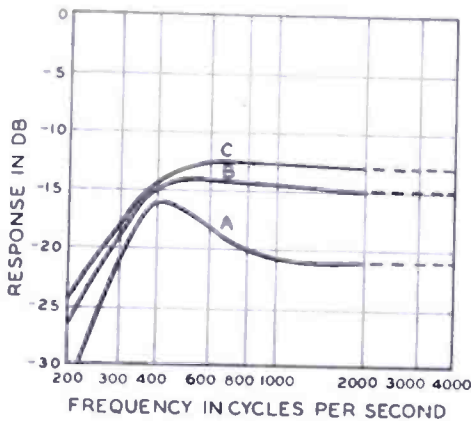


Fig. 4—Theoretical response frequency characteristics for the three mechanisms of Figure 1 operating in the case of Figure 2. Curve A obtained with mechanism A. Curve B obtained with mechanism B. Curve C obtained with mechanism C. 0 decibels corresponds to an efficiency of 100 per cent.

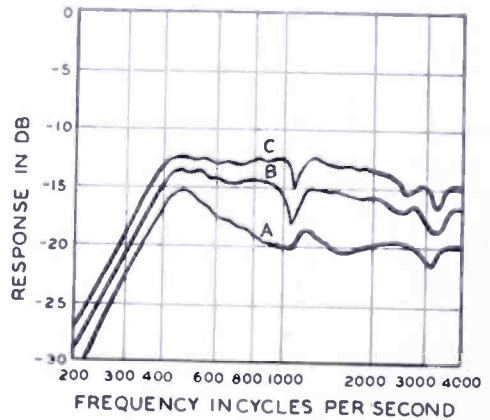


Fig. 5—Experimental response frequency characteristics for the three mechanisms of Figure 1 operating in the case of Figure 2. Curve A obtained with mechanism A. Curve B obtained with mechanism B. Curve C obtained with mechanism C. 0 decibels corresponds to an efficiency of 100 per cent.

The response frequency characteristic computed from the data of Figures 1, 2 and 3 and Equation (1) for the frequency range 500 to 2000 cycles is shown in Figure 4. The measured response frequency characteristic of the loud speaker operating in the case is shown in Figure 5. The measured efficiency was computed from the measured sound pressure over the surface of a sphere and the measured electrical power input. This is fair agreement between the theoretically predicted and experimentally determined efficiency.

A consideration of Equation (1) shows that the efficiency can be increased by increasing the air gap flux. The theoretically predicted and experimentally determined increased output obtained by increasing

the air gap flux from 10,000 to 21,000 gausses is shown in Figures 4 and 5. The gain is of the order of 6 decibels. The efficiency in the range from 500 to 2000 cycles is about 2.4 per cent.

A further consideration of Equation (1) shows that the efficiency can also be increased by substituting an aluminum voice coil for the copper voice coil, while retaining the same mass, since the density resistivity product of aluminum is one-half that of copper. The theoretically predicted and experimentally determined increased output obtained by the substitution of an aluminum voice coil for a copper voice coil is shown in Figures 4 and 5. The increase in efficiency is about 3 decibels.

The weight of the cone used in the above experiments was about as light as could be tolerated even for the small power requirements. For the above conditions on diaphragm mass and dimensions and case volume, a slight increase in efficiency can be obtained with existing materials. For example, the air gap flux could be increased to 23,000 gausses and the mass of the voice coil made equal to the mass of the cone and air load. Employing these expedients, the increase in efficiency would be about one decibel. However, the added magnet material required is not justified by the small increase in efficiency.

For the above conditions on diaphragm dimensions and case volume, the efficiency is practically as high as can be realized with a mass controlled direct radiator loud speaker operating in a small case. It appears that some other type of vibrating system must be used to obtain an appreciable increase in efficiency. Two of these, namely, the acoustical phase inverter loud speaker and the horn loud speaker will be considered in the sections which follow.

ACOUSTICAL PHASE INVERTER LOUD SPEAKER¹

The acoustical phase inverter consists of a direct radiator loud speaker mounted in a ported cabinet as shown in the perspective view of Figure 6. A sectional view of the vibrating system and the mechanical network is also shown in Figure 6. From the mechanical network the velocity, in centimeters per second, in branch 1 is

$$\dot{x}_1 = \frac{f_M(z_{M2} + z_{M3})}{z_{M1}z_{M2} + z_{M1}z_{M3} + z_{M2}z_{M3}}, \quad (16)$$

where $f_M = Bli$, the driving force, in dynes,

B = flux density in the air gap, in gausses,

l = length of the voice coil conductor, in centimeters,

i = current in the voice coil, in abamperes,

$$z_{M1} = r_{MA} + r_{MS} + j\omega(m_c + m_A) + \frac{1}{j\omega C_{MS}},$$

$$z_{M2} = \frac{1}{j\omega C_{MV}},$$

$$z_{M3} = r_{MP} + j\omega m_P,$$

r_{MA} = mechanical resistance due to radiation from the diaphragm, in mechanical ohms,

r_{MS} = mechanical resistance of the suspension system, in mechanical ohms,

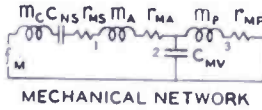
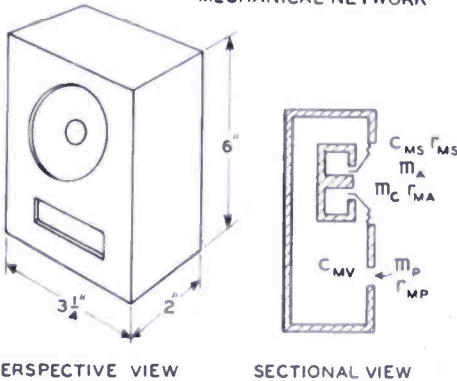


Fig. 6—Perspective and sectional views and the mechanical network of a phase inverter direct radiator loud speaker. In the mechanical network: f_M = driving force. m_c = mass of the cone and coil. C_{MS} = compliance of the suspension system. r_{MS} = mechanical resistance of the suspension system. m_A = mass of the air load. r_{MA} = mechanical resistance of the air load. C_{MV} = compliance of the case volume. m_P = mass of the air in the port. r_{MP} = mechanical resistance of the air load at the port.



m_c = mass of the cone and voice coil, in grams,

m_A = mass of the air load on the cone, in grams,

C_s = compliance of the suspension system, in centimeters per dyne,

C_v = compliance of the case volume, in centimeters per dyne,

r_{MP} = mechanical resistance due to radiation from the port, in mechanical ohms, and

m_P = mass of the air in the port and the air load on the port, in grams.

The velocity in branch 2 is

$$\dot{x}_2 = \frac{f_M z_{M2}}{z_{M1} z_{M2} + z_{M1} z_{M3} + z_{M2} z_{M3}} \tag{17}$$

The sound power output, in ergs per second, is

$$P_A = r_{MA} \dot{x}_1^2 + r_{MP} \dot{x}_2^2. \quad (18)$$

In computing the radiation mechanical resistances r_{MA} and r_{MP} , and the masses m_A and m_P , cognizance must be taken of the reaction of the port on the diaphragm and the reaction of the diaphragm upon the port with the appropriate phase relations.

The electrical power input, in ergs per second, is

$$P_E = r_E i^2, \quad (19)$$

where i = current, in abamperes.

The electrical resistance r_E is the real part of

$$z_E = r_{EV} + jx_{EV} + z_{EM}, \quad (20)$$

where r_{EV} = damped electrical resistance of the voice coil, in abohms,

x_{EV} = damped electrical reactance of the voice coil, in abohms,

z_{EM} = motional electrical impedance, in abohms,

$$z_{EM} = \frac{(Bl)^2}{z_{MT}},$$

z_{MT} = total mechanical impedance, in mechanical ohms,

$$z_{MT} = \frac{z_{M1}z_{M2} + z_{M1}z_{M3} + z_{M2}z_{M3}}{z_{M2} + z_{M3}}.$$

The efficiency, in per cent, of the acoustical phase inverter is

$$\mu = \frac{P_A}{P_E} \times 100. \quad (21)$$

From the above considerations it will be seen that the acoustical phase inverter loud speaker increases the efficiency by a reduction in mechanical reactance due to a system of two degrees of freedom, and by an increase in the radiation mechanical resistance due to the increase in the effective area of the radiating system.

The theoretically predicted and experimentally determined output frequency characteristics of the system of Figure 6 using the driving

mechanism *C* of Figure 1 are shown in Figure 7. A considerable increase in efficiency is obtained over a frequency range of one octave. The magnitude of the efficiency is an inverse ratio of the frequency range of the gain in output. Therefore, the range of high efficiency is limited to about an octave. This frequency range is not sufficient even for a small personal type loud speaker.

HORN LOUD SPEAKER¹

The principal virtue of a horn lies in presenting almost any value of mechanical resistance to the driving system. The horn serves as an acoustical transformer between the relatively small acoustical impedance of air and the large acoustical impedance of the diaphragm. This

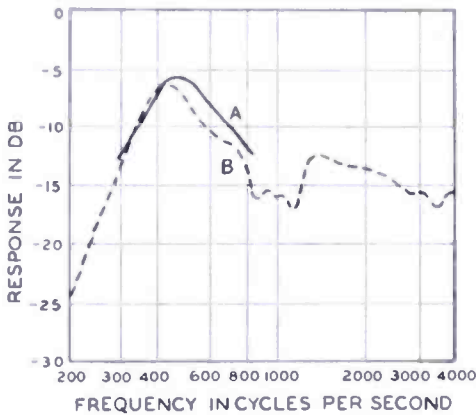


Fig. 7—Theoretical and measured response frequency characteristics of the phase inverter direct radiator loud speaker of Figure 6 using mechanism *C* of Figure 1. A. Theoretical response. B. Measured response. 0 decibels corresponds to an efficiency of 100 per cent.

feature makes it possible to obtain a higher efficiency than in the case of the mass controlled direct radiator loud speaker. The application of a horn to a personal type radio receiver presents some difficulties. Several horn systems were developed, built and tested. These included collapsible horns employing different types of bellows as well as nests of conical and pyramidal sections. In another section the electrical components in the receiver case were arranged so as to form an acoustical path of varying cross-sectional area. Of these arrangements, a collapsible type in which one side of the horn is used for the antenna appeared to be the most practical, because it provided a means of separating the loop antenna from the case. This is desirable from the standpoint of obtaining a high ratio of electrical reactance to electrical resistance in the loop. Perspective and sectional views, and the mechanical network of this horn loud speaker system are shown in Figure 8. It will be seen that the cross-sectional area of the horn increases linearly along the axis. The equation expressing the cross-sectional area as a function of the distance along the axis in a parabolic form is

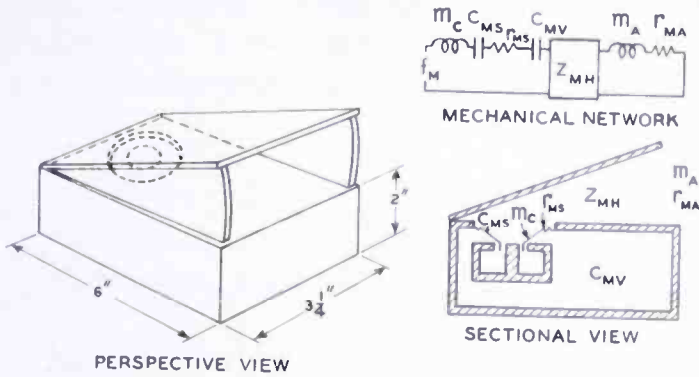


Fig. 8—Perspective and sectional views and the mechanical network of a horn loud speaker. In the mechanical network: f_M = driving force. m_c = mass of the cone and coil. C_{MS} = compliance of the suspension system. C_{MV} = compliance of the case volume. Z_{MH} = quadripole representing the horn. m_A = mass of the air load at the horn mouth. r_{MA} = mechanical resistance of the air load at the horn mouth.

$$S = S_1 x_1. \tag{22}$$

The mechanical impedance at the throat of a parabolic horn in terms of the mechanical impedance at the mouth and the dimensions of the horn is

$$z_{M1} = j\rho ck S_1 \left[\frac{z_{M2} [J_0'(kl_2) Y_0(kl_1) - J_0(kl_1) Y_0'(kl_2)]}{z_{M2} [J_0'(kl_2) Y_0'(kl_1) - J_0'(kl_1) Y_0'(kl_2)]} + \frac{j\rho ck S_2 [J_0(kl_1) Y_0(kl_2) - J_0(kl_2) Y_0(kl_1)]}{j\rho ck S_2 [J_0'(kl_1) Y_0(kl_2) - J_0(kl_2) Y_0'(kl_1)]} \right], \tag{23}$$

- where J_0 = Bessel function of the first kind,
- Y_0 = Bessel function of the second kind,
- l_1 = distance from the apex to the throat, in centimeters,
- l_2 = distance from the apex to the mouth, in centimeters,
- S_1 = area of the throat, in square centimeters,
- S_2 = area of the mouth, in square centimeters,
- ρ = density of air, in grams per cubic centimeter,
- c = velocity of sound, in centimeters per second,
- $k = 2\pi/\lambda$,
- λ = wavelength, in centimeters,
- $z_{M2} = r_{M2} + jx_{M2}$ mechanical impedance at the mouth, in mechanical ohms.

The mouth is considered to radiate into 4π solid angles. Under these conditions the mechanical resistance, in mechanical ohms, of the air load upon the mouth of the horn is given by

$$r_{M2} = \frac{1}{4\pi^2} \rho c k^2 S_2^2 \quad (24)$$

The approximate mass, in grams, of the air load upon the mouth is

$$m_{A2} = .35\rho S_2^{3/2}. \quad (25)$$

The mechanical reactance, in mechanical ohms, of the air load upon the mouth is

$$x_{M2} = \omega m_{A2}. \quad (26)$$

From the mechanical network the velocity, in centimeters per second, is,

$$\dot{x} = \frac{f_M}{z_{MT}} \quad (27)$$

where $f_M = Bli$, the driving force, in dynes,

B = flux density, in gaussess,

l = length of the voice coil conductor, in centimeters,

i = current in the voice coil, in abamperes,

$$z_{MT} = r_{MS} + j\omega m_c + \frac{1}{j\omega C_{MS}} + \frac{1}{j\omega C_{MV}} + z_{M1} \left(\frac{S_c}{S_1} \right)^2$$

r_{MS} = mechanical resistance of the suspension system of the loud speaker mechanism, in mechanical ohms,

m_c = mass of the cone and the air load on the back of the cone, in grams,

C_{MS} = compliance of the suspension system, in centimeters per dyne,

C_{MV} = compliance of the case volume, in centimeters per dyne,

z_{M1} = impedance at the throat of the horn, in mechanical ohms,

S_c = area of the cone, in square centimeters, and

S_1 = area at the throat of the horn, in square centimeters.

The resistive and reactive components at the throat of the horn shown in Figure 8 are shown in Figure 9.

The acoustical power output, in ergs per second, is

$$P_A = r_{M1} \dot{x}^2, \tag{28}$$

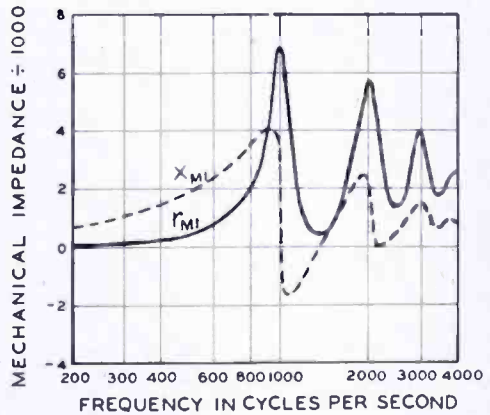
where r_{M1} = real part of the mechanical impedance at the throat of the horn, in mechanical ohms.

The electrical power output, in ergs per second, is

$$P_E = r_E i^2, \tag{29}$$

where i = current, in abamperes.

Fig. 9—Mechanical impedance frequency characteristics at the throat of the horn. r_{M1} = mechanical resistance. x_{M1} = mechanical reactance.



The electrical resistance r_E is the real part of

$$z_E = r_{EV} + jx_{EV} + z_{EM}, \tag{30}$$

where r_{EV} = damped electrical resistance of the voice coil, in abohms,
 x_{EV} = damped electrical reactance of the voice coil, in abohms,
 z_{EM} = motional electrical impedance, in abohms,

$$z_{EM} = \frac{(Bl)^2}{z_{MT}}$$

The efficiency, in per cent, of the horn loud speaker is

$$\mu = \frac{P_A}{P_E} \times 100. \tag{31}$$

The theoretically predicted and experimentally determined output frequency characteristics of the system of Figure 8 using driving mechanism *C* of Figure 1 are shown in Figure 10.

The output frequency characteristics of the same unit as a direct radiator loud speaker are shown in Figures 4 and 5. It will be seen that an increase of efficiency over the direct radiator system of about 6 decibels is obtained in the frequency from 700 to 5000 cycles. The response falls off below 700 cycles. To obtain a uniform response down to 300 cycles would require a larger horn. This is practically impossible for a case of the dimensions specified in Figure 2. However, there is another possibility, namely, the combination of a horn and phase inverter.

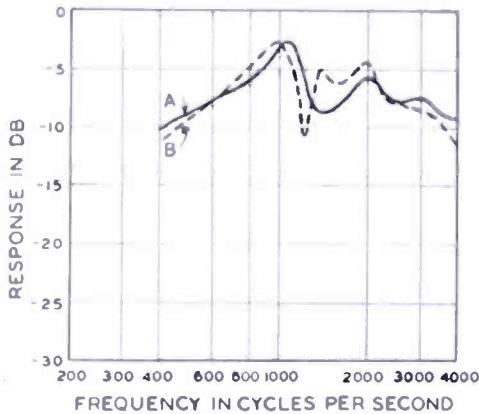


Fig. 10—Theoretical and measured response frequency characteristics of the horn loud speaker of Figure 8 using mechanism *C* of Figure 1. A. Theoretical response. B. Measured response. 0 decibels corresponds to an efficiency of 100 per cent.

COMBINATION HORN AND PHASE INVERTER LOUD SPEAKER

From the considerations in the two preceding sections, it appears that a combination horn and direct radiator loud speaker with phase inversion would be the logical solution for a high efficiency loud speaker for personal radio receivers. Perspective and sectional views and the mechanical network of a combination horn and phase inverter loud speaker are shown in Figure 11. With the horn collapsed, the dimensions are the same as those of the case for the back enclosed direct radiator loud speaker of Figure 2. The experimentally determined response frequency characteristic of the combination horn and acoustical phase inverter loud speaker, using the driving mechanism *C* of Figure 1, is shown in Figure 12. Comparing this characteristic with the response frequency characteristic of Figure 5, it will be seen that the gain in efficiency by the use of a horn and acoustical phase inverter system, over a direct radiator loud speaker using the same driving mechanism, is 6 decibels. In comparison to a conventional small direct radiator loud speaker unit, that is, the same diaphragm but a copper

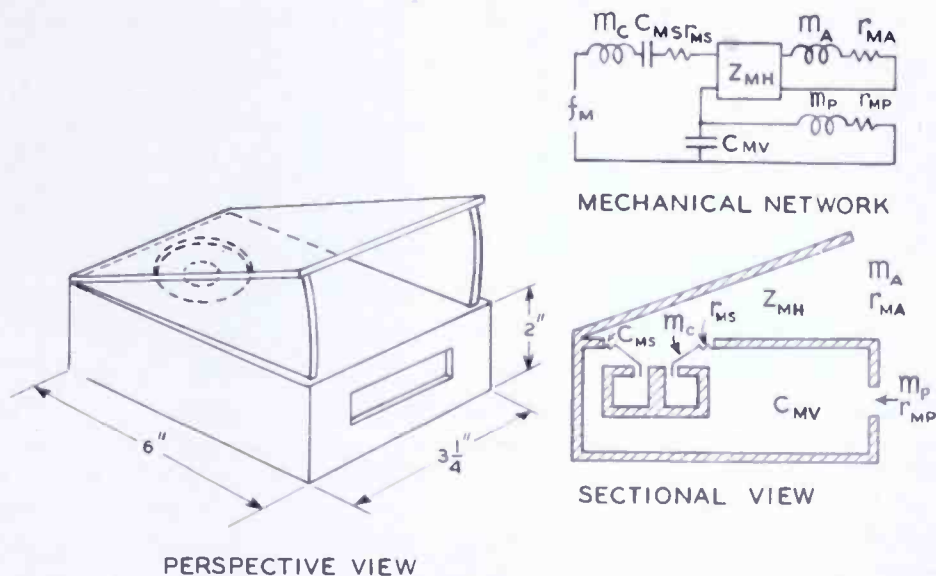
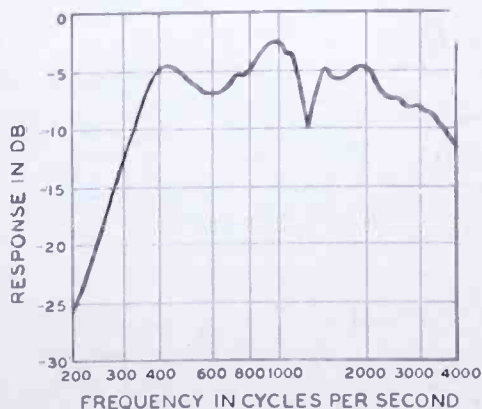


Fig. 11—Perspective and sectional views and the mechanical network of a combination horn and phase inverter loud speaker. In the mechanical network: f_M = driving force. m_c = mass of the cone and coil. C_{MS} = compliance of the suspension system. r_{MS} = mechanical resistance of the suspension system. C_{MV} = compliance of the case volume. Z_{MH} = quadripole representing the horn. m_A = mass of the air load at the horn mouth. r_{MA} = mechanical resistance of the air load at the horn mouth. m_P = mass of the air in the port. r_{MP} = mechanical resistance of the air load of the port.

voice coil and 10,000 gauss in the air gap, unit A, the gain is 15 decibels or 32 to 1 in efficiency.

With a loud speaker having an efficiency of 25 per cent, it is possible to obtain a sound level of 84 decibels at three feet with an input of 10 milliwatts. This level is somewhat higher than conversational speech. This loud speaker makes it possible to use subminiature tubes and very small B batteries. For example, the output of subminiature output tubes with 45 volt plate supply and plate current of 1.2 milliamperes for 10 per cent distortion is 15 milliwatts. With a loss of .6 decibels

Fig. 12—Measured response frequency characteristic of the combination horn and phase inverter loud speaker of Figure 11 using mechanism C of Figure 1. 0 decibels corresponds to an efficiency of 100 per cent.



in the transformer this turns out to be 13 milliwatts at the loud speaker.

PERSONAL RECEIVERS EMPLOYING COMBINATION HORN AND DIRECT RADIATOR LOUD SPEAKER

Personal radio receivers employing the combination horn and phase inverter loud speaker have been developed and built. The electrical circuit of the receiver used is shown in Figure 13. This is a conventional superheterodyne receiver employing four subminiature tubes. The loop for the receiver is located in the lid, that is, the large flat surface of the collapsible horn. The sensitivity is comparable to that of a conventional personal radio receiver using miniature tubes. A

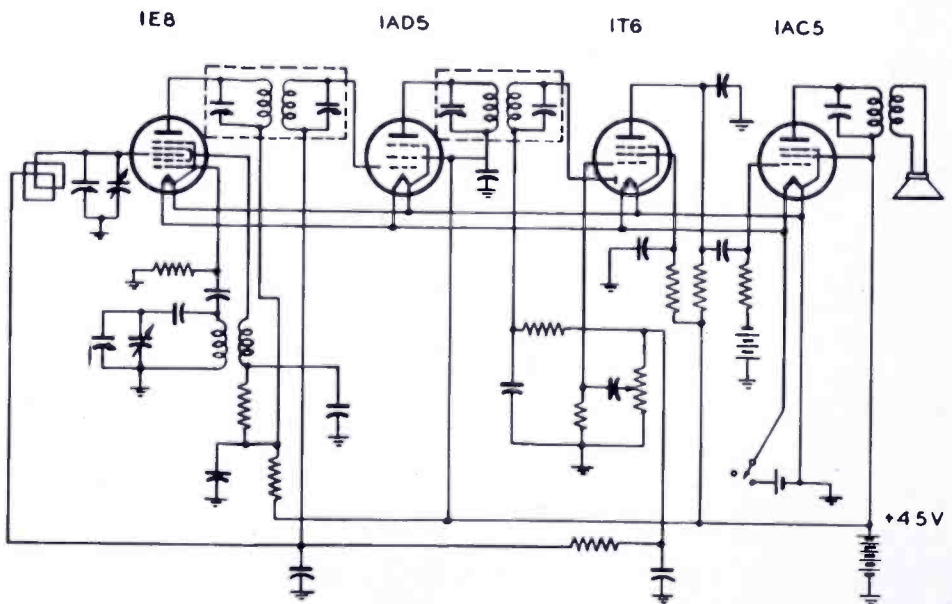


Fig. 13—Electrical circuit diagram of the laboratory model personal radio receiver using subminiature tubes.

photograph of a laboratory model of a personal radio receiver having the case dimensions of Figure 11 with the lid closed, or in the non-operating condition, is shown in Figure 14. The same receiver with the lid open forming the horn, which is the operating condition, is shown in Figure 15. The exterior content of this radio receiver is 41 cubic inches.

Following the work outlined in this paper it was found that a further reduction in size could be obtained without much reduction in low frequency response. Photographs of a smaller radio receiver are shown in Figures 16, 17 and 18. The exterior content of this radio receiver is 25 cubic inches.

A photograph of the RCA-BP10 and the RCA-54B commercial



Fig. 14—Photograph of the laboratory personal radio receiver model 1 with the lid closed. Dimensions: $6'' \times 3\frac{3}{8}'' \times 2\frac{1}{32}''$.



Fig. 15—Photograph of the laboratory personal receiver model 1 with the lid open forming the horn which is the operating condition.

personal radio receivers, and the two laboratory model personal radio receivers described above are shown in Figure 19. The exterior content of the BP10 is 105 cubic inches and the exterior content of the 54B is 89 cubic inches.

A graph showing the exterior cubical content of portable radio receivers as a function of time, starting with the year 1923, is shown in Figure 20. The reduction in size has been accomplished through the continuous research and development of tubes, batteries, transformers, capacitors, resistors, and loud speakers with the object of reducing the size and improving the performance.

The electrical input to the loud speaker in the two laboratory models of personal radio receivers using the combination horn and direct radiator loud speaker with phase inversion is 13 milliwatts at the loud speaker. The electrical input to the direct radiator loud

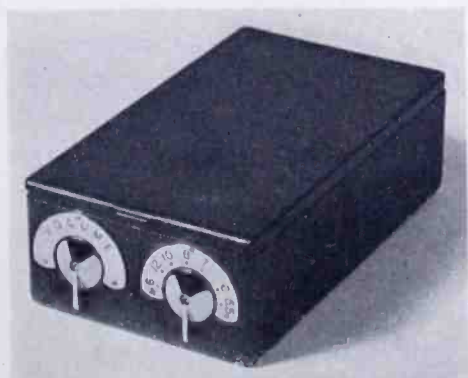


Fig. 16—Photograph of the laboratory personal radio receiver model 2 with the lid closed. Dimensions: $5\frac{1}{8}'' \times 3'' \times 1\frac{5}{8}''$.

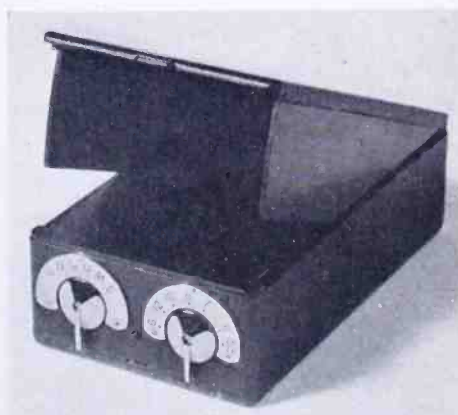


Fig. 17—Photograph of the laboratory model of the personal radio receiver model 2 with the lid open forming the horn which is the operating condition.

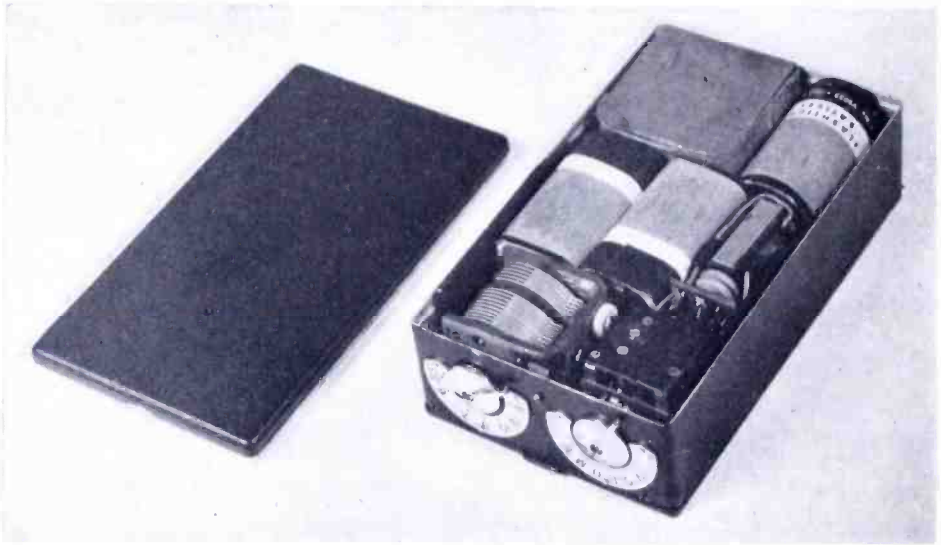


Fig. 18—Photograph of the laboratory model of the personal radio receiver model 2 with the back lid removed showing the arrangement of the components of the receiver.



Fig. 19—Photograph of the RCA-BP10 and RCA-54B commercial personal radio receivers and the two laboratory models, 1 and 2.

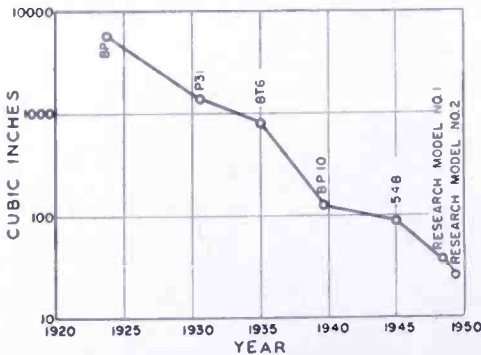


Fig. 20—Graph showing the exterior cubical content of portable and personal radio receivers starting with the year 1923.

speaker in the 54B is 65 milliwatts. In spite of the large difference in size and electrical output, the frequency range and maximum acoustical output of the small radio receivers with the combination horn and direct radiator loud speaker with phase inversion are comparable to, or better than, the large personal radio receivers with direct radiator loud speakers.

A STUDY OF COCHANNEL AND ADJACENT-CHANNEL INTERFERENCE OF TELEVISION SIGNALS*

A Report

BY

RCA LABORATORIES DIVISION, PRINCETON, N. J.

Part I—Cochannel Studies

Summary—The reduction of cochannel television interference with monochrome signals, color television signals, and combinations of monochrome and color signals by the use of the offset-carrier (10.5 kilocycles) method has been investigated in the laboratory through the medium of observer tests. Included in the study are the field-sequential, the line-sequential, and the dot-sequential color systems. The results of extensive field and laboratory experiments with synchronization of monochrome television carriers are reported in detail. On the basis of subjective viewing of interference by observers, ratios of desired to interfering carrier strengths are listed for tolerable interference and perceptible interference. Such data lead to a rational criterion for the allocation of monochrome and color television stations on an offset carrier (10.5 kilocycles) basis.

GENERAL DISCUSSION

IN THE Fall of 1948, when the Federal Communications Commission (FCC) held hearings on the problem of cochannel interference of very-high-frequency (VHF) television stations, established the Ad Hoc Committee to review the available data on tropospheric propagation in order to arrive at an acceptable method of predicting interference, and instituted the "freeze" on new television station construction, the Radio Corporation of America accelerated its program of development on a television carrier synchronizing system. At the engineering conference, December 2, a report on the laboratory tests concerning television carrier synchronization was made and the equipment used in the Princeton laboratory to synchronize WNBT, New York, with WNBW, Washington was described.

Early in 1949, the synchronizing equipment was moved to a field site midway between New York and Washington and field observations of the operation of the system were made for a period of several months. Concurrent with these tests, further laboratory development

* Decimal Classification: R171×R430.11×R583.16.

was progressing which resulted in "offset carrier" operation. This latter method was simpler in operation, was more economical of equipment, and yielded results superior to television carrier synchronization. Field experience with a number of Channel 4 stations followed. In the Summer of 1949, quantitative data was obtained in the laboratory, in cooperation with the Joint Technical Advisory Committee (JTAC) of the Institute of Radio Engineers and the Radio Manufacturers Association with a large number of observers, to determine the probable desired-to-undesired signal ratio for unsynchronized signals, for synchronized signals, and for signals using offset carriers. These laboratory tests, as well as much field experience, firmly established the fact that offset carrier was a simple and effective method of reducing co-channel interference.

It is the purpose of this report to describe the early work on television carrier synchronizing, to discuss the offset carrier method and describe field observations of the method, to discuss briefly the JTAC observer tests, and to describe more recent work carried out by RCA in determining the desired-to-undesired signal ratios for offset carrier operation as applied to the RCA dot-sequential color television system and the Columbia Broadcasting System field-sequential color television system and in attempting to determine the appropriate ratios for the Color Television, Incorporated line-sequential color television system.

PRELIMINARY EXPERIMENTS WITH SYNCHRONIZED TELEVISION CARRIERS

When two cochannel television stations are operated normally, the carrier frequencies may differ by only a few cycles, by fifty to one hundred cycles, and at times by several hundred cycles. The resultant beat between the carrier of the desired signal and the carrier of the interfering signal appears as horizontal moving black bars in the television picture. With increased interfering signal, the undesired picture appears in the background of the desired picture. Experience has shown that the horizontal bars due to carrier beat become objectionable when the undesired picture in the background is barely visible. With the two carriers precisely synchronized in frequency, the moving bars are completely eliminated and the undesired picture becomes the next source of interference to be considered. Under this condition of precise synchronization, the improvement to be obtained depends upon the relative phases of the two carriers at the receiving point. If the two carriers could be held precisely in time quadrature, the largest improvement would be secured. The least improvement is achieved when the carriers are in phase or in phase opposition. Hence, in observer tests carried out in the laboratory to determine improvement ratios, it

seemed desirable to determine the improvement ratios which applied in the least favorable phase condition.

A laboratory test was conducted with twenty-five observers. The observers were shown a television picture with an unsynchronized signal as a source of interference. The interfering signal was adjusted to a value which the observer indicated to be objectionable. Then the carrier frequencies were synchronized, adjusted to the least favorable phase, and the undesired signal increased until the observer felt that the interference was of the same degree of objectionableness as for the unsynchronized condition. The improvement factor was taken as the number of decibels which the undesired signal was increased from the unsynchronized case to the synchronized case. The results of this laboratory test are shown in Figure 1, expressed as a probability distribution in terms of the percentage of observers noting an improvement greater than the corresponding ordinate value. It may be noted from Figure 1 that fifty per cent of the observers experienced an improvement of 17 decibels in favor of carrier synchronization.

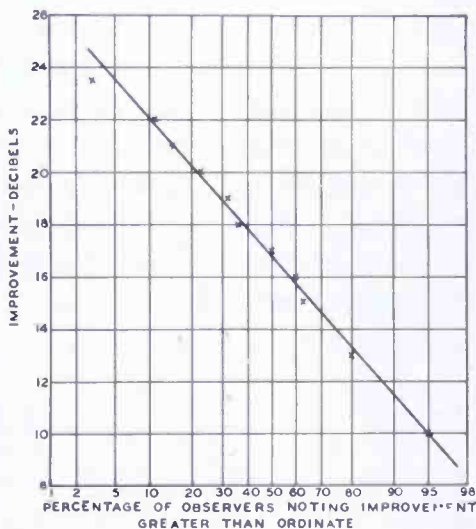


Fig. 1—Improvement in reception of a television signal in the presence of a cochannel interfering signal. (The improvement factor is that obtained with synchronized carriers in the least favorable relative phase, with nonsynchronous operation used as the reference standard.)

To obtain field experience under home receiving conditions, equipment was assembled which made possible the carrier synchronization of television station WNBT, New York, with WNBW in Washington. The equipment used in conducting the synchronizing test consisted of two units. The first unit was located in the RCA Laboratories in Princeton, New Jersey, and the second was located at Station WNBT in New York. The equipment at the Princeton Laboratories included two narrow-band superheterodyne receivers. The voltage from a single local oscillator was applied to the first detectors of both receivers, thus the frequency difference between the two incoming signals was retained. The output signals from the two intermediate-frequency amplifiers were mixed in a phase discriminator, the output voltage of which was a measure of the phase difference between the two incoming carriers. The output voltage of the phase discriminator was used to

the WNBT signal was in an open field and had a back lobe of 12 per cent, so the antenna was turned slightly to further suppress the WNBW signal.

The transmitter control gear was installed at WNBW and a telephone line connected the receiving equipment at Brandywine with WNBW control equipment. Both the transmitter control equipment and the receiving equipment were those previously used at Princeton. Synchronization of WNBW and WNBT, using the Brandywine installation, began on January 22, 1949, and continued for several months. Shortly after the start of operations at Brandywine, the RCA Victor Division supplied new equipment of a more advanced design for use at Brandywine and at WNBW. This equipment included refinements not used in the original equipment, and in addition provided the means for synchronizing three stations. This was done in anticipation of the time when WGAL-TV, in Lancaster, Pennsylvania, would begin broadcasting on Channel 4. This latter receiving station synchronizing equipment and the transmitter control units are shown in Figure 5 and Figure 6, respectively.

Continued observations of signal reception in the fringe areas of WNBT and WNBW showed that the application of carrier synchronization had indeed proven beneficial to viewers who had been troubled by cochannel interference. As a result of the experience gained with the Brandywine installation, plans were made with the General Electric Company and the Westinghouse Radio Stations, Incorporated, to establish a receiving point at Wilbraham, Massachusetts, with the necessary equipment to synchronize WBZ-TV in Boston and WRGB in Schenectady with WNBT. Receiving antennas were erected and some equipment was installed at Wilbraham in preparation for this next step. This project was halted by the advent of "offset carrier" operation, which had resulted from continued research at RCA Laboratories on the problem of cochannel interference. Since it was soon apparent that offset operation was extremely simple, very economical, and yielded results superior to television carrier synchronization, the Wilbraham project was dropped, the Brandywine operation ceased, and offset carrier experiments were immediately started with WNBT and WNBW.

EXPERIMENTS WITH OFFSET CARRIERS

For the condition of nonsynchronous operation where there are four or five horizontal black bars in the picture, there are sections of positive and negative interfering pictures corresponding to the cycles of the beat between the two carriers. With this observation as a basis, it was concluded that if the beat difference between the two carriers were made to correspond exactly to one-half the line frequency, a

condition would be obtained where not only would the beat between carriers be a very fine pattern, but also the odd and even lines would contain interfering pictures of opposite polarities, with a tendency to integrate out when observed at normal viewing distance. To check this condition, an experimental arrangement was made in the laboratory

where the carrier of the local signal was offset by precisely 7,875 cycles with respect to the interfering signal. A group of twenty-five observers was used to obtain the data shown in Figure 7, which

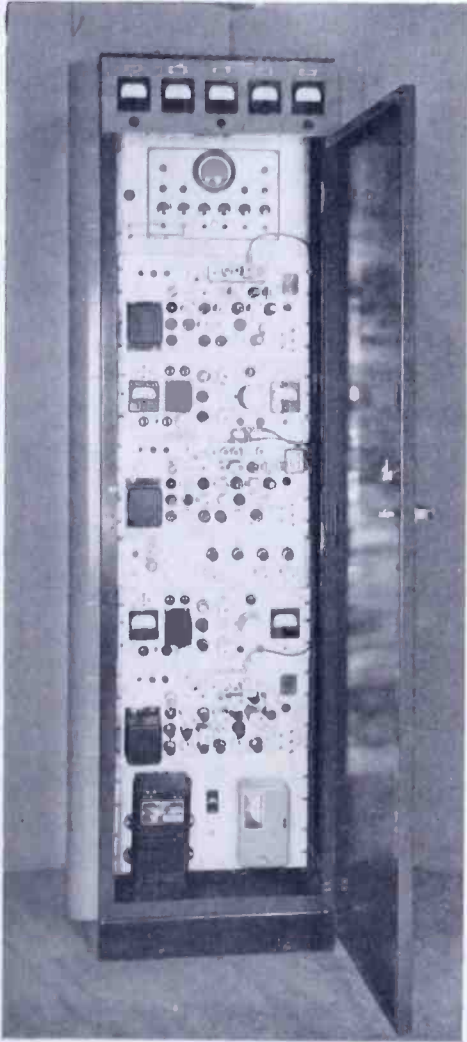


Fig. 5—Television carrier synchronization equipment, receiving station rack.

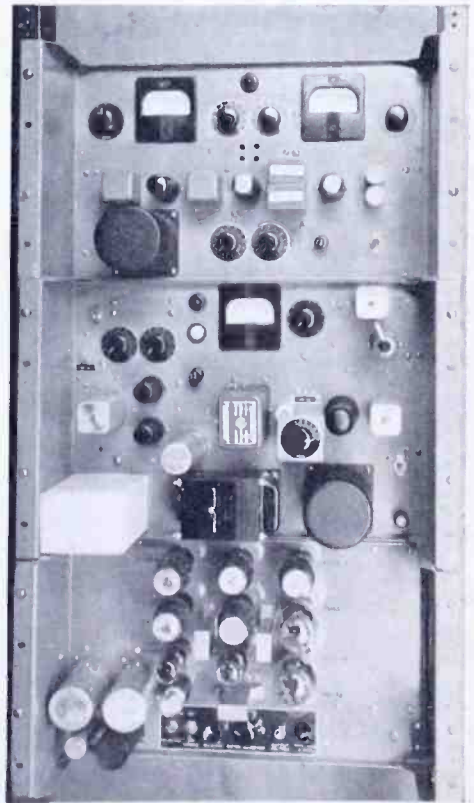


Fig. 6—Television carrier synchronization equipment, transmitter control units.

shows the improvement obtained by this precise offset method with respect to the normal unsynchronized condition. It may be seen from Figure 7 that fifty per cent of the observers experienced an improvement of at least 25 decibels. This was an improvement of approximately 8 decibels over the synchronized carrier condition.

To operate two stations under this condition requires the same equipment as used for carrier synchronization plus a few items of

auxiliary equipment required to produce the precise displacement of one-half line frequency, or 7,875 cycles obtained by dividing the actual received line frequency by 2. The precision of frequency control required to obtain the full advantage of this method of operation requires that the synchronizing generators at both transmitters be operated from crystals, rather than from 60-cycle power supplies which may not be tied into the same power network.

At the completion of this series of laboratory tests, it was thought that perhaps the frequency tolerance specified above for the half-line frequency condition could be reduced in exchange for some of the 8-

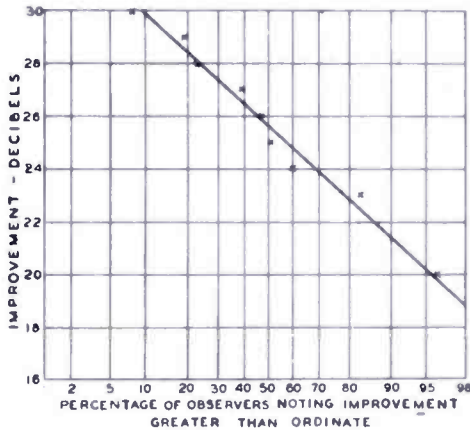


Fig. 7—Improvement in reception of a television signal in the presence of a cochannel interfering signal. (The improvement factor is that obtained with carriers offset by one-half line frequency, 7875 cycles, with nonsynchronous operation used as a reference standard.)

decibel improvement obtained over the synchronized condition. In other words, if the frequency tolerance for the half-line frequency operating condition could be made the same as the normally-specified transmitter crystal stability, the 8-decibel improvement over the synchronous condition could be sacrificed to obtain this simple operating condition. If this arrangement were at least equal to the synchronized condition, it would be without the equipment difficulties, telephone line charges, personnel and plant facilities required for synchronized operation.

To determine the improvement as a function of the difference frequency between the two transmitter carriers, additional laboratory measurements were made. A group of observers made observations at a number of offset carrier frequencies. The curve of Figure 8 was the result. To obtain this data, the difference frequency between the two carriers was adjusted to give the fine horizontal black bars their most objectionable appearance, that is, they moved slowly either up or down in the picture. The data presented in Figure 8 is for the worst condition that could be realized for a given nominal offset or difference frequency between the two carriers. From the curve of Figure 8, it is seen that at a nominal half-line frequency difference between the two carriers, an improvement of approximately 20 decibels is obtained, as compared to the 25-decibel improvement obtained at the precise half-line frequency.

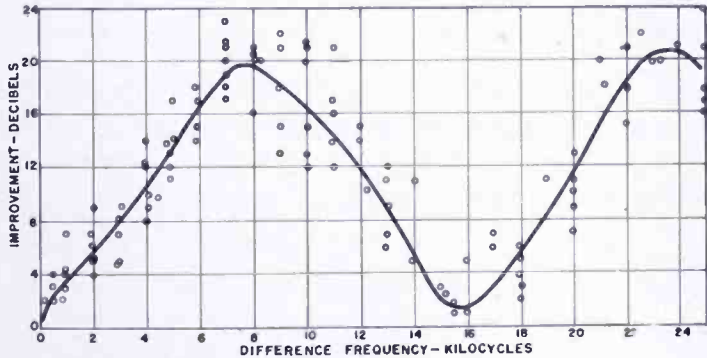
8-

decibel improvement obtained over the synchronized condition. In other words, if the frequency tolerance for the half-line frequency operating condition could be made the same as the normally-specified transmitter crystal stability, the 8-decibel improvement over the synchronous condition could be sacrificed to obtain this simple operating condition. If this arrangement were at least equal to the synchronized condition, it would be without the equipment difficulties, telephone line charges, personnel and plant facilities required for synchronized operation.

To determine the improvement as a function of the difference frequency between the two transmitter carriers, additional laboratory measurements were made. A group of observers made observations at a number of offset carrier frequencies. The curve of Figure 8 was the result. To obtain this data, the difference frequency between the two carriers was adjusted to give the fine horizontal black bars their most objectionable appearance, that is, they moved slowly either up or down in the picture. The data presented in Figure 8 is for the worst condition that could be realized for a given nominal offset or difference frequency between the two carriers. From the curve of Figure 8, it is seen that at a nominal half-line frequency difference between the two carriers, an improvement of approximately 20 decibels is obtained, as compared to the 25-decibel improvement obtained at the precise half-line frequency.

From Figure 8, it is seen that as the difference frequency between the two carriers is further increased, a minimum improvement is approached at line frequency, and again another favorable interference condition is reached at one and one-half times line frequency. With the data of Figure 8 in mind, it is seen that in a situation where three stations are involved, one station could be on frequency, the second station displaced half-line frequency above, and the third station displaced half-line frequency below. With this arrangement, the interference between stations 1 and 2 and between stations 1 and 3 would be at a minimum. However, the interference between stations 2 and 3, which would have a carrier difference corresponding to line frequency, could be very severe or at best little if any improvement would be noticed. To overcome this difficulty in a three-station situation, it was proposed that a displacement in carrier frequency of not half-line frequency but 10.5 kilocycles be used. Again referring to Figure 8, it is

Fig. 8—Improvement in reception in the presence of a co-channel interfering signal as a function of the frequency difference between carriers. (Fine adjustment of frequency for maximum visibility of interference.)



seen that with an offset of 10.5 kilocycles, an improvement of approximately 15 decibels is obtained. Also the frequency difference between stations 2 and 3 is now 21 kilocycles, with an improvement of approximately 15 decibels.

In order to put laboratory experience to a field test in the simplest form, it was only necessary to obtain a new crystal for the WNBT picture transmitter and another new crystal for the WNBT frequency monitor and to secure permission from the FCC to make this slight shift in frequency for experimental purposes. During the late Spring of 1949, observations in home receiving locations were made in the Princeton area. It was soon apparent that this simple offset carrier method was extremely effective in reducing cochannel interference on Channel 4 in the fringe area. Many demonstrations were made during this period where the WNBT frequency was periodically returned to its normally assigned value. The improvement due to offset carrier operation was indeed striking.

On June 17, 1949, WNBT in New York was returned to its normally

assigned frequency. At the same time, WBZ-TV, WRGB, and WNBW were offset 10.5 kilocycles from WNBT. Station WGAL-TV, Lancaster, began offset operation on June 24. Thus by late June, these five Channel 4 stations were operating in offset conditions planned to yield substantial mutual protection. The offset frequency conditions are listed in Table I.

Table I—Offset Carrier Conditions of Channel 4 Stations

Station	Effective Radiated Power (kilowatts)	Antenna Height Above Average Terrain (feet)	Frequency (kilocycles)
WRGB, Schenectady, N. Y.	18.25	832	67,250+10.5
WBZ-TV, Boston, Mass.	14.3	547	67,250-10.5
WNBT, New York, N. Y.	7.0	1280	67,250
WNBW, Washington, D. C.	20.5	330	67,250-10.5
WGAL-TV, Lancaster, Pa.	1.0	260	67,250+10.5

A panel truck was equipped with measuring gear for making observations and measurements in the field. An RCA-8TS30 television receiver, an RCA-WX1A Field Intensity Meter with Esterline-Angus recorder, a Hewlett Packard 200C audio oscillator, and an RCA-TMV122B oscillograph were included. The field intensity meter, together with the oscillograph and audio oscillator, afforded a simple and accurate means of determining the frequency difference between pairs of stations.

Picture observations were made in fringe area cities, localities where average field intensities ranged from 200 to 800 microvolts



Fig. 9—Fringe area cities where observations of cochannel interference were made.

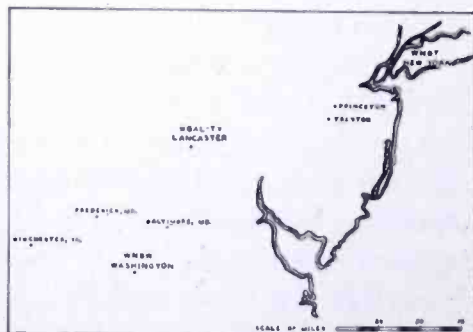


Fig. 10—Fringe area cities where observations of cochannel interference were made.

per meter. In each of the fringe area cities, the field intensity meter and recorder were used to make a survey through the particular city to determine the range of variation of field intensity and the median field intensity. Figures 9 and 10 show the fringe area cities visited during the Summer of 1949. Table II shows the results of field intensity measurements in these cities.

Table II—Field Strength in Fringe Area Cities

	Distance Miles	Surveyed Station	Field Intensity Corrected to 30 feet Microvolts per Meter		
			Median Field	Minimum	Maximum
Adams, Mass.*		WRGB			
Baltimore, Md.	13.0	WNBW	320	80	1200
Bridgeport, Conn.	3.2	WNBT	240	80	480
Fall River, Mass.	2.5	WBZ-TV	150	80	400
Frederick, Md.	2.2	WNBW	300	60	400
N. Adams, Mass.*		WRGB			
Newburgh, N. Y.	1.7	WBZ-TV	90	60	140
Norwalk, Conn.	3.3	WNBT	500	240	1200
Peekskill, N. Y.	1.4	WNBT	1100	240	8000
Pittsfield, Mass.	2.1	WRGB-TV	320	100	520
Providence, R. I.	5.4	WBZ-TV	120	40	400
Westport, Conn.	1.0	WNBT	590	240	1200
Worcester, Mass.	4.3	WBZ-TV	300	80	1400
Newport, R. I.	0.8	WNBT	120	40	280

* Field strength too low to be usable.

While observations were being made in each locality, the desired station and the nearest cochannel interfering station were operated, first with nominally the same frequencies but nonsynchronous, and secondly with carriers offset 10.5 kilocycles. Thus direct comparisons of the two modes of operation were made under like receiving conditions.

Characteristic moving bars or flickering pictures were generally seen in the first case and fine bars in the second. In every case where it was possible to see the fine bars of offset carrier operation, the picture deteriorated severely when the operation was shifted to the same nominal frequencies. The change was conspicuous and was seen repeatedly. The observers were thoroughly convinced by many field demonstrations of the value of offset carrier operation.

It should be pointed out that the most objectionable thing about nonsynchronous operation is either the movement of the bars or the

overall changes in average brightness of the picture which appears as flicker when the frequency difference is between frame frequency and zero beat.

During the field tour, WNBT picture was received well in Peekskill, Newburgh and Poughkeepsie, New York, except in depressions. WRGB is evidently quite well eliminated from this area by the Catskill Mountains which are also responsible for poor reception in Catskill, New York, of WRGB. Only a few miles east in Hudson, New York, WRGB was received well with little WNBT interference. In and to the north and south of Catskill, WNBT interference was very severe, with either nonsynchronous or offset operation. In many places in this locality, WNBT field strength exceeded WRGB. In western Massachusetts, WRGB was received well in Pittsfield and poorly in Great Barrington, Adams and North Adams. There was very little cochannel interference, day or night, probably because of the proximity of the Berkshires. All of these towns are surrounded by large hills.

Reception of WBZ-TV in Fitchburg, Worcester, Providence and Fall River, Massachusetts, was very good, with only slight traces of fine bars due to cochannel interference with offset operation. Severe interference from WNBT was observed in Newport, Rhode Island, at times, but again the improvement due to offset carrier operation was apparent.

WNBT was received well in Bridgeport and Norwalk, Connecticut. There was interference from WBZ-TV in Norwalk and interference from both WBZ-TV and WRGB in Bridgeport. However, with offset carrier operation, the pictures from WNBT were quite satisfactory. Good pictures from WNBT (over 110 miles across Long Island Sound) were seen in Mystic, Connecticut, in spite of strong WBZ-TV interference.

Very acceptable pictures were received from WNBT in Princeton and Trenton, New Jersey, throughout the Summer. Close scrutiny of the received picture revealed fine lines due to cochannel interference when offset carrier operation was used, while nonsynchronous operation usually resulted in a far from satisfactory picture.

The RCA Service Company reports that the Washington area cochannel interference problem has never been serious. Fringe area cities include only Baltimore, Annapolis and Frederick, Maryland. Baltimore television viewers are discouraged from use of Channel 4 because it is noisy relative to Baltimore stations and therefore cochannel interference complaints have been very few. In Frederick, the Channel 4 pictures are very noisy with no complaints of cochannel

interference. Annapolis cochannel interference complaints have been greatly reduced by offset carrier operation.

During the field tour, no cochannel interference was seen in Baltimore, but slight interference was observed a few miles north of Baltimore. No cochannel interference was observed in Frederick or reported by the local RCA dealer.

Severe cochannel interference was observed in Winchester, Virginia, where field strengths of WNBW are seldom over 300 microvolts per meter. Again offset carrier operation proved beneficial.

OBSERVER TESTS OF COCHANNEL INTERFERENCE,
IN COLLABORATION WITH JTAC

In the research phases of the program on television carrier synchronization and on offset carrier operation, observer data were obtained which showed the improvement of the two methods in terms of nonsynchronous operation. To be useful for allocation purposes, the data must consist of ratios of desired to undesired signal for a given method of operation, rather than of an improvement factor of one system over another. The assembly of such data requires a large amount of equipment and observations by many observers under controlled conditions.

In July, 1949, the facilities and assistance of RCA Laboratories were made available to JTAC in order to accumulate the desired data.

The television system tested was the standard black-and-white signal using 60 fields and 525 lines, interlaced in the usual manner. One hundred observers were used in the tests, and threshold and tolerable ratios of desired to undesired signal were obtained for three conditions of operation: 1, nonsynchronous; 2, synchronous; and 3, 10.5-kilocycle offset. A complete description of the tests and delineation of the data is contained in Proceedings of JTAC, Vol. 4, September 26, 1949, COMMENTS ON THE PROPOSED ALLOCATIONS OF TELEVISION BROADCAST SERVICES. A summary of the pertinent data is shown in Table III.

Table III—Minimum Ratios of Desired RF Signal to Undesired RF Signal as Obtained for Fifty Per Cent of the Observers in the JTAC Observer Tests, July, 1949.

	Type of Interference		
	Nonsynchronous	Synchronous	10.5-Kilocycle Offset
Threshold ratio	54.5 decibels	40.0 decibels	36.0 decibels
Tolerable ratio	44.6 decibels	32.4 decibels	27.2 decibels

These observer tests showed that synchronous operation was twelve decibels better than nonsynchronous operation with respect to tolerable ratios of desired to undesired signal, while 10.5-kilocycle offset was seventeen decibels better than nonsynchronous operation. The results of these extensive JTAC tests fully demonstrated the soundness of the philosophy behind the principle of offset carrier operation.

OBSERVER TESTS OF COCHANNEL INTERFERENCE WITH COLOR TELEVISION SYSTEMS

During the course of the hearings before the FCC in the Fall of 1949, three color television systems were advanced, namely, the field-sequential system, the line-sequential system, and the dot-sequential system. In order to establish a television allocation plan which included one of the above color systems as well as the present monochrome system, it will be necessary to have knowledge of the tolerable desired to undesired cochannel interference ratios for the color system in question as well as for the color system versus a standard monochrome system. Experiments were begun in October, 1949, in order to obtain data on this important question for the three color systems under consideration.

A. Field-sequential color television system

In the standard monochrome television system with 525 lines, 60 fields, and 30 frames, the line frequency is 15,750 cycles per second. Figure 8 showed that the maximum improvement in the operation of the offset carrier system occurred at one-half of line frequency or 7,875 cycles per second. A minimum improvement appeared at 15,750 cycles where beats occurred between the line frequency and the interfering carrier. It may be recalled that an offset of 10,500 cycles was chosen as a compromise which also gave protection in a three-station plan. The proposed field-sequential color television system has 405 lines, 144 fields, and 72 frames. Hence the line frequency is 29,160 cycles per second. From previous experience with offset operation, one quickly arrives at the conclusion that for maximum protection to this field-sequential system when the interfering signal is a similar field-sequential signal, the carriers should be offset by 14,580 cycles and that little improvement would be achieved with the carriers offset 29,160 cycles. It would seem reasonable to expect that 10,500 cycles and 21,000 cycles of offset carrier would be as effective for the field-sequential system as it was for standard monochrome.

The Columbia Broadcasting System has proposed that a dual set of standards be established which would permit some stations to operate

in color with the field-sequential system, while others continued to operate on the present monochrome standards. It seemed desirable to first investigate the interference conditions for this dual-standards condition.

An experiment was made with a small number of observers, using a field-sequential color signal as the desired signal and a standard black-and-white signal as the source of interference. Threshold (perceptible) interference ratios were determined as a function of difference between carrier frequencies. The results are shown in Figure 11, with the least interference occurring at a separation of 14,580 cycles, one-half the line frequency of the desired picture, and with practically no improvement over nonsynchronous operation at a separation of 29,160 cycles. It may be seen that 10,500 and 21,000 cycle offset is effective for a field-sequential signal. Since the interference is largely caused by beating of the undesired carrier with frequency components in the desired signal, it seems logical to conclude that the shape of a curve like that of Figure 11 is largely determined by the characteristics of the desired signal and that the interfering signal may be field-sequential, line-sequential, dot-sequential, or standard black-and-white without changing the major interfering effects.

It may be noted that a limited number of observers found a ratio of 38 decibels to be just perceptible for this combination with carriers offset by 10.5 kilocycles, while in the JTAC tests with 100 observers the corresponding ratio with standard monochrome for both the desired and undesired signals was found to be 36 decibels.

A group of fifteen observers was then assembled for a series of tests to determine cochannel ratios for a variety of conditions. Because of the great amount of time necessary for these types of tests and because Figure 11 showed the large improvement obtained by offset frequencies of 10.5 kilocycles, the remainder of the data was taken only for this condition of carriers.

The receiver used for observing the field-sequential pictures consisted of a modified chassis from an RCA-9T240 television receiver using a ten-inch tube with a picture equivalent to a seven-inch tube and a magnifying lens to give the equivalent of a ten-inch picture. A rotating color wheel was included.

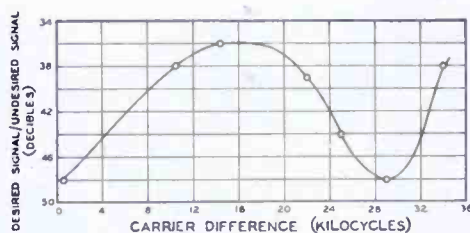


Fig. 11—Ratio of desired signal to interfering signal for threshold perceptibility as a function of the difference between carrier frequencies. The desired signal is field-sequential color. The interfering signal is standard monochrome.

For observations where the desired picture was standard monochrome, an unmodified RCA-9T240 television receiver was used.

A color slide was used for the desired picture in all cases. This slide is reproduced in black and white in Figure 12. The receivers were adjusted to achieve a high-light brightness of 15 foot-lamberts. The ambient room illumination was maintained at approximately four foot-candles.

Two field-sequential signals and a monochrome signal were used for the determination of threshold and tolerable ratios. At the same time, ratios were obtained using a standard monochrome signal interfering with a standard monochrome signal. The results for this latter condition are shown as Curves 5, Figure 14C and Figure 15C, where Figure 14 applies to threshold ratios and Figure 15 applies to tolerable ratios.

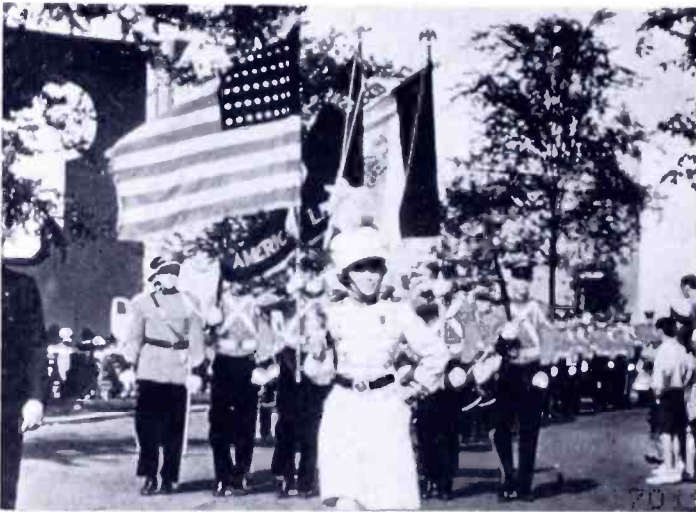


Fig. 12—Black-and-white reproduction of the color slide used as the desired picture in the co-channel tests.

Data were taken with a field-sequential picture as the desired signal and with another field-sequential signal as the interfering signal. The results are given by Curves 3, Figures 14B and 15B.

Next, the desired signal continues to be the field-sequential picture viewed on a color receiver, with standard monochrome signal as the interference. Curves 4, Figures 14B and 15B, depict the results of this test.

Then a standard monochrome signal was viewed on the black-and-white receiver, with a field-sequential signal as the source of interference, with the ratios displayed as Curves 6, Figures 14C and 15C.

Some difficulty was experienced when the field-sequential color picture was the desired signal, since many of the observers complained of flicker in the desired picture and felt that it was difficult to separate this effect from the interfering effects.

B. Line-sequential color television system

The line-sequential system uses the standards of normal monochrome, as far as the number of lines and scanning fields. A flying spot scanner, developed to produce color signals of the simultaneous type, was used as a picture source, together with suitable circuitry to

		LINE SEQUENCE B						
		FIELD→						
		I	II	III	IV	V	VI	VII
←LINE	1	RED		GREEN		BLUE		RED
	2		GREEN		RED		BLUE	
	3	GREEN		BLUE		RED		GREEN
	4		BLUE		GREEN		RED	
	5	BLUE		RED		GREEN		BLUE
	6		RED		BLUE		GREEN	
	7	RED		GREEN		BLUE		RED
	8		GREEN		RED		BLUE	

		LINE SEQUENCE C						
		FIELD→						
		I	II	III	IV	V	VI	VII
←LINE	1	RED		GREEN		RED		GREEN
	2		BLUE		RED		BLUE	
	3	GREEN		BLUE		GREEN		BLUE
	4		RED		GREEN		RED	
	5	BLUE		RED		BLUE		RED
	6		GREEN		BLUE		GREEN	
	7	RED		GREEN		RED		GREEN
	8		BLUE		RED		BLUE	

Fig. 13—Line-scanning sequences of the line-sequential color system. Sequence C was used to obtain Curves 8, Figures 14C and 15C.

provide sequential line selection from first the red signal, then the green signal, and then the blue signal. The necessary circuits were added to the receiver¹ to select the proper line sequence according to the transmitted synchronizing information. The sampler normally present in the dot-sequential color television receiver was not used, and the

¹ Radio Corporation of America, "A Six-Megacycle Compatible High-Definition Color Television System", pamphlet, September 26, 1949, Figure 10.

scanning and video signals were applied to the red, green and blue kinescopes in sequence. The two line-scanning sequences used in these tests are shown in Figure 13. When viewed on the color receiver, scanning sequence B was seen to have very coarse line structure and flickered badly on small objects or on nearly horizontal lines. Sequence C exhibited coarse line structure and had very poor vertical resolution. The pictures for either sequence were so poor in character that to determine interference ratios appeared to be without meaning, and no data was taken on this phase.

Interference ratios were determined where the desired signal was a standard monochrome picture viewed on a standard television receiver, with the line sequential signal using sequence C, Figure 13, as the interfering signal. The results are shown in Curves 8, Figures 14C and 15C.

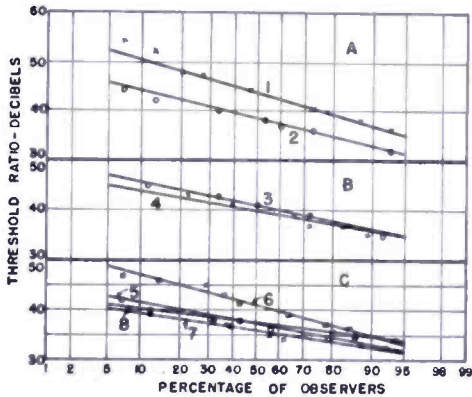


Fig. 14—Threshold values of co-channel interfering television signals, as a function of the percentage of observers requiring ratios greater than the ordinate values.

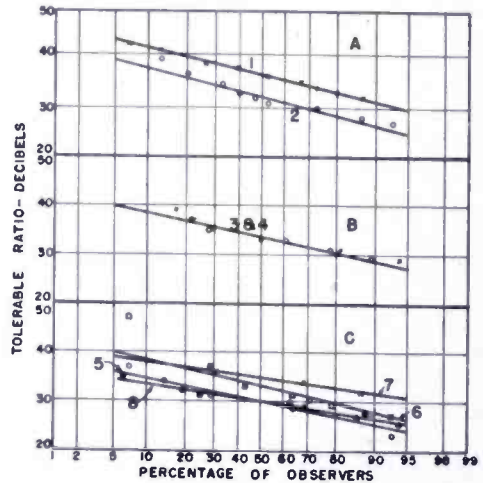


Fig. 15—Tolerable values of co-channel interfering television signals, as a function of the percentage of observers requiring ratios greater than the ordinate values.

C. Dot-sequential color television system

Interference ratios pertaining to the dot-sequential color television system were next determined. The direct-view receiver shown in Figure 16 of Reference (1) was used for observations. In the first run, the color picture was viewed on this receiver, with a standard monochrome signal as the interference (Curves 1, Figure 14A and 15A). Then the same color picture was viewed on an RCA-9T246 monochrome receiver, again with a standard monochrome signal as the interference, with the results shown in Curves 2, Figures 14A and 15A.

A third test was made, where a standard monochrome picture was received on a standard television receiver, with the dot-sequential signal as the interfering signal (Curves 7, Figures 14C and 15C).

The results of the observer tests on the three systems, field sequential, line sequential, and dot sequential, are summarized in Table IV. It may be seen that the tolerable ratios average five decibels higher than the corresponding ratio obtained in the previous JTAC tests, using standard monochrome for both the desired and undesired signal. This may be because only fifteen observers were used in these later tests on color television, while one hundred observers were used in the JTAC tests.

Table IV—Summary of Tolerable and Threshold Ratios of Desired to Undesired Cochannel Television Signals with Carriers Offset 10.5 Kilocycles.

Curve	Fig- ure	Sym- bol	Desired signal	Undesired signal	Average ratio re- quired by the observers (decibels)	
					Thresh- old	Toler- able
1	A	X	Dot-sequential color viewed on color receiver	Standard monochrome	42.0	36.0
2	A	O	Dot-sequential color viewed on standard monochrome receiver	Standard monochrome	37.0	32.0
			Dot-sequential color viewed on color receiver	Dot-sequential color	35.0	29.0
			Dot-sequential color viewed on standard monochrome receiver	Dot-sequential color	37.0	31.0
3	B	O	Field-sequential color viewed on color receiver	Field-sequential color	40.0	33.0
4	B	X	Field-sequential color viewed on color receiver	Standard monochrome	39.0	33.0
5	C	O	Standard monochrome viewed on standard monochrome receiver	Standard monochrome	36.0	29.0
6	C	□	Standard monochrome viewed on standard monochrome receiver	Field-sequential color	40.0	32.0
7	C	X	Standard monochrome viewed on standard monochrome receiver	Dot-sequential color	35.0	29.0
8	C	•	Standard monochrome viewed on standard monochrome receiver	Line-sequential color, Se- quence C	36.0	30.0
			Standard monochrome viewed on standard monochrome receiver (JTAC results)	Standard monochrome	36.0	27.2

The JTAC tests showed an average required ratio of approximately 45 decibels for monochrome pictures, using nonsynchronous operation of carriers. The observer tests conducted by RCA on the color television systems as well as the JTAC observer tests, both groups of tests with 10.5 kilocycles for the offset value, indicate that a ratio of 30 decibels is a very acceptable value, in round numbers. Figures 16, 17, 18, and 19 have been prepared to assist the reader in relating these interference ratios in terms of cochannel station separation. These curves were prepared by methods described in the report of the Ad Hoc Committee.*

In the above figures, only the effects on a line joining the desired station with the undesired station are considered. D is the distance between the two transmitters, d is the distance from the desired station to the receiving point along the line between the stations, and A is the ratio in decibels of the desired to the undesired signal. All four

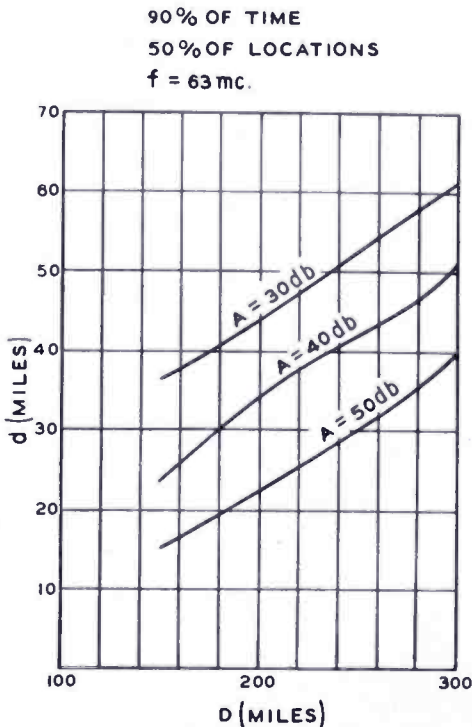


Fig. 16—Protection ratios A decibels existing at 50 per cent of the locations for 90 per cent of the time at a distance d miles from the desired station on a line toward the undesired station, with the stations separated D miles. The frequency is 63 megacycles.

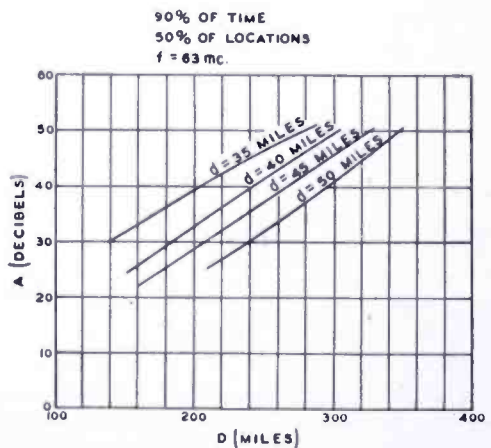


Fig. 17—Protection ratios A decibels existing at 50 per cent of the locations for 90 per cent of the time at a distance d miles from the desired station on a line toward the undesired station, with the stations separated D miles. The frequency is 63 megacycles.

* REPORT OF THE AD HOC COMMITTEE FOR THE EVALUATION OF THE RADIO PROPAGATION FACTORS CONCERNING THE TELEVISION AND FREQUENCY MODULATION BROADCASTING SERVICES IN THE FREQUENCY RANGE BETWEEN 50 AND 250 MEGACYCLES, Volume I, May, 1949.

figures relate to the probability of the particular ratio A occurring at 50 per cent of the locations for 90 per cent of the time. Figures 16 and 17 are estimates for a frequency of 63 megacycles, and may be considered to apply for Channels 2 to 6, inclusive, while Figures 18 and 19 are for the frequency of 195 megacycles and may be considered to apply for Channels 7 to 13, inclusive.

The reader may wish to draw conclusions of his own from these figures, together with a number of interference ratios. As an example of the type of information which may be readily extracted from these figures, one may assume a separation of two cochannel stations of 200 miles. If the stations are operating with offset carriers of 10.5 kilocycles, and a ratio A of 30 decibels is assumed, Figure 16 shows that this protection value holds for 50 per cent of the locations and 90 per cent of the time out to a service radius of 43.5 miles on the line toward the interfering station. If the two stations are operating nonsynchronously, the protected distance is shrunk to 28 miles if an interference ratio of 45 decibels is assumed for the nonsynchronous operation. On the other hand, it may be noticed that if the stations

are nonsynchronous and it is desired to give the same order of protection for the nonsynchronous operation as for offset operation, the stations should be separated by

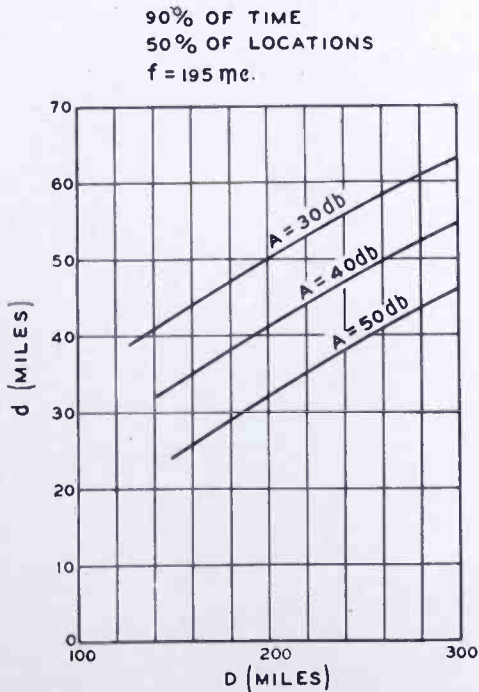


Fig. 18—Protection ratios A decibels existing at 50 per cent of the locations for 90 per cent of the time at a distance d miles from the desired station on a line toward the undesired station, with the stations separated D miles. The frequency is 195 megacycles.

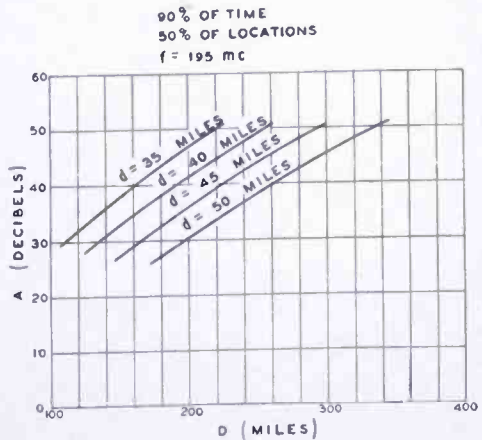


Fig. 19—Protection ratios A decibels existing at 50 per cent of the locations for 90 per cent of the time at a distance d miles from the desired station on a line toward the undesired station, with the stations separated D miles. The frequency is 195 megacycles.

a distance of 300 miles. The above observations apply to a frequency of 63 megacycles, or to the five lower television channels.

A similar inspection of Figure 18 reveals that at a frequency of 195 megacycles, or the upper seven television channels, offset carrier operation gives protection to a distance of 50 miles, with a protection ratio of 30 decibels and a station separation of 200 miles. With the same station separation, a protection ratio of 45 decibels (nonsynchronous operation) exists to a distance of 36 miles. Again, if the stations are nonsynchronous, the station separation must be 300 miles to secure a protection ratio of 45 decibels out to a distance of 50 miles.

A rough rule to apply seems to be as follows: (1) with a fixed separation of stations, offset carrier operation extends the service radius in the direction of the undesired station by about 50 per cent over nonsynchronous operation, or (2) for a fixed protected radius, nonsynchronous operation requires an increase in station separation of approximately 50 per cent over the separation required for offset carrier operation.

CONCLUSION

Television carrier synchronization has been demonstrated to be extremely advantageous in reducing cochannel television interference. Offset carrier operation has been shown to be superior in results and more economical to apply than television carrier synchronization.

Extensive application of offset carrier operation to existing television stations, many observations in a mobile laboratory and in homes, and the JTAC observer tests have fully demonstrated a remarkable improvement in television service when compared to conventional nonsynchronous operation.

Limited observer tests demonstrate that offset carrier operation is equally applicable to standard monochrome transmissions, the dot-sequential color television system and the field-sequential color television system. Limited data indicate that the line-sequential color television system interferes with a standard monochrome signal to the same extent as an interfering standard monochrome signal. No observer tests using a line-sequential signal as the desired picture were made for the reasons stated earlier.

It is recommended that for either standard monochrome or for color transmissions the amount of carrier offset shall be 10.5 kilocycles, or in a three-station combination one station shall remain on the assigned frequency, the second station shall be offset 10.5 kilocycles above the first, while the third shall be offset 10.5 kilocycles below the first.

NOTE: It is planned to print Part II of this paper—Adjacent-Channel Studies—in the June, 1950 issue.

RESONANT FREQUENCIES AND CHARACTERISTICS OF A RESONANT COUPLED CIRCUIT*

BY

C. L. CUCCIA

Research Department, RCA Laboratories Division,
Princeton, N.J.

Summary—The characteristics of a resonant coupled circuit are derived and charted so that they may be used in predicting the performance of ultra-high-frequency electron-tube systems which employ an external resonant circuit for tuning, frequency modulation, and control. The resonant frequencies of a basic circuit, the rate of change of system frequency as a function of the rate of change of frequency of the secondary circuit, and various important impedance and energy considerations are plotted.

"Much has been written about coupled circuits and they have been studied in all kinds of manners."

—B. D. H. TELLEGEN

IN VIEW OF the vast number of papers published in recent years which have been concerned with the analysis and characteristics of coupled circuits, it is difficult to believe from casual inspection that another equation could be derived or another curve plotted which could add useful information to this literature. However, since the advent of the use of ultra-high-frequency systems and techniques, information of a new type and from a different point of view is often found to be necessary for certain new systems and the coupled-circuit equations are therefore examined in the following presentation from the particular standpoint of their use in predicting the performance of ultra-high-frequency electron-tube systems which are intended for frequency modulation and control.

Among the first important new applications of coupled-circuit phenomena and theory in the communications field were those brought about by the use of new types of ultra-high-frequency vacuum tubes such as klystrons and magnetrons whose systems are made up of more than one resonant circuit; the application of coupled-circuit theory to electron-tube systems such as klystrons in which such considerations as transfer admittance are important, has been treated in considerable detail. In more recent years, coupled-circuit theory has become useful

* Decimal Classification: R142.

for determining the performance of frequency changing systems for tuning, frequency modulation, and frequency stabilization—in particular, those ultra-high-frequency generators employing an external secondary cavity whose frequency can be controlled mechanically or electronically using a reactance tube or spiral electron beam. In such systems it is essential to know the new resonant frequencies of the resulting coupled system and such useful considerations as the limits in frequency shift possible, stored energy ratio, and power-loss ratio at these resonant frequencies.

Although the equivalent circuit of coupled-circuit electron-tube systems will vary depending on the type of tubes involved and the method of coupling, the series parameter circuit pictured in Figure 1 permits an analysis which is actually applicable to many practical systems. This analysis is very fundamental and is also applicable to

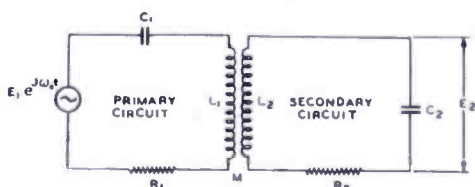


Fig. 1—Two-loop inductively-coupled circuit.

many systems and considerations which are not basically ultra-high-frequency in nature; e.g., tuned grid—tuned plate oscillators and frequency “pulling” which is caused by the inadvertent coupling of two resonant circuits.

Much of the information in this paper has been presented in analytical form; this paper represents a generalization of this information into a set of reference curves to which the engineer and the student of electrical circuits can refer. The analytical treatment is an extension of the works of Pierce, Tellegen, Sherman, and others.

The paper is in two parts—Part I which identifies the resonant frequencies of the coupled circuit shown in Figure 1, and Part II which uses the results of Part I to chart various characteristics of the system.

PART I—THE RESONANT FREQUENCIES OF A TWO-LOOP INDUCTIVELY-COUPLED RESONANT CIRCUIT

When the primary circuit in Figure 1 is excited in isolation by a voltage $Ee^{j\omega_1 t}$, the circuit will exhibit resonance (voltage will be in phase with the primary current) when

$$\omega_1 = 1/\sqrt{L_1 C_1}. \quad (1)$$

Consider the secondary circuit whose resonant angular velocity measured in isolation is

$$\omega_2 = 1/\sqrt{L_2 C_2}. \quad (2)$$

When this circuit is removed from isolation and is coupled to the primary circuit by the coupling factor, K , where

$$K = M/\sqrt{L_1L_2}, \tag{3}$$

then the generator exciting the primary circuit sees a unity power factor circuit (system exhibits resonance) when the angular velocity is ω_0 . ω_0 is related to ω_1 , ω_2 and Q_2 by the exact expression*

$$\left[\frac{\omega_0^2}{\omega_1^2} \right]^3 (1 - K^2) - \left[\frac{\omega_0^2}{\omega_1^2} \right]^2 \left(1 + \frac{\omega_2^2}{\omega_1^2} \left(2 - K^2 - \frac{1}{Q_2^2} \right) \right) + \left[\frac{\omega_0^2}{\omega_1^2} \right] \frac{\omega_2^2}{\omega_1^2} \left(2 + \frac{\omega_2^2}{\omega_1^2} - \frac{1}{Q_2^2} \right) - \frac{\omega_2^4}{\omega_1^4} = 0. \tag{4}$$

In this expression, the ratio, ω_0/ω_1 , which yields the new system angular velocity, ω_0 , in terms of the isolated primary circuit angular velocity, ω_1 , is conveniently made a function of the ratio, ω_2/ω_1 .

Equation (4) is a third order algebraic equation in ω_0^2/ω_1^2 . Its solution for various values of Q_2 and K is presented as follows:

Case 1— $Q_2 \rightarrow \infty$

When Q_2 is very large, Equation (4) reduces to

$$\left[\frac{\omega_0^2}{\omega_1^2} \right]^3 (1 - K^2) - \left[\frac{\omega_0^2}{\omega_1^2} \right]^2 \left(1 + \frac{\omega_2^2}{\omega_1^2} (2 - K^2) \right) + \left[\frac{\omega_0^2}{\omega_1^2} \right] \frac{\omega_2^2}{\omega_1^2} \left(2 + \frac{\omega_2^2}{\omega_1^2} \right) - \frac{\omega_2^4}{\omega_1^4} = 0, \tag{5}$$

which can be written in the form:

* This equation is prescribed by the loop equations,

$$E = I_1R_1 + j \left(\omega L_1 - \frac{1}{\omega C_1} \right) I_1 - j\omega MI_2, \quad 0 = I_2R_2 + j \left(\omega L_2 - \frac{1}{\omega C_2} \right) I_2 - j\omega MI_1,$$

when the input susceptance, as seen by the driving generator, is set equal to zero thereby yielding the general resonant angular velocity, ω_0 , which satisfies this condition. Q_1 and Q_2 are described as follows:

$$Q_1 = \frac{\omega_1 L_1}{R_1} = \frac{1}{\omega_1 C_1 R_1}, \quad Q_2 = \frac{\omega_2 L_2}{R_2} = \frac{1}{\omega_2 C_2 R_2}.$$

Note that Q_1 does not appear in Equation (4), showing that ω_0 is dependent on ω_1 , ω_2 , and Q_2 , only.

$$\left(\frac{\omega_0^2}{\omega_1^2} - \frac{\omega_2^2}{\omega_1^2} \right) \left(\left[\frac{\omega_0^2}{\omega_1^2} \right]^2 (1 - K^2) - \left[\frac{\omega_0^2}{\omega_1^2} \right] \left(1 + \frac{\omega_2^2}{\omega_1^2} \right) + \frac{\omega_2^2}{\omega_1^2} \right) = 0. \quad (6)$$

The roots of Equation (6) are

Root 1 (upper frequency):

$$\frac{\omega_0}{\omega_1} = \left[\frac{\left[1 + \frac{\omega_2^2}{\omega_1^2} \right] + \sqrt{\left[1 + \frac{\omega_2^2}{\omega_1^2} \right]^2 - 4 \frac{\omega_2^2}{\omega_1^2} (1 - K^2)}}{2(1 - K^2)} \right]^{1/2}, \quad (7)$$

Root 2 (lower frequency):

$$\frac{\omega_0}{\omega_1} = \left[\frac{\left[1 + \frac{\omega_2^2}{\omega_1^2} \right] - \sqrt{\left[1 + \frac{\omega_2^2}{\omega_1^2} \right]^2 - 4 \frac{\omega_2^2}{\omega_1^2} (1 - K^2)}}{2(1 - K^2)} \right]^{1/2}. \quad (8)$$

Root 3: $\omega_0/\omega_1 = \omega_2/\omega_1$. (9)

The general form of the solution of (6) is shown in Figure 2 where the abscissa is ω_2/ω_1 and the ordinate is ω_0/ω_1 . Root 3 is a straight line with unity slope. The lower frequency root starts from zero and is asymptotic to $\omega_0/\omega_1 = 1$. The upper frequency root starts at $\omega_2/\omega_1 = 0$ at an ordinate intercept whose value may be shown to be given by the expression

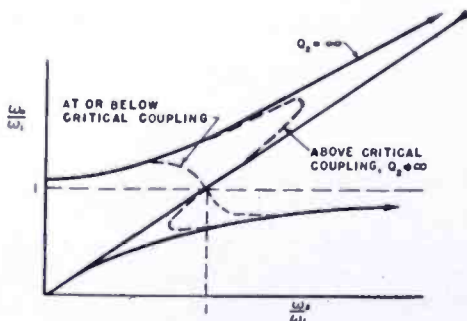


Fig. 2—General behavior of the resonant frequencies of a coupled circuit as a function of the mutual coupling coefficient, K , and the Q of the secondary cavity.

$$\left[\frac{\omega_0}{\omega_1} \right]_{\frac{\omega_2}{\omega_1} = 0} = \frac{1}{\sqrt{1 - K^2}}, \quad (10)$$

and is asymptotic to the line described by Root 3.

The general solution of (6) is pictured in Figure 3 for values of coupling coefficient from $K = 0.1$ to $K = 0.9$. It is seen that as K increases in magnitude, the upper

and lower frequencies, corresponding to a particular value of ω_2/ω_1 , become farther apart—the increase in the upper frequency being greater than the corresponding increase in the lower frequency. The frequency denoted by Root 3 is, in general, not of interest except at or below critical coupling (see Case II) due to the relatively low magnitude of the circulating currents which can be shown to exist at this frequency.

Illustration of the use of Figure 3

Consider two high Q resonators which, when measured in isolation, yield the values, $\omega_1 = 2\pi \cdot 500,000$ radians per second and $\omega_2 = 2\pi \cdot 720,000$ radians per second. Then $\omega_2/\omega_1 = 1.44$. If $K = 0.3$, it is seen from Figure 3 that $\omega_0/\omega_1 = 0.975$ and 1.49 . It follows then, that $\omega_0 = 2\pi \cdot 487,500$ and $2\pi \cdot 745,000$ radians per second.

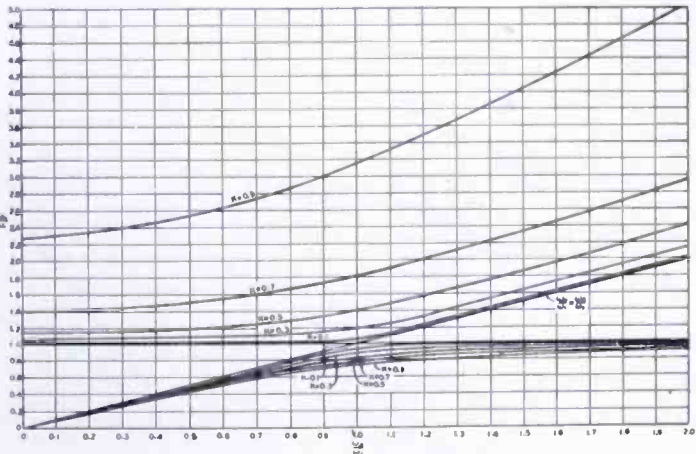


Fig. 3—Resonant frequencies of coupled-circuit as a function of K for $Q_2 = \infty$.

Case II— $Q_2 \ll \infty$

When Q_2 is not extremely large, the roots of Equation (4) occur as shown in Figures 4a, 4b, and 4c for $K = 0.1, 0.3,$ and 0.5 and $10 < Q_2 < \infty$.

When dealing with finite- Q secondary circuits, one of the most important considerations is the relationship between K and Q_2 which determines “critical coupling”. Critical coupling is that value of coupling coefficient, which, when combined with an appropriate value of Q_2 , determines the transition point from the region where the system has three resonant frequencies (three real roots) to the region where the system has only one resonant frequency (one real root and two imaginary roots). It is seen in Figure 4a that as Q_2 decreases in value for the case when $K = 0.1$, the range of values of ω_2/ω_1 over which Equation (4) will have three real roots decreases—the shrinkage taking place about the line $\omega_2/\omega_1 = 1$. Critical coupling will take place when the curve relating ω_2/ω_1 and ω_0/ω_1 for any value of K becomes single-

valued for all values of ω_2/ω_1 and passes through the point $\omega_2/\omega_1 = \omega_0/\omega_1 = 1$ with infinite slope. The relationship which specifies critical coupling may be derived by taking the derivative of $(\omega_2/\omega_1)^2$ in Equation (4) with respect to $(\omega_0/\omega_1)^2$ and setting the result equal to zero at $\omega_2/\omega_1 = 1$. This manipulation will yield the expression,

$$Q_2 K = 1. \tag{11}$$

It is evident in Figure 4a that for $K = 0.1$, the curve which represents $Q_2 = 10$, and which satisfies Equation (11) is single-valued for all

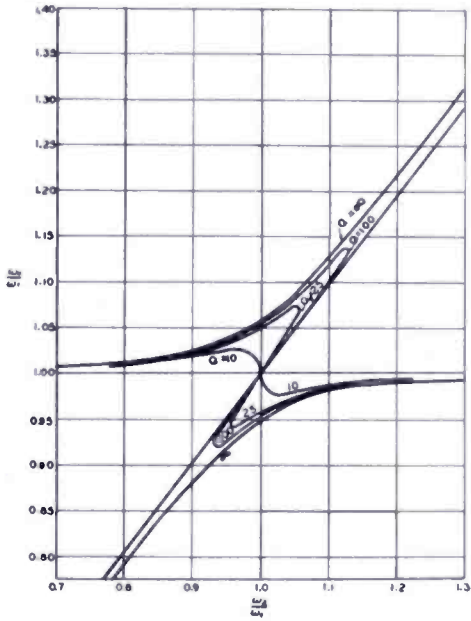


Fig. 4a

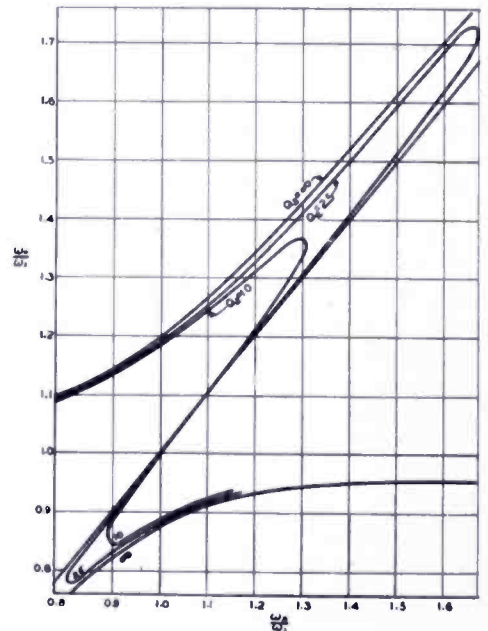


Fig. 4b

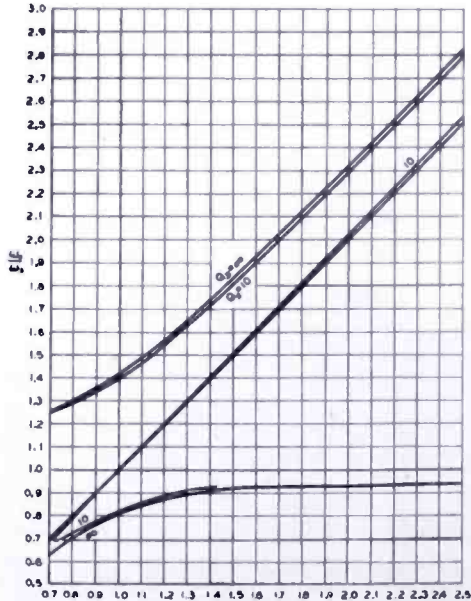


Fig. 4c

Fig. 4—Resonant frequencies of a coupled circuit as a function of K for finite values of Q_2 . (a) $K = 0.1$, (b) $K = 0.3$, (c) $K = 0.5$.

values of ω_2/ω_1 and passes through the point, $\omega_2/\omega_1 = \omega_0/\omega_1 = 1$, with infinite slope.

When K is large, then for practical values of Q_2 , the frequencies specified by Figure 3 may be used with good accuracy. When both Q_2 and K are small and in the vicinity of critical coupling, then the

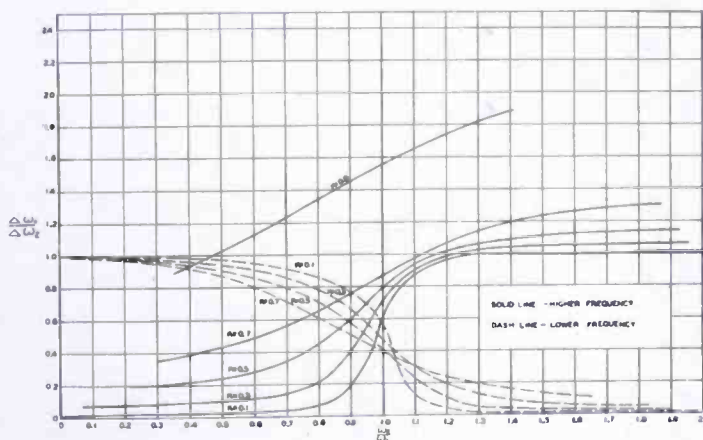
curves in Figure 3 will no longer be usable and it will be necessary to use solutions of Equation (4).

The Change in ω_0 as a Function of a Change in ω_2

If the secondary circuit is to be varied in frequency by use of a suitable frequency changing element such as a reactance tube, then it is convenient to know $\Delta\omega_0$ which is the change in the angular velocity of the system, as a function of $\Delta\omega_2$ which is the change in the secondary circuit frequency. A chart of $\Delta\omega_0/\Delta\omega_2$ versus ω_2/ω_1 is shown in Figure 5 for very large values of Q_2 . This chart is obtained graphically from Figure 3.

If the values of K and Q_2 are such that the system coupling is near or below critical coupling, then it is necessary to determine this information from Figure 4 or from appropriate charted solutions of Equation (4).

Fig. 5—Curves which yield the change $\Delta\omega_0/2\pi$ in the system frequency as a function of a change $\Delta\omega_2/2\pi$ in the frequency of the secondary circuit for the case when $Q_2K \gg 1$.



PART II—POWER, STORED ENERGY, AND IMPEDANCE CONSIDERATIONS IN A RESONANT TWO-LOOP INDUCTIVELY COUPLED CIRCUIT

Introduction

Part II will present curves for power ratio, stored energy ratio and impedance changes in a resonant two-loop inductively coupled circuit. These charts are computed using the upper and lower frequency sets in Figure 3 which is described by Equations (7) and (8). For regions of interest where the frequency sets in Figure 3 do not apply—near critical coupling, for example—then values of ω_0/ω_1 corresponding to ω_2/ω_1 , Q_2 , and K should be taken from Figures 4a, 4b, or 4c or from appropriate solutions of Equation (4) and substituted into the equations which describe the following cases.

Power Loss Ratio in a Resonant Coupled Circuit

In the coupled circuit in Figure 1, if P_1 is the power loss in the primary loop and P_2 is the power loss in the secondary loop, then

$$P_1/P_2 = (I_1^2 R_1)/(I_2^2 R_2). \tag{12}$$

It follows that

$$\frac{P_1}{P_2} = \frac{1}{K^2} \frac{\omega_1}{\omega_2} \left[\left(\frac{\omega_1}{\omega_0} \cdot \frac{\omega_2}{\omega_1} \right)^2 \frac{1}{Q_1 Q_2} + \frac{Q_2}{Q_1} \left(1 - \left(\frac{\omega_1}{\omega_0} \cdot \frac{\omega_2}{\omega_1} \right)^2 \right) - j2 \frac{\omega_1}{\omega_0} \cdot \frac{\omega_2}{\omega_1} \frac{1}{Q_1} \left(1 - \left(\frac{\omega_1}{\omega_0} \cdot \frac{\omega_2}{\omega_1} \right)^2 \right) \right]. \tag{13}$$

For practical values of Q_1 and Q_2 , this equation reduces to the form

$$\frac{P_1}{P_2} \cdot \frac{Q_1}{Q_2} \approx \frac{1}{K^2} \cdot \frac{\omega_1}{\omega_2} \left[1 - \left(\frac{\omega_1}{\omega_0} \cdot \frac{\omega_2}{\omega_1} \right)^2 \right] \tag{14}$$

Choosing values of ω_0/ω_1 from Figure 3, $(P_1/P_2)(Q_1/Q_2)$ versus ω_2/ω_1 may be plotted as shown in Figure 6 for $K = 0.1, 0.3, 0.5,$ and 0.7 for both the upper and lower set of frequencies when $KQ_2 \gg 1$.

Stored Energy Ratio

If \mathcal{E}_1 is the stored energy in the primary loop in Figure 1 and if \mathcal{E}_2 is the stored energy in the secondary loop, then

$$\mathcal{E}_1 = (Q_1 P_1)/\omega_1, \tag{15}$$

$$\mathcal{E}_2 = (Q_2 P_2)/\omega_2, \tag{16}$$

and

$$\mathcal{E}_1/\mathcal{E}_2 = (Q_1/Q_2) (P_1/P_2) (\omega_2/\omega_1). \tag{17}$$

Using Equation (14), it follows from (17) that

$$\left| \frac{\mathcal{E}_1}{\mathcal{E}_2} \right| \approx \frac{1}{K^2} \left[1 - \left(\frac{\omega_1}{\omega_0} \cdot \frac{\omega_2}{\omega_1} \right)^2 \right]^2. \tag{18}$$

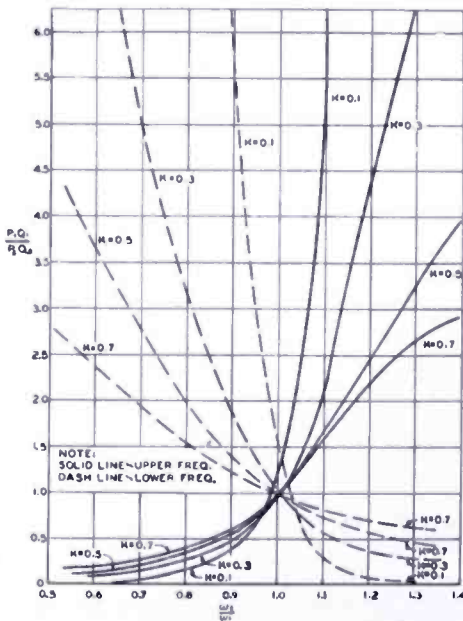


Fig. 6—Power-loss ratio in a two-loop resonant coupled circuit as a function of Q_1/Q_2 and K for $Q_2 K \gg 1$.

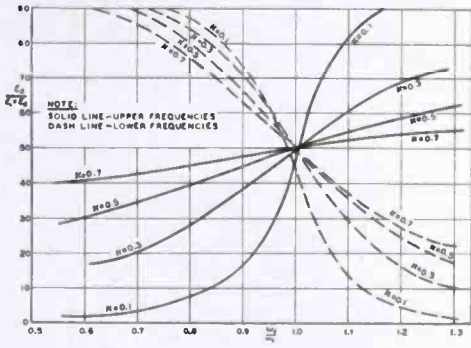


Fig. 7—Stored energy ratio in a resonant two-loop inductively coupled circuit when $Q_2K \gg 1$.

The stored energy in the secondary loop may be described in terms of the total stored energy of the system by using the following expression:

$$\frac{E_2/E_1}{1 + E_2/E_1} = E_2/(E_1 + E_2). \quad (19)$$

Figure 7 pictures $E_1/(E_1 + E_2)$ versus ω_2/ω_1 for both the upper and lower frequency set from Figure 3 for $K = 0.1, 0.3, 0.5, \text{ and } 0.7$.

Considerations of the Resistive Impedance of a Parallel Resonant Circuit When a Secondary Circuit Is Inductively Coupled to It.

Consider the circuit pictured in Figure 8. When the secondary circuit is decoupled, the resistive impedance, as measured across the terminals a and b , is, for higher values of Q ,

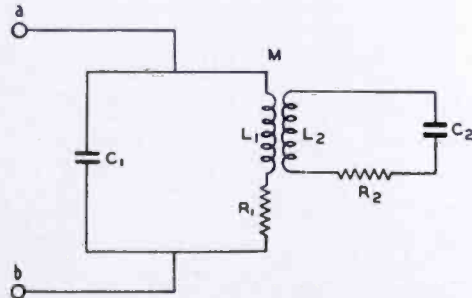


Fig. 8—Parallel resonant tank circuit to which has been coupled a secondary loop circuit.

$$Z_{ab} = L_1/(C_1R_1), \quad (20)$$

where, in general, for this RLC circuit in isolation,

$$\omega_1 = \sqrt{\frac{1}{L_1C_1} - \frac{R_1^2}{L_1^2}}. \quad (21)$$

When the secondary circuit is inductively coupled to the primary circuit, the ratio of L_1 and R_1 will change by the factor, η , such that for the coupled circuit in Figure 8 at resonance,

$$Z_{ab} = (L_1/(C_1R_1)) \eta. \quad (22)$$

Although the circuits shown in Figures 1 and 8 are not equivalent, the resistance and the reactance which are reflected from the secondary circuit into the primary circuit in Figure 1 may be used in deriving the expression for η provided that

$$\omega_0 \gg R_1/(\eta L_1). \quad (23)$$

Since the driving point impedance in Figure 1 is

$$Z_s = \frac{E_1}{I_1} = R_1 + R_2 \frac{\omega^2 M^2}{R_2^2 + \left[\omega L_2 - \frac{1}{\omega C_2} \right]^2} \quad (24)$$

$$+ j \left[\left[\omega L_1 - \frac{1}{\omega C_1} \right] - \left[\omega L_2 - \frac{1}{\omega C_2} \right] \frac{\omega^2 M^2}{R_2^2 + \left[\omega L_2 - \frac{1}{\omega C_2} \right]^2} \right],$$

it is easily shown that

$$Z_s = R_1 \left[1 + \frac{\frac{\omega_0^4 K^2 Q_1}{\omega_2^3 \omega_1 Q_2}}{\left(\frac{\omega_0}{\omega_1} \cdot \frac{\omega_1}{\omega_2} \right)^2 \frac{1}{Q_2^2} + \left[\left(\frac{\omega_0}{\omega_1} \cdot \frac{\omega_1}{\omega_2} \right)^2 - 1 \right]^2} \right] \quad (25)$$

$$+ j \left[\omega_0 L_1 \left\{ 1 - \frac{K^2 \left(\frac{\omega_0}{\omega_1} \cdot \frac{\omega_1}{\omega_2} \right)^2 \left[\left(\frac{\omega_0}{\omega_1} \cdot \frac{\omega_1}{\omega_2} \right)^2 - 1 \right]}{\left(\frac{\omega_0}{\omega_1} \cdot \frac{\omega_1}{\omega_2} \right) \frac{1}{Q_2^2} + \left[\left(\frac{\omega_0}{\omega_1} \cdot \frac{\omega_1}{\omega_2} \right)^2 - 1 \right]^2} \right\} - \frac{1}{\omega_0 C_1} \right],$$

from which it follows that

$$\eta = \frac{\beta - K^2 \left(\frac{\omega_0}{\omega_1} \cdot \frac{\omega_1}{\omega_2} \right)^2 \left[\left(\frac{\omega_0}{\omega_1} \cdot \frac{\omega_1}{\omega_2} \right)^2 - 1 \right]}{\beta + \frac{\omega_0^3}{\omega_2^3} \cdot \frac{\omega_0}{\omega_1} K^2 \frac{Q_1}{Q_2}}, \quad (26)$$

where

$$\beta = \left(\frac{\omega_0}{\omega_1} \cdot \frac{\omega_1}{\omega_2} \right)^2 \frac{1}{Q_2^2} + \left[\left(\frac{\omega_0}{\omega_1} \cdot \frac{\omega_1}{\omega_2} \right)^2 - 1 \right]^2. \quad (27)$$

Curves of η versus ω_2/ω_1 are shown in Figures 9a, 9b, and 9c for $K = 0.1, 0.3, 0.5,$ and 0.7 and $Q_1/Q_2 = 0.1, 1.0,$ and 10 , using values of ω_0/ω_1 from Figure 3.

It is often of interest to determine the conditions during which

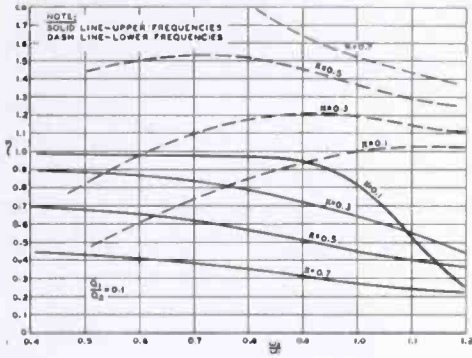


Fig. 9a

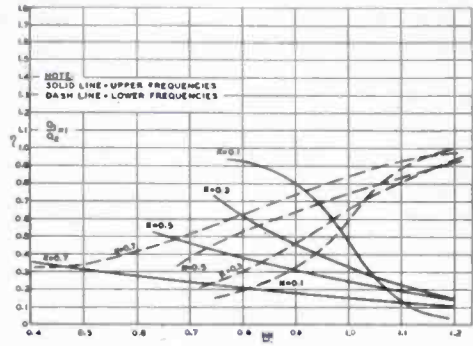


Fig. 9b

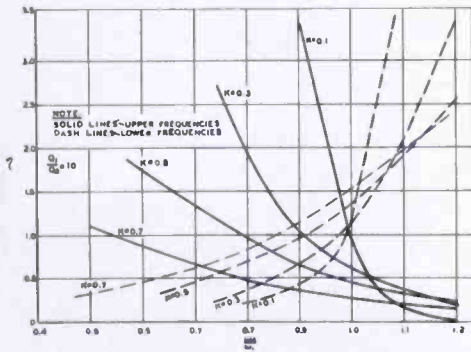


Fig. 9c

Fig. 9—Curves of η which is a factor describing the change in the resistive impedance of the primary circuit in Figure 8 at the new resonant frequencies when a secondary circuit is inductively coupled to it for the case when $Q_2K \gg 1$. (a) $Q_1/Q_2 = 0.1$, (b) $Q_1/Q_2 = 1.0$, (c) $Q_1/Q_2 = 10$.

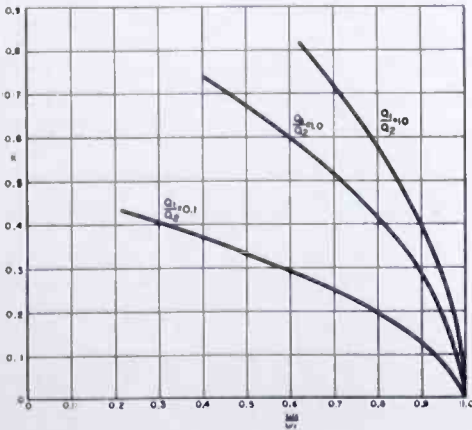


Fig. 10—Chart describing the values of K , Q_1 and Q_2 at which the resonant coupled circuit in Figure 8 presents the same values of resistive impedance, Z_{ab} , at both the upper and lower resonant frequencies.

the resistive impedances at both frequencies are equal. These are found by using the intersections of the curves in Figures 9a, 9b, and 9c; the results are plotted in Figure 10. Note that the intersections take place only when $\omega_2/\omega_1 < 1$ with the slopes of the curves decreasing as the magnitude of the ratio, Q_1/Q_2 , is decreased.

ACKNOWLEDGMENT

The author wishes to acknowledge the valuable criticism and advice of R. A. Braden.

BIBLIOGRAPHY

1. G. W. Pierce, **ELECTRIC OSCILLATIONS AND ELECTRONIC WAVES**, Chapters VII-IX, McGraw-Hill Book Co., N.Y., 1920.
2. L. Cohen, "Frequencies and Damping Factors of Coupled Circuits", *Proc. I.R.E.*, Vol. 9, No. 2, pp. 150-164, April, 1921.
3. B. Van der Pol, "On Oscillation Hysteresis in a Triode Generator with Two Degrees of Freedom", *Phil. Mag.*, Vol. 43, pp. 700-719, April, 1922.
4. E. A. Guillemin, **COMMUNICATION NETWORKS**, pp. 323-356, John Wiley and Sons, N.Y., 1931.
5. W. L. Everitt, **COMMUNICATION ENGINEERING**, Chapter IX, McGraw-Hill Book Co., N.Y., 1932.
6. L. A. Kelley, "Direct Solution of Tuned Coupled Circuits", *Elec. Eng.*, Vol. 51, pp. 789-794, November, 1932.
7. Ronold King, "Amplitude Characteristics of Coupled Circuits having Distributed Constants", *Proc. I.R.E.*, Vol. 21, No. 8, pp. 1142-1182, August, 1933.
8. B. Van der Pol, "The Nonlinear Theory of Electric Oscillations", *Proc. I.R.E.*, Vol. 22, pp. 1051-1086, September, 1934.
9. C. B. Aiken, "Two-Mesh Tuned Coupled Circuit Filters", *Proc. I.R.E.*, Vol. 25, No. 2, pp. 230-272, February, 1937, and errata, Vol. 26, No. 6, p. 672, June, 1937.
10. J. B. Sherman, "Some Aspects of Coupled Circuits", *Proc. I.R.E.*, Vol. 30, No. 11, pp. 505-510, November, 1942.
11. R. L. Sproull, "Reactance Tube Frequency Modulation of Microwave Oscillators", Report No. 20, U.S. Navy Contract NXsa-35042.
12. R. L. Sproull, "The Diode Frequency Modulator", Report No. 16, U.S. Navy Contract NXsa-35042.
13. B. D. H. Tellegen, "Coupled Circuits", *Philips Research Reports*, Vol. 2, No. 1, pp. 1-19, February, 1947.
14. J. S. Donal, Jr., C. L. Cuccia, B. B. Brown, C. P. Vogel and W. J. Dodds, "Stabilized Magnetron for Beacon Service", *RCA Review*, Vol. III, No. 2, pp. 352-372, June, 1947.
15. G. B. Collins, **MICROWAVE MAGNETRONS**, Part IV, McGraw-Hill Book Co., N.Y., 1948.
16. D. R. Hamilton, J. K. Knipp and J. B. Horner Kuper, **KLYSTRONS AND MICROWAVE TRIODES**, Chapter 11, McGraw-Hill Book Co., 1948.
17. S. H. Chang, "Parabolic Loci for Two Tuned Coupled Circuits", *Proc. I.R.E.*, Vol. 36, pp. 1384-1388, November, 1948.
18. A. E. Harrison and N. W. Mather, "Graphical Analysis of Tuned Coupled Circuits", *Proc. I.R.E.*, Vol. 37, pp. 1016-1020, September, 1949.
19. M. S. Wheeler, "Frequency Contours for Microwave Oscillator with Resonant Load", *Proc. I.R.E.*, Vol. 37, pp. 1332-1336, November, 1949.

A BROADBAND TRANSITION FROM COAXIAL LINE TO HELIX*

BY

C. O. LUND†

Research Department, RCA Laboratories Division,
Princeton, New Jersey

Summary—A new type coaxial line to helix transition is described, which incorporates a section of non-uniform helix. The transition has a fairly broad band of operation and permits the coupling of helices to coaxial lines of impedances used commonly for transmission lines.

An approximate theory for this transition, based upon an impedance concept developed for helices and the theory for non-uniform transmission lines is outlined. The performance of practical transitions is discussed and shows that although the simple theory does not hold in all cases, transitions with reasonable lengths that have a voltage-standing-wave-ratio of less than 1.5 over a very wide band can be constructed.

INTRODUCTION

THE helix has recently gained importance as a transmission element for ultra-high frequencies. Its special peculiarities, low velocity of wave propagation and a high axial electrical field, justify its use in the traveling wave tube; other aspects of the field configuration make it useful as an antenna.

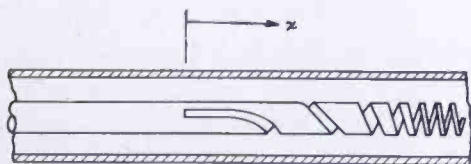


Fig. 1—The helix to coaxial line transition, schematic.

In connection with work on the traveling-wave tube it was found necessary to develop a transition from the helix to other transmission elements such as waveguides and coaxial lines. The result is the transition shown in Figure 1. It consists of a cylinder with a helical slot, whose pitch is gradually varied between infinity and the pitch of the uniform helix.

The advantage of this transition is that it acts as a transformer between a helix and a coaxial line with reasonable dimensions of the center conductor, and is mechanically rigid compared with the kind of transition, where the conductor, i.e., the helix wire, has the same

* Decimal Classification: R117.3.

† Now with the Microwave Section, Laboratory for Telegraphy and Telephony, Royal Technical College, Copenhagen, Denmark.

dimension over the transition. For application in the traveling wave tube, the transition has the advantage that it completely encloses the electron beam, and so introduces very little distortion into the electron-optical system.

This coaxial line to helix transition can also be used as a part of a waveguide to helix transition, since the coaxial line can be coupled to a waveguide by conventional means, although this might not have as wide an operating bandwidth as other schemes.

Helices have been used for some time as delay lines¹⁻⁴ and high-frequency cables for video frequencies.⁵ For these applications the helix has been described in terms of distributed low frequency reactances. Various relations between velocity of propagation, impedance, pitch, diameter and diameter of outer shield have been developed for the uniform helix and its variations.⁶

The high-frequency behavior has been investigated briefly by Ollendorf⁷ who sets up the field equations for a helical conducting sheet in free space. Solutions for this case in terms of phase constant have been worked out by Pierce,⁸ and Shulman and Heagy.⁹

The field equations for a helical conducting sheet with a conducting outer cylindrical shield have been solved for the propagation constant by W. M. Surber, Department of Electrical Engineering, Princeton University (unpublished work), Loshakov and O'Derogge,¹⁰ and C. Shulman and the author (unpublished, but the results are given later in this paper).

The nonuniform helix has been studied for the case of video

¹ Von H. Kaden, "Properties of an RF Cable Whose Inner Conductor is a Helix", *Telegraphen Fernsprech Funk- und Fernseh-Technik*, Vol. 32, No. 9, p. 195, September, 1943.

² K. H. Zimmermann, "Spiral Delay Lines", *Electrical Communications*, Vol. 23, p. 327, September, 1946.

³ J. P. Blewett and J. H. Rubel, "Video Delay Lines", *Proc. I.R.E.*, Vol. 35, p. 1580, December, 1947.

⁴ L. N. Brillouin, "Electromagnetic Delay Lines", *Proceedings of a Symposium on Large Scale Digital Calculating Machinery*, Harvard University Press, 1948.

⁵ Keutner, "Die Bemessung Koaxialer Kabel mit Gewendelten Leitern", *Telegraphen Fernsprech Funk- und Fernseh-Technik*, Vol. 32, No. 9, September, 1943.

⁶ H. E. Kallmann, "Equalized Delay Lines", *Proc. I.R.E.*, Vol. 34, No. 9, p. 646, September, 1946.

⁷ F. Ollendorf, *DIE GRUNDLAGEN DER HOCHFREQUENZ-TECHNIK*, pp. 79-87, Julius Springer, Berlin, 1926.

⁸ J. R. Pierce, "Theory of the Beam-Type Traveling-Wave Tube", *Proc. I.R.E.*, Vol. 35, No. 2, p. 111, February, 1947.

⁹ C. Shulman and M. S. Heagy, "Small-Signal Analysis of Traveling-Wave Tube", *RCA Review*, Vol. 8, No. 4, December, 1947.

¹⁰ L. N. Loshakov and O'Derogge, "On the Theory of a Coaxial Spiral Line", *Radiotekhnika* (Moscow), Vol. 3, No. 2, p. 11, March/April, 1948.

frequencies, by Keutner,¹¹ who uses a low-frequency impedance concept as a basis for design of an exponentially nonuniform line.

DESIGN PROCEDURES

The geometry of the helix to coaxial line transition, as shown in Figure 1, is of such nature that it can not readily be treated by using Maxwell's equations. This makes an exact analysis impractical.

It was decided to use an approach similar to Keutner's. This includes the development of an impedance concept for a model of the physical helix, the helical conducting sheet as used by Ollendorf and others, and the use of this impedance in the theory for tapered lines, which gives the optimum impedance function for low reflection in the transmission band. This procedure involves several approximating steps since the definition of the impedance of a helix at high frequencies is difficult to formulate. It is doubtful what impedance to assign to the helix with outer shield. It is the same difficulty encountered with waveguides and other structures that propagate other than transverse electromagnetic modes. However, since the helix has to be transformed from a coaxial line, it is necessary for this purpose to develop some relation between the helix impedance and that of the corresponding coaxial line. An impedance concept is developed for the helical conducting sheet, which might not hold in all cases for the physical slot-in cylinder type of helix.

The field equations for the helical conducting sheet with outer shield do not suggest any usable impedance function. The approach actually used is rather artificial, being based on the fact that if a coaxial line is joined to a helix, the reflection from the joint can be measured. To this reflection an impedance ratio can be assigned. The same applies to the case where two helices of different pitch are joined. Such measurements were made for a junction between a coaxial line and a helix where the inner conductor, which is joined to the helix, has the same diameter as the helix, and the outer conductor is common.

An effort was then made to discover a simple equation which would fit the experimental results. A relation was discovered which has the same dependence on pitch as the measured results, but which yields somewhat lower impedance values. It is to be expected that this calculated impedance would be lower than the measured value, since the measured impedance includes the effect of mode transformations

¹¹ Keutner, "Hochfrequenzkabel mit veranderlichem Wellenwiederstand", *Elektrische Fernmeldetechnik*, No. 62, 1943.

for the joint between the coaxial line and the helix. It has not been possible to make any estimates of the order of magnitude of these reflections.

Consider Figure 2. If a distributed inductance L is assigned to the helix, and the static distributed capacitance C between the shield and the helical conducting sheet is introduced, the following definitions can be made:

$$\text{Helix impedance, } Z = \sqrt{\frac{L}{C}}, \quad (1)$$

$$\text{velocity of propagation, } v_H = \frac{1}{\sqrt{LC}}, \quad (2)$$

$$\text{and by eliminating } L, \quad Z = \frac{1}{Cv_H}. \quad (3)$$

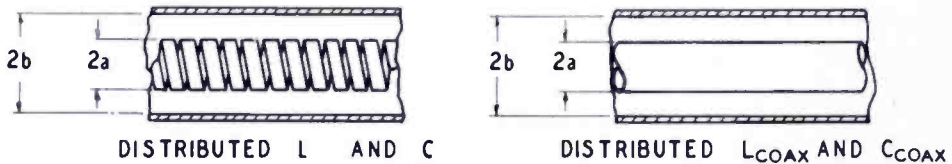


Fig. 2—Geometry of uniform helix and corresponding coaxial line.

Consider now a coaxial line and a helix with common outer conductor, where the diameter of the inner conductor is the same as that of the helix (see Figure 2). For this condition

$$Z_{\text{coax}} = \frac{1}{C_{\text{coax}} c}, \quad (4)$$

where C_{coax} is the capacity per unit length between inner and outer conductor, and c is the phase velocity in the coaxial line.

The concept of distributed reactances is probably very artificial for the helix at these frequencies as it is known from measurements that the fields for small pitch and high frequencies are very close to the helix. Also, the whole picture breaks down when the circumference of the helix approaches half a wave-length. This region of higher modes of propagation will not be considered here.

However, if it is assumed that $C = C_{\text{coax}}$, a simple relation is obtained. This probably holds for the slotted-cylinder type of helix,

but not for the helix transition where the wire has constant dimensions over the transition. The relation is

$$Z = Z_{\text{coax}} \frac{c}{v_H} = Z_{\text{coax}} \frac{\lambda}{\lambda_H} \tag{5}$$

This happens to be a good approximation to the actual measured impedances, whatever the physical significance may be.

The velocity of propagation can be computed to the first order of approximation, assuming that the waves travel with the speed c in the conducting direction of the helical conducting sheet.

A better approximation is obtained by solving the field equations for the helical conducting sheet with outer conductor. The different authors mentioned above find, for the relative phase velocity v_H/c of this line, the following expression:

$$\frac{v_H}{c} = \frac{\lambda_H}{\lambda} = \left[1 + \left(a\mu \cdot \frac{\lambda}{2\pi a} \right)^2 \right]^{-1/2} \tag{6}$$

where μ is the solution of the implicit expression

$$\left[2\pi \frac{a}{\lambda} \frac{2\pi a}{p} \right]^2 = (a\mu)^2 \frac{I_0(a\mu)K_0(a\mu)}{I_1(a\mu)K_1(a\mu)} \left[\frac{1 - \frac{I_0(a\mu)K_0(b\mu)}{K_0(a\mu)I_0(b\mu)}}{1 - \frac{I_1(a\mu)K_1(b\mu)}{K_1(a\mu)I_1(b\mu)}} \right],$$

where a = radius of helix, b = radius of shield, p = pitch of helix.

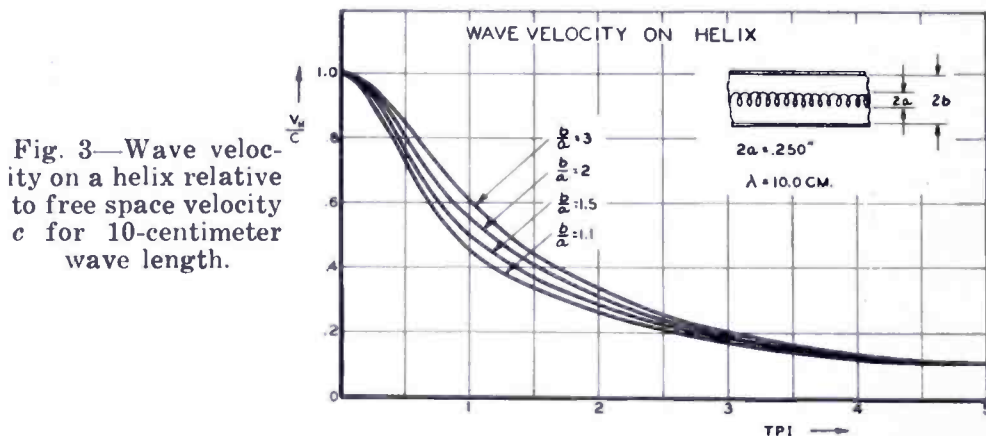
A particular case is shown in Figure 3. It can be seen that the shield has some influence on the velocity of propagation at large pitches.

The velocity of propagation can be determined by measuring the length of standing waves on the helix with a traveling probe. This has been done for slotted-cylinder type helices of different pitches, and the results check very well with the values computed from the formulas above. Further, the phase fronts have been determined by measuring the position of the minimum when the helix is rotated around its axis. This showed that the phase fronts are essentially normal to the axis of the helix with only a small perturbation at the slot. The slot was, in this case, .045 inch wide on a .375-inch diameter

helix. This is another justification for using the helical conducting sheet as a model.

THEORY FOR TAPERED LINES

The theory for tapered lines gives the optimum impedance function Z_y along the taper for a given frequency band, impedance ratio, minimum reflection in the pass band and length of taper. The theory is based on the work of L. P. Smith in an unpublished report. It is shown that the optimum taper has one or more derivatives of $\log Z_y$ con-



tinuous. Smith shows that if $\log Z_y$ has q continuous derivatives over the taper, the voltage reflection coefficient for the taper, r , will be

$$r = \frac{1}{2} \left(\frac{i}{2\beta} \right)^q \int_0^l \left[\frac{d^q}{dy^q} (\log Z_y) \right] e^{2i\beta y} dy \quad (7)$$

where Z_y is the impedance function, $\beta = \frac{2\pi}{\lambda}$, y = electrical length from the beginning of the taper, l = total electrical length of taper and $i = \sqrt{-1}$. This formula applies only where at least the first derivative is continuous. The curve for exponential tapers is taken from the work of Frank.¹² Some examples are shown in Figure 4. The exponential taper is best only for very short tapers.

These results have not had too much significance before, as the impedances to be matched by tapers have usually had a ratio of less than one to five, so it mattered very little what impedance function was

¹² N. H. Frank, "Reflections from Sections of Tapered Transmission Lines and Waveguides", Radiation Laboratory Report 43-17.

chosen. In the case of the helix to coaxial line transition, however, it is necessary to match impedances of ratios higher than one to ten. This requires that the optimum impedance function be used. In practice, the tapers are made long enough that the region of minor maxima on the reflection curve can be regarded as the pass band.

The theory for tapered lines, as worked out by Smith, applies only to cases where the velocity of propagation along the taper is constant, which is not the case for helix transition. If attempts are made to apply the theory for this case, the equations become implicit, and will not readily give any design formulas.

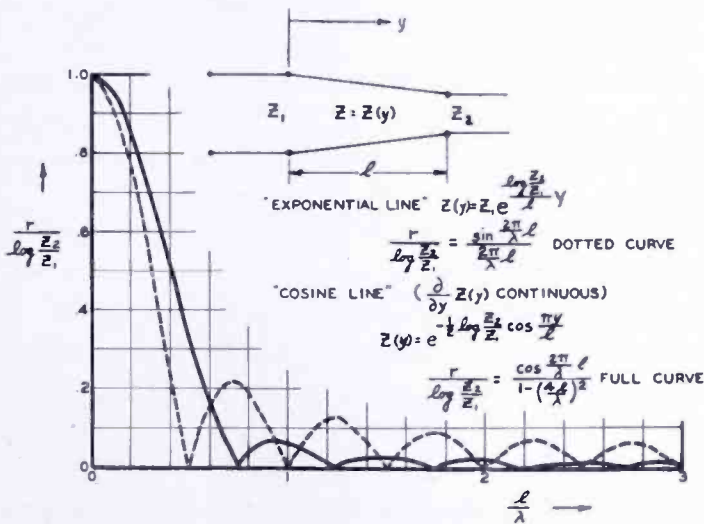


Fig. 4—Voltage reflection coefficient as a function of taper form and electrical length of taper.

If, instead of the axial distance, x , along the helix transition (Figure 1), the electrical length,

$$y = \int_0^x \frac{2\pi}{\lambda_H} dx \equiv \int_0^x \beta_x dx \tag{8}$$

is used in the theory, the impedance as a function of electrical length can be found. The theory applies in this case, the only difference

being that the electrical length, $y = \int_0^x \beta_x dx$, is substituted for the physical length, x . The result in terms of y is the same as in the constant velocity case.

As the relation between the impedance and the velocity of propagation is known, the impedance function can be converted from a function of y to a function of x . This must be done graphically. The operation is actually the solution of an implicit function at the stage where it is rather general. It has the reasonable physical meaning that the rate of change of impedance per wavelength should follow a specified law.

These are the tools. They are used as follows.

Usually the dimensions of a helix and its outer shield are given, as well as a certain specified operating waveband, where the highest frequency should be below the region for higher modes on the helix.

The electrical length is computed from the helix parameters, which give the helix impedance as outlined earlier, the lowest operating frequency, and the permissible reflection in the pass band. Since this is an approximate theory only, it is advisable to provide a safety factor in the maximum allowed reflection.

Figure 5 shows an example in which the impedance for a taper with 3 continuous derivatives is plotted against electrical length, y . The electrical length y is normalized as l .

Using the relation between helix impedance and axial phase velocity, v_H , (Equation (5)) and the relation between v_H and pitch, p , (Equation (6) or Figure 3), this function can be transformed to read turns per

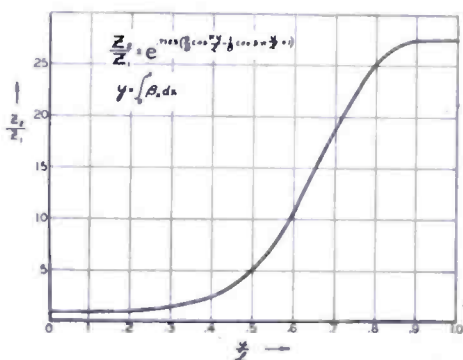


Fig. 5—Impedance as a function of electrical length for taper.

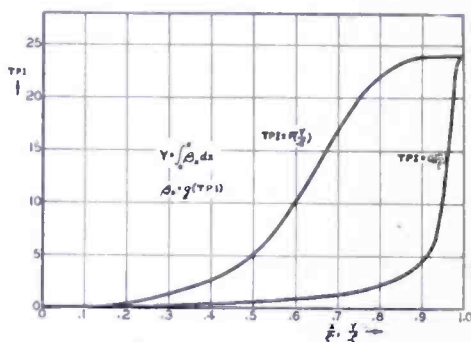


Fig. 6—TPI for helix transition as function of normalized electrical length, y/l , and normalized axial length, x/l .

inch (TPI) as a function of electrical length. This is shown in the upper curve of Figure 6.

From Equation (5) the velocity of propagation is known and therefore β_x is known and a graphical transformation of turns per inch as a function of electrical length, y , to physical length, x , can be made. This is shown in the lower curve of Figure 6. Both lengths, y and x , are normalized.

For machining purposes, an integrated turns-per-inch curve is useful as it gives the form of the unfolded cylindrical sheet directly. The transitions can be made by rolling a properly cut sheet, but this is difficult to do accurately. It has been found that a better way is to mill a slot in a cylindrical sleeve. An example of two such sleeves is shown in Figure 7. Tests show that it is very important that the slot width be constant.

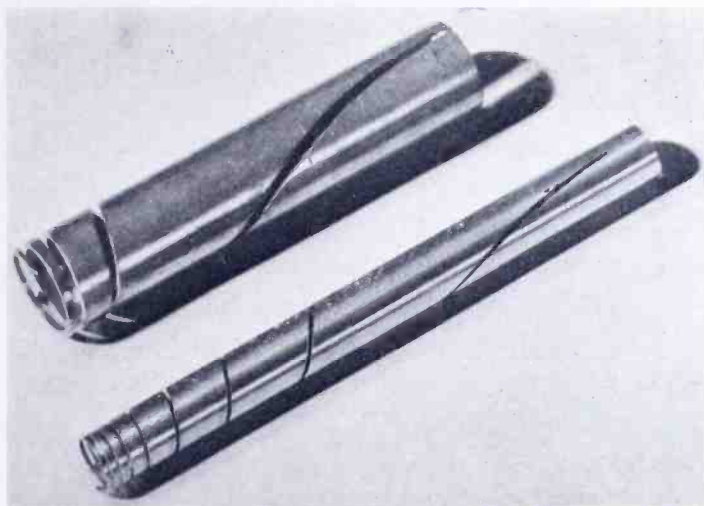


Fig. 7—Two transitions for traveling-wave tube helices.

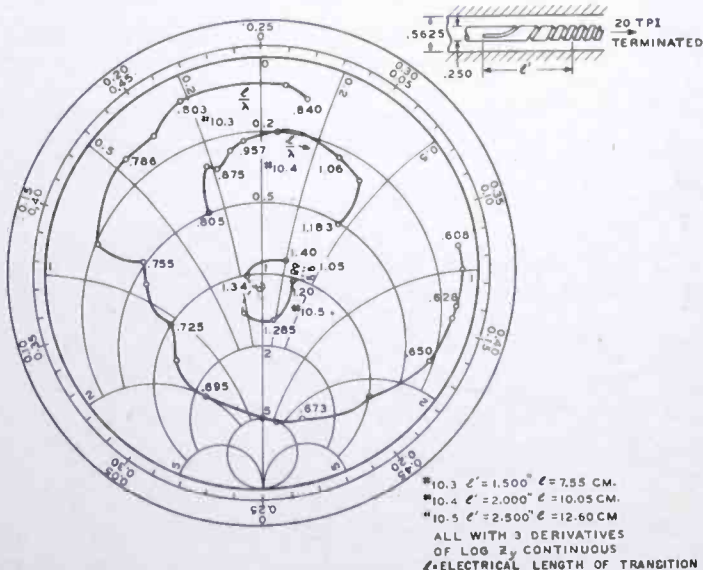
MEASUREMENT OF PERFORMANCE

In order to check these assumptions, measurements were made in which the voltage-standing-wave-ratio versus frequency was measured for a transition, terminated by a lossy helix, joined to a coaxial line with the same diameter inner conductor as the diameter of the transition, and common outer conductor.

Some of the results are shown in Figure 8, where the voltage-standing-wave-ratio and relative phase are plotted for three different transitions with the same impedance function, but different lengths.

The shortest is not operating as a proper transformer, probably due to the neglected influence of mode transformations. The 2-inch long transition shows the proper transformer behavior, but the maximum reflections in the operating band are too large for some purposes.

Fig. 8—Smith diagram for various helix transitions in the region 8.5- to 13.5-centimeter wave length. l is the total electrical length of the transition at $x = 10$ centimeters.



The longest ($2\frac{1}{2}$ -inch) transition, shows typical behavior of a good transition, although the details of the pattern cannot be accounted for by the theory.

Several transitions of this kind have been built for different helices, and have behaved satisfactorily in operating tubes. As the spurious peaks in the reflection curve are higher than the peaks expected from the simple theory outlined here, it is better to use a maximum design reflection of 10 to 20 per cent of that actually allowable.

Several transitions of this type have also behaved satisfactorily in operating tubes, and have been helpful in investigating various helix circuits, as they directly allow measurements on helices from coaxial lines with a good match.

ACKNOWLEDGMENT

The author wishes to thank R. A. Braden, L. S. Nergaard, W. J. Dodds and R. W. Peter, all of RCA Laboratories, for considerable help and encouragement during the work, and the two last named for their valuable advice concerning the preparation of this paper.

AN AUTOMATIC PLOTTER FOR ELECTRON TRAJECTORIES*

BY

DAVID B. LANGMUIR†

Formerly with RCA Laboratories,
Harrison, N. J.

Summary—A device is described which uses electromechanical means to plot automatically the trajectories of charged particles in electrostatic potential fields. A scale model of the field is produced in an electrolytic trough. A pair of wire probes dipped into the electrolyte measure E_n , the potential gradient normal to the direction of motion, and V , the potential (proportional to the total kinetic energy of the charged particle). The ratio $E_n/2V$ is equal to the radius of curvature of the trajectory of the charged particle. The plot is made by continuously adjusting the radius of curvature of the path of the probes to the correct value as the probes move through the fluid. Mechanical design, electrical circuits, and performance are discussed.

INTRODUCTION

THE motion of charged particles in electrostatic fields is a subject of practical interest in electron and ion optics and in the design of many electronic devices. Much study has been given to methods of calculating ion trajectories.¹ Since considerable labor is generally involved, aids to computation offer attractive possibilities. This paper describes a device of the analogue type which automatically plots trajectories simulating the paths of charged particles in electrostatic fields. A brief account of preliminary work has been previously published.²⁻⁴

The potential field in which the motion is to be studied is simulated by means of the familiar electrolytic trough.⁵ Motion of the particle

* Decimal Classification: R138.3×537.67.

† The work described in this paper was performed from 1936 to 1939. The author is now with the U. S. Atomic Energy Commission, Washington, D. C.

¹ Zworykin, Morton, Ramberg, Hillier, and Vance, *ELECTRON OPTICS AND THE ELECTRON MICROSCOPE*, Wiley and Sons, 1945.

² D. Gabor, "Mechanical Tracer for Electron Trajectories," *Nature*, Vol. 139, No. 3513, p. 373, February 27, 1937.

³ D. B. Langmuir, "Automatic Plotting of Electron Trajectories," *Nature*, Vol. 139, No. 3529, p. 1066, June 19, 1937.

⁴ L. M. Myers, *ELECTRON OPTICS*, Chapman-Hall, London, 1939.

⁵ Reference (1), page 389.

is derived by computing its radius of curvature in terms of the potential field as follows. If v is the velocity of an ion at a point P at which the electrostatic potential is V , then

$$Ve = \frac{1}{2} mv^2 \quad (1)$$

where e and m are the charge and mass of the ion respectively. If E_n is the electrostatic gradient at P normal to the direction of electron motion, there will be a force $E_n e$ exerted at right angles to the path. If r is the radius of curvature at P

$$E_n e = mv^2/r \quad (2)$$

Combining (1) and (2),

$$r = 2V/E_n \quad (3)$$

In the case of an electron with zero initial velocity, V is the potential relative to the cathode. Initial velocity may be taken into account by adding a constant correction to V .

A simulated trajectory can be constructed by drawing a series of arcs each of which has a radius corresponding to the position and direction of motion in the potential field, as defined by Equation (3). In the device described here, an exploring probe consisting of two fine wires was dipped into the electrolyte to simulate the charged particle. This probe was supported rigidly on a movable carriage so designed that the radius of curvature of its motion could be continuously and automatically adjusted to the correct value. When moved from a chosen starting point in a given initial direction, the carriage automatically carried the probes along a simulated trajectory.

ELECTRICAL CIRCUITS

a. Determination of E_n

The input circuit is shown in Figure 1a. The exploring electrodes dip into the liquid L at the point M , a field being applied between the cathode and anode electrodes (K and A respectively). It was found that the output, E_n , varied to a large extent with the voltage of the point M relative to ground (indicated by P in the diagram). In general, a null output could not be obtained for any orientation of the points unless the probes were at ground potential ($P = 0$). The difficulty resulted from the distributed capacity of the transformer primary

and its leads, and from the resistivity of the fluid. Figure 1b shows an equivalent circuit. R_1 and R_2 represent the resistance to the respective exploring wires through the fluid. C_1 and C_2 are the distributed capacities to ground. If the point M , midway between the exploring wires, is at an alternating potential relative to ground, then in general a voltage will develop across the transformer because the bridge circuit is unbalanced. While it was possible, by adding some capacitance to one or another of the primary leads, to balance the circuit, this balance was sensitive to changes in electrolyte conductivity, depth of

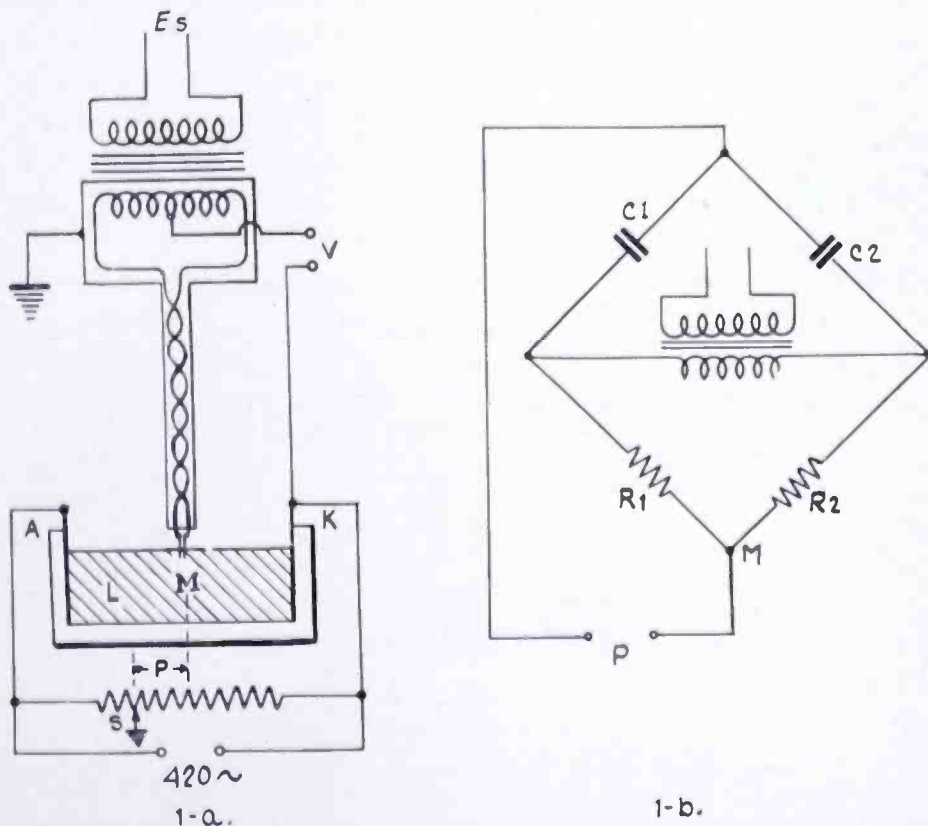


Fig. 1—Schematic diagram of input system and its equivalent circuit, showing the effect of distributed capacitance in the primary of the transformer.

the exploring electrodes and other factors. It was found that a balance seldom stayed in adjustment for more than half an hour, and a slight mismatch produced appreciable errors in the indicated value of E_n .

This difficulty was at first avoided by moving the point of ground potential through the liquid in coincidence with the motion of the pick-up electrodes. This was accomplished by means of a motor control on the slider S of the potentiometer which shunted the tank. This required bulky and complicated equipment. By the use of a feed back

amplifier, the same result was later obtained without appreciable time lag and without mechanical moving parts. The method essentially degenerated the distributed capacities C_1 and C_2 by a factor of from 1,000 to 2,000, with a proportional reduction of the spurious signal. The shield around the primary (Figure 1a), instead of being grounded, was maintained at an alternating potential approximating closely that of the primary center tap. The voltage across C_1 and C_2 was thus reduced to a small fraction of its former value, and a proportionately smaller unbalance voltage was built up.

Figure 2 shows the circuit employed. The primary, including input leads and center tap is completely enclosed in an electrostatic shield.

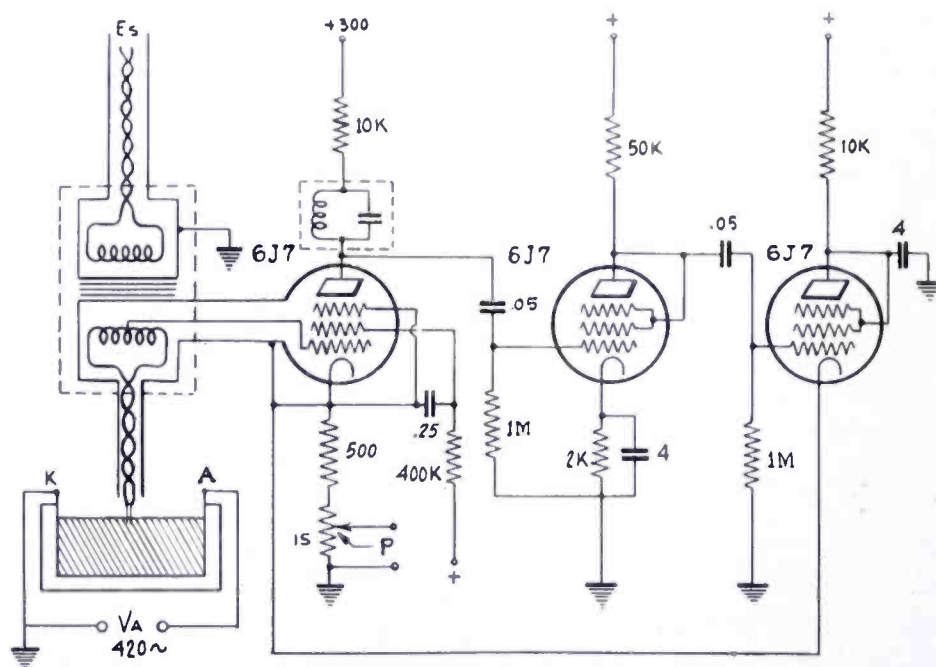


Fig. 2—Diagram of the input system together with the feed-back amplifiers for degenerating the distributed capacitance in the primary. The dotted lines indicate magnetic shielding consisting of nests of three boxes of 0.020-inch nicaloi. P is a 17-ohm Leeds-Northrup Kohlrausch slide wire.

The center tap goes to the grid cap of a tube, the shield being connected to the metal shell. It is essential that the shielding be very complete, and that the screen grid of the first tube be by-passed to the cathode and not to ground. The entire shield should have as low a capacity to ground as is convenient. A grounded shield around the secondary is necessary to prevent electrostatic pick-up between the primary shield and the secondary coil.

Two stages of amplification were employed; the first sharply tuned and having a voltage gain of 220, and the other covering a much wider band with a gain of 8. The third tube produced a gain somewhat less

than unity, but served as a convenient means of coupling input and output completely together. The problem of realizing 60 decibels of feedback was simplified in this case by the very narrow frequency band used. Some difficulty with low frequency motorboating was experienced until an arrangement of by-pass condensers was found which produced stability. The use of voltage-regulator tubes should further increase the margin of safety from instability due to common coupling through the power supply, but this was not actually tried.

With an over-all gain of G , coupled totally to the input, the voltage between center tap and shield is $1/G$ times its value with the shield grounded. The arrangement shown therefore should be capable of reducing the spurious signal by a factor of over 1,000, and experimental measurements showed this to be the case.

The total voltage across the tank was limited to about one volt peak to peak, so as not to drive the amplifier beyond the range of accurate following. A frequency of 420 cycles was used.

When the spurious signals were eliminated, the output of the transformer secondary, E_s (Figure 2), was measured as a function of angle of rotation of the probe about a vertical axis. The output was accurately a sine function of this angle. It also was found to vary accurately as $1/r$ in a field between coaxial cylinder electrodes. It was therefore concluded that the output, E_s , was proportional to the potential gradient.

An amplifier employing enough negative feedback to assure linearity and stability of gain was employed to raise the voltage E_s to an appropriate value. The circuit of this amplifier is shown in Figure 3.

b. Determination of V

With the electrode in the tank corresponding to the cathode grounded, the voltage of the primary shield of the probe transformer was very precisely equal to the voltage V of the probe relative to the cathode, owing to the use of negative feedback. A potentiometer in series with the common cathode resistor, as shown in Figure 2, therefore experienced a voltage drop proportional to V . A potentiometer of resistance 17 ohms was used at this point in the circuit.

c. Determination of E_n/V

The circuit of Figure 4 shows how the ratio E_n/V was determined. The voltage across the slide-wire potentiometer in the cathode circuit may be designated as aV , a being a proportionality constant dependent upon relative resistances in the circuit. Similarly, the output of the second amplifier equals bE_n , where b depends upon the amplifier gain

and other factors such as separation between the probes. If f is the position of the slider on the potentiometer shown in Figure 4 as indicated on a linear scale comprising a range -1 to $+1$, then the condition for null reading in the amplifier is that

$$f = \frac{2b}{a} E_n/V. \quad (2)$$

From Equation (3) it is seen that f is proportional to the curvature $1/r$. The constant b was adjustable for purposes of calibration by varying the gain of the E_n amplifier.

The adjustment of the potentiometer to the balanced position was accomplished by a motor controlled by the output of the null amplifier

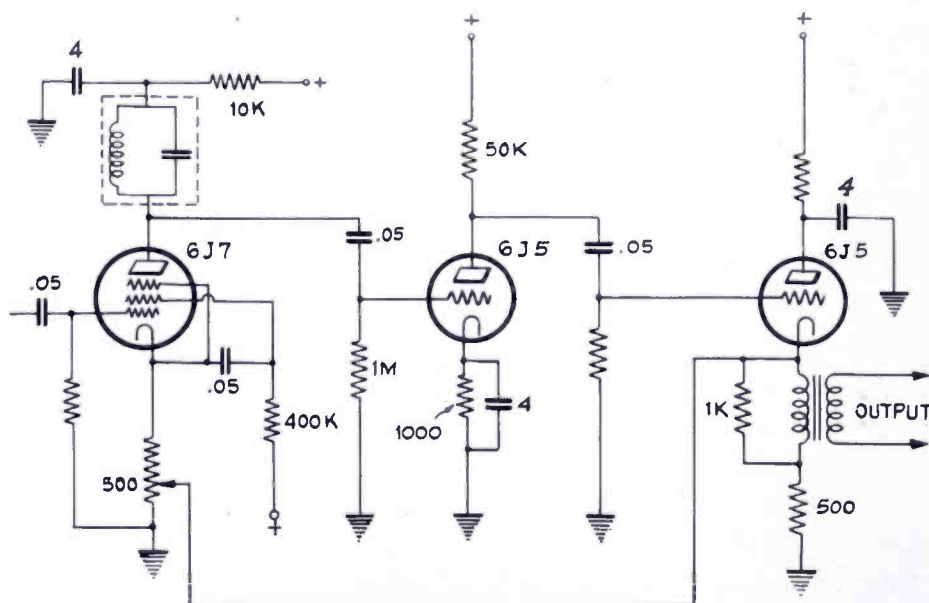


Fig. 3—Amplifier for E_n . Feedback is applied between 3rd and 1st stages to provide linearity and stability. Actually, two such three-stage amplifiers were used in tandem, with resistance coupling between 3rd and 4th stages.

(Figure 4) in such a way as always to move the slider of the potentiometer toward the position of balance. Figure 5 shows a circuit which performed this control satisfactorily.

Since the motor must reverse when the phase of the control signal reverses, a fixed-phase voltage was supplied for comparison by the transformer T_2 . The primary of this was connected to the main 420-cycle supply which energized the electrolytic tank. A balanced form of the grid control circuit was adopted so as to neutralize the effect of fluctuations of the 420-cycle supply. The reference voltage produces no bias on the thyratron grids when the balanced circuit is used, and

therefore no changes in bias can result if it varies. With a resistance inserted in the appropriate place (shown as R in Figure 5), complete failure of the 420-cycle voltage resulted in a slightly increased negative bias on the thyatron grids, thus preventing both thyratrons from conducting simultaneously.

Relays are shown in the output circuits of the 2051 thyratrons. Mercury-vapor thyratrons have been used instead of relays. Their grids can conveniently be connected to the cathodes of the 2051 tubes, if a separate cathode resistor is supplied for each 2051. Mercury tubes cannot be conveniently driven directly by the amplifier without

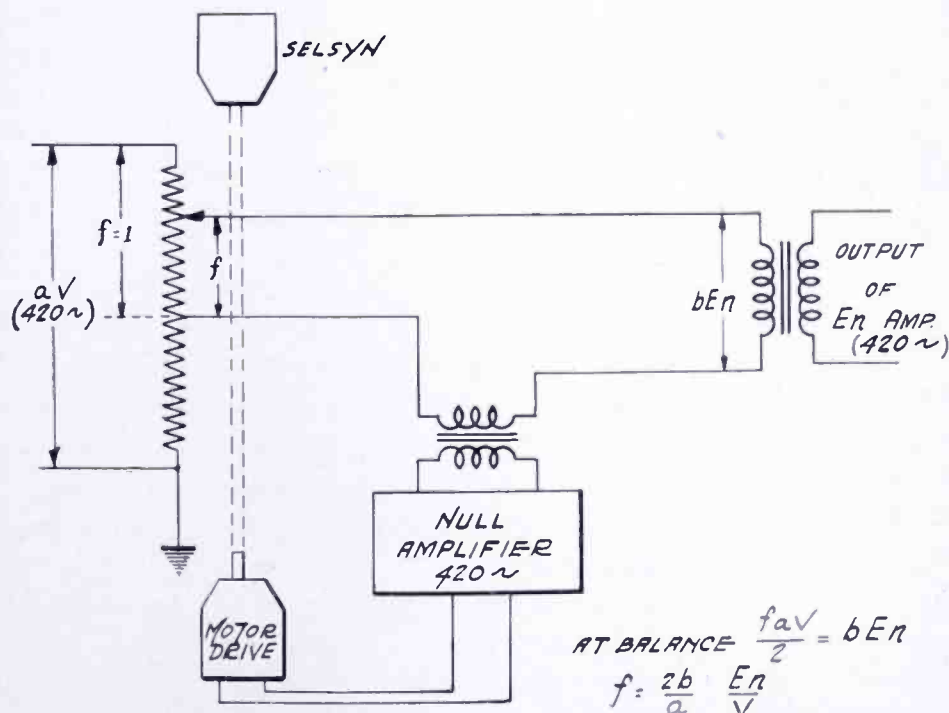


Fig. 4--Circuit for determining ratio E_n/V . The displacement f of the slide wire is transmitted to the lead screw on the carriage by a pair of selsyns.

loss of sensitivity, because of the large voltage margin which must be allowed for protection against ambient temperature variations.

MECHANICAL CARRIAGE

A schematic diagram of the moving carriage is shown in Figure 6. It is seen that the curvature $1/r$ is a linear function of the lead screw. Since the potentiometer setting is linear in E_n/V , Equation (3) shows that a direct coupling of potentiometer to lead screw is required. This was accomplished by a pair of self-synchronous motors.

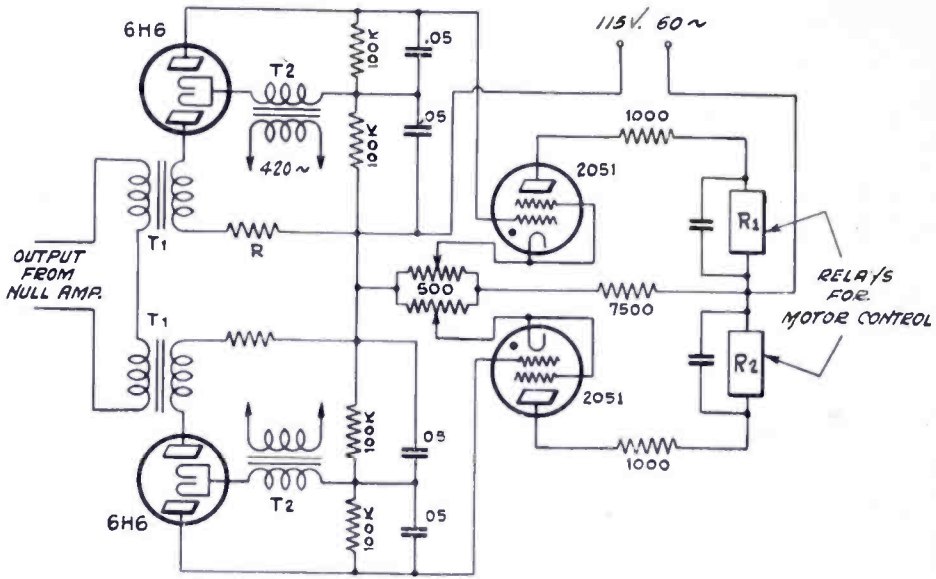


Fig. 5—Circuit showing how drive motor in Figure 4 is controlled by output of null amplifier.

CALIBRATION

If the proportionality factor between $1/r$ and E_n/V is not equal to $1/2$, the paths plotted will not correspond to those of electrons in electrostatic fields. By using an adjustable proportionality factor it should be possible to draw trajectories in transverse magnetic fields and at relativistic speeds. For the simple electrostatic case, the calibration will depend upon the separation of the exploring points, the over-all voltage gains of the amplifiers for V and E_n up to the balancing potentiometer, and the mechanical coupling ratio between the potentiometer and the moving carriage. In order to calibrate the instrument, plane-parallel electrodes a distance d apart were set up in the bath, fringe fields being avoided by means of flat insulating side walls perpendicular to the electrodes. The exploring points were placed at the position half way between the plates ($V/V_a = 0.5$) and in such an orientation that they are parallel to the lines of force. In this position, they pick up maximum

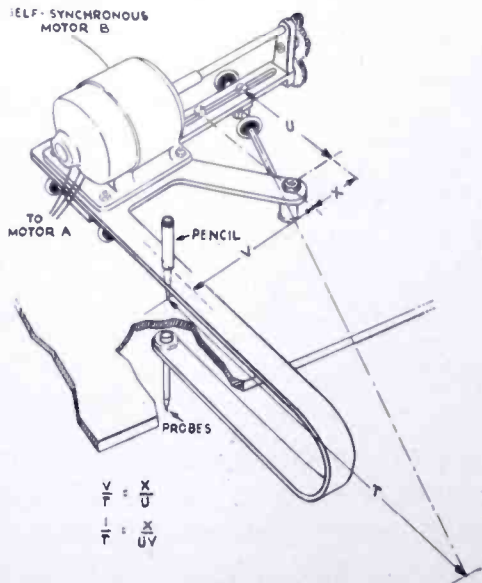


Fig. 6 — Sketch showing basic features of moving carriage.

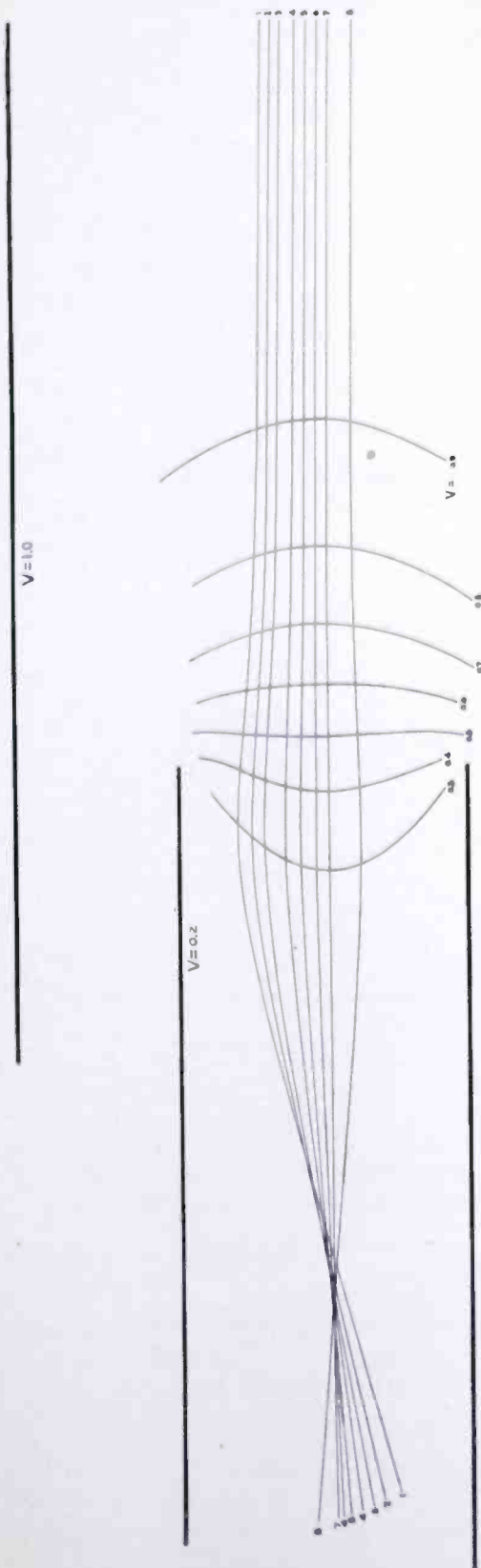


Fig. 7—Trajectories as drawn by machine.

signal, and the angular adjustment is not critical. In this position the correct value of $1/r = 1/d$. The gain of the E_n amplifier was adjusted until the machine balanced itself at the correct setting.

Electron paths could be then plotted automatically by moving the carriage steadily along on the course it chose for itself. A small electric motor was used for driving.

RESULTS

Figures 7 and 8 show a set of curves traced with the machine. The electrodes were flat plates perpendicular to the page, forming a two-dimensional potential field. The other curves were all started parallel to the axis and allowed to take their course from right to left. The spherical aberration of the rays farther from the axis is apparent.

COMMENTS

The precision of the instrument was limited by the follow-

ing difficulties, some of which can be eliminated, while others may be difficult to overcome: 1) *Vibration*—Horizontal and vertical oscillations of the probe were quite troublesome due to the long supporting arm which was required. An improved design of this arm, incorporating greater rigidity and damping would help. Ripples in the water would probably then become a limiting factor. Increased viscosity might be feasible to reduce ripples. 2) *Effects near the probes*—Because of variable meniscus formations it was found necessary to coat the probes with glass except near the tips, and to immerse them completely. Beyond a depth of 1-2 millimeters, the output was practically inde-

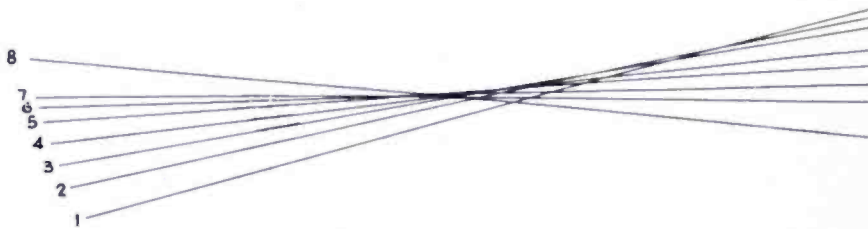


Fig. 8—Enlargement of region of focus in Figure 7.

pendent of depth. For higher accuracy, and in other than two dimensional fields, this factor might not be negligible, and the variation with depth might be unacceptable. 3) *Phase shifts*—The non-ohmic character of the water makes perfect balances of E_n against V rarely obtainable. The phase of E_n with respect to V varies from point to point over the fluid surface. This phase shift is most pronounced in regions of intense and rapidly varying gradients. The effect of this upon accuracy was not investigated.

OTHER FORMS OF THE INSTRUMENT

The most serious limitation of the machine was the finite lower limit to its radius of curvature. By combining the approach described

here with that of Gabor², a device can be made which will go around sharp corners, like his, and also have the automatic features of the machine described above.

Figure 9 shows the schematic design. The carriage is shown in 9(a). W_1 and W_2 are wheels whose axles are rigidly fixed to the frame. The wheel W_3 rotates about the point O so that its axle makes a variable angle ϑ with the common axis of W_1 and W_2 . ϑ is controlled by the positions of the pins P_1 or P_2 one of which bears on one of the arms A attached to W_3 . P_1 and P_2 move in opposite directions along the lengths of the twin lead screws S_1 and S_2 which are geared together. The arms A extend at angles of 45 degrees to the direction of the axle of W_3 . A spring exerts a continuous clockwise torque upon W_3 . The

arms A are therefore always pressed against either P_1 or P_2 . As rotation counterclockwise proceeds, the left arm of A , whose length is accurately fixed, engages P at the symmetrical position, and upon further rotation P_2 lags behind and loses contact with the arm.

The associated potentiometer circuit is shown in Figure 9c. A standard-type slide-wire potentiometer can be used if it can be center tapped.

By reference to Figure 9b, application of the law of sines proves

that $\frac{x}{p-x} = \tan \vartheta$. x in this case

may be taken equal to the deflection of P_1 or P_2 from the equilibrium position, and p is then the total

length of sweep throughout which P_1 or P_2 is in contact with the

arm A . It is clear that $\frac{1}{r} = \frac{\tan \vartheta}{H}$ and hence that $\frac{1}{r} = \frac{1}{H} \frac{x}{p-x}$. Com-

bining this with the condition for balance of the potentiometer as shown in Figure 9c and with Equation (3), we obtain the following equation as the condition that the combined electrical and mechanical systems describe a correct trajectory:

$$\frac{2b}{aH} \frac{x}{p-x} = \frac{y}{q-y}$$

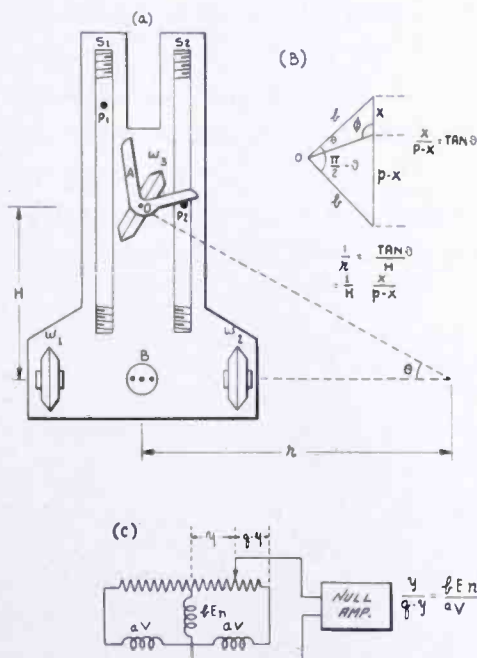


Fig. 9—Proposed modified carriage and circuit to permit shorter radii of curvature to be attained.

This can be satisfied provided $x/p = y/q$; and $2b/aH = 1$. The first requires that the potentiometer and lead screws be coupled together so that sweeping the complete range on the former causes a total rotation of 180 degrees on the part of W_3 . The second condition can be fulfilled by adjustment of the amplifier gains.

The exploring probe and stylus are located on the vertical line through B , the point where a line from W_3 intersects the axis of W_1 and W_2 at right angles.

When sharply curved trajectories are described, the U tube which supports the probe will occasionally strike the edge of the table and have to be rotated about a vertical axis to a new position. B. J. Thompson suggested that this adjustment could be made automatic by connecting the exploring probe to the carriage by means of a flexible shaft. By gearing this to the carriage at the top and to the probe at the bottom, the U tube (through which the shaft might run) could be left free to rotate about a vertical axis passing through the probe and recording stylus. Any rotation of the U tube would not affect the angular orientation of the probe electrodes in the fluid, and the machine would be able to describe curves such as circles, ellipses or spirals without interruption.

ACKNOWLEDGMENT

The author gratefully acknowledges the ideas and suggestions of many of his colleagues in RCA Laboratories in connection with this work, and particularly the leadership of the late B. J. Thompson. The skilled mechanical work of Joseph Egles was very helpful.

RCA TECHNICAL PAPERS†

Fourth Quarter, 1948

Any request for copies of papers listed herein should be addressed to the publication to which credited.

- "Analysis of Residual Gas in Electron Tubes with the Light Spectrograph", R. H. Zachariason, *Analytical Chemistry* (October) 1949
- "Artificial Lines for Video Distribution and Delay", A. H. Turner, *RCA Review* (December) 1949
- "Attenuation in a Dielectric Circular Rod", Walter M. Elsasser, *Jour. Appl. Phys.* (December) 1949
- "Counter Circuits Using Transistors", E. Eberhard, R. O. Endres and R. P. Moore, *RCA Review* (December) 1949
- "Design Procedures for Pi-Network Antenna Couplers", L. Storch, *Proc. I.R.E.* (December) 1949
- "A Direct-Drive Deflection and High Voltage System for Television Receivers", W. E. Scull, Jr., R. G. Wolcott and S. I. Tourshou, *RCA Licensee Bulletin LB-789* (December 23) .. 1949
- "Direct-Reading Electronic Timer", R. R. Freas, *RCA Review* (December) 1949
- "Double-Probe Method for Determination of Electron Temperatures in Steady and Time-Varying Gas Discharges", E. O. Johnson and L. Malter, *Phys. Rev.* (November 1) 1949
- "Duo-Cone Loud Speaker", H. F. Olson, J. Preston and D. H. Cunningham, *RCA Review* (December) 1949
- "The Evaluation of Chromium-Iron Alloys for Metal Kinescope Cones", A. S. Rose and J. C. Turnbull, *RCA Review* (December) 1949
- "Experimental Tube for F-M Detection", L. J. Giacoletto, *Electronics* (November) 1949
- "An Experimental UHF Television Tuner", Bulletin, RCA Laboratories Division (December) 1949
- "Formation of Insulating Layers by the Thermal Decomposition of Ethyl Silicate", H. B. Law, *Rev. Sci. Instr.* (December) 1949
- FREQUENCY MODULATED RADAR, D. G. C. Luck, McGraw Hill Book Co., New York, N.Y. 1949
- "A Functional Sound Reproducing System", H. F. Olson, A. R. Morgan and J. Preston, *RCA Licensee Bulletin LB-787* (December 1) 1949
- "Harmonic Analyzer and Synthesizer", J. Lehmann, *Electronics* (November) 1949
- "Hints on Using Sweep Generators for TV Receiver Alignment", John A. Cornell, *Radio News* (December) 1949
- "Illumination for Television Studios—Part II", H. M. Gurin, *Tele-Tech*, (October) 1949
- "An Investigation of Dielectric Rod as Wave Guide", C. H. Chandler, *Jour. Appl. Phys.* (December) 1949

† Report all corrections or additions to RCA Review, Radio Corporation of America, RCA Laboratories Division, Princeton, N. J.

- "Mass Spectrometric Studies of Oxide Cathode Sublimation Phenomena", R. H. Plumlee, *Amer. Phys. Soc. Bul.* (December) 1949
- "Microwave Q Measurements in the Presence of Series Losses", L. Malter and G. R. Brewer, *Jour. Appl. Phys.* (October) .. 1949
- "A New Direct-Reading Loran Indicator for Marine Service", F. E. Spaulding, Jr. and R. L. Rod, *RCA Review* (December) 1949
- "A New Image Orthicon", R. B. Janes, R. E. Johnson and R. R. Handel, *RCA Review* (December) 1949
- "New 15-inch Duo-Cone Loudspeaker", H. F. Olson, J. Preston and D. H. Cunningham, *Audio Eng.* (October) 1949
- "Notes on a Coaxial Line Bead", D. W. Peterson, *Proc. I.R.E.* (November) 1949
- "Photicon", V. K. Zworykin, *Electronics* (December) 1949
- "Photomultipliers for Scintillation Counting", G. A. Morton, *RCA Review* (December) 1949
- "The Provisional Frequency Board", P. F. Siling, *RCA Review* (December) 1949
- RADIO OPERATOR'S LICENSE Q & A MANUAL, Milton Kaufman, John F. Rider, Publisher, New York, N.Y. 1949
- "A Secondary-Emission Electron Multiplier Tube for the Detection of High Energy Particles", R. P. Stone, *Rev. Sci. Instr.* (December) 1949
- "Sensitivity, Directivity and Linearity of Direct Radiator Loudspeakers", H. F. Olson, *RCA Licensee Bulletin LB-786* (November 10) 1949
- "Six-Megacycle Compatible High-Definition Color Television System", *RCA Review* (December) 1949
- "Some New Complex Silicate Phosphors Containing Calcium, Magnesium, and Beryllium", A. L. Smith, *Jour. Electrochem. Soc.* (November) 1949
- "A Special Wide-Band Scope Amplifier", Milton Kaufman, *Radio and Television News* (October) 1949
- "Synchronization for Color Dot Interlace in the RCA Color Television System", Bulletin, RCA Laboratories Division (October) 1949
- "Television Service, Part VIII—Vertical Oscillator Troubles", John R. Meagher, *RCA Rad. Serv. News* (November and December) 1949
- "TVI-Free Rig for 10!", A. M. Seybold, *CQ* (October and November) 1949
- "A Two-Color Direct-View Receiver for the RCA Color Television System", Bulletin, RCA Laboratories Division (November) 1949
- "A 15 by 20-inch Projection Receiver for the RCA Color Television System", Bulletin, RCA Laboratories Division (October) 1949

NOTE—Omissions or errors in these listings will be corrected in the yearly index.

AUTHORS



JOHN C. BLEAZEY received the B.S. degree in Electrical Engineering from the Drexel Institute of Technology in 1940. In 1941 he was commissioned in the U.S. Army Signal Corps. While in the Army, he was promoted to the rank of Captain and commanded a Radar Maintenance Unit in the European Theatre till the end of the war. In 1945 he joined the RCA Laboratories Division, Princeton, N. J. and has been engaged in research in acoustics. Mr. Bleazey is a member of the Acoustical Society of America.

C. LOUIS CUCCIA received the B.S. degree in E.E. in 1941 and the M.S. degree in 1942 from the University of Michigan. From 1941 to 1942 he was affiliated with the department of engineering research of the University of Michigan for Fisher Body Division of the General Motors Corporation. In June 1942, he joined the research department of the RCA Manufacturing Company in Harrison, N. J. In November 1942, he transferred to the research staff of RCA Laboratories Division in Princeton, N. J. Mr. Cuccia is an Associate Member of the Institute of Radio Engineers and a member of Sigma Xi.



ALBERT W. FRIEND received the B.S. (E.E.) degree in 1932 and the M.A. (Physics) degree in 1936 from West Virginia University, and the S.D. degree in Communication Engineering from Harvard University in 1948. Previous to 1934 he consulted on communications systems, and was a divisional transmission and distribution engineer for the Ohio Power Company. From 1934 to 1944 he was Instructor and Assistant Professor of Physics (West Virginia University); Research Fellow, Blue Hill Meteorological Observatory; Research Fellow, Cruft Laboratory; Instructor in Physics and Communication Engineering (Harvard University), Research Associate and Staff Member, Radiation Laboratory; Technical Director, Heat Research Laboratory (Massachusetts Institute of Technology) and special consultant to Division 5 of N.D.R.C. From 1944 to 1947 he was television advance development engineer with the RCA Victor Division in Camden, N. J. From 1946 to 1948 he also did research work under government contracts at Cruft Laboratory, Harvard University. In 1947 he transferred to the RCA Laboratories Division at Princeton, N. J. Dr. Friend is a Senior Member of the Institute of Radio Engineers, a Member of the American Institute of Electrical Engineers, American Meteorological Society, the Acoustical Society of America, the American Geophysical Union, the American Association for the Advancement of Science, Tau Beta Pi, Sigma Pi Sigma, and Sigma Xi. He is a registered professional engineer.



RAYMOND F. GUY was a radio amateur from 1911 until 1916 when he joined the professional ranks as a ship's radio officer and radio inspector. He was subsequently employed by the Marconi Wireless Telegraph Company, the Independent Wireless Telegraph Company and the Shipowner's Radio Service. He served with the Signal Corps during the first World War, after which he entered Pratt Institute, graduating in 1921 with a degree in Electrical Engineering. In the same year he joined the staff of Radio Station WJZ. In 1924 he transferred to the RCA Research Laboratories and in 1929 to the

National Broadcasting Company. During the second World War he participated in projects of the OSS, the CIAA and the OWI. He is presently Manager of Radio and Allocations Engineering for the National Broadcasting Company. Mr. Guy is a member of the Society of Professional Engineers and the Radio Executives Club, a charter member of the Radio Pioneers, a life member of the Veteran Wireless Operator's Association, a fellow of the Radio Club of America, and a fellow and President for the year 1950 of the Institute of Radio Engineers.

R. A. HACKLEY received the B.S. degree in 1931 and the M.S. degree in E.E. in 1933 from Yale University, where from 1931 to 1933 he was a Graduate Assistant and Instructor in Electrical Engineering. In 1933 he became a member of the Research Division of the RCA Manufacturing Company at Camden, N. J. Since 1942 he has been a research engineer at RCA Laboratories Division, Princeton, N. J. engaged in work of underwater sound. Mr. Hackley is a Member of the Acoustical Society of America, the Institute of Radio Engineers, Tau Beta Pi, and Sigma Xi.



DAVID B. LANGMUIR received the degree of B.Sc. from Yale University in 1931, and the Ph.D. degree in Physics from Massachusetts Institute of Technology in 1935. He was engaged in research at the RCA Manufacturing Company, Harrison, New Jersey, from 1935 to 1941, working on cathode ray tubes, television light valves and short wave transmitting tubes. He served as Liaison Officer for the Office of Scientific Research and Development in Washington and London from 1941 to 1945; as Secretary, Guided Missiles Committee, Joint Chiefs of Staff, 1945-1946; Director, Planning Division, Research

and Development Board, 1946-1948. Dr. Langmuir is presently employed by the Atomic Energy Commission, Washington, D. C.

C. O. LUND received the M.S. degree in Electrical Engineering from the Technical University of Denmark in 1947. In the same year he became a research engineer at the Laboratory for Telegraphy and Telephony at the University. He was an Honorary Fellow of the American Scandinavian Foundation from July 1947 to July 1949 as a trainee at the RCA Laboratories Division, Princeton, N. J. Mr. Lund is now with the Microwave Section of the Laboratory for Telegraphy and Telephony at the Technical University of Denmark.





T. MURAKAMI received the B.S. degree in E.E. from Swarthmore College in 1944, and the M.S. degree from the Moore School of Electrical Engineering, University of Pennsylvania in 1947. From 1944 to 1946 he was an assistant and research associate in the department of electrical engineering at Swarthmore College. Since 1946 he has been with the Advanced Development Section of the Home Instrument Department, RCA Victor Division, Camden, N. J., working on radio frequency circuit development. Mr. Murakami is an Associate Member of the Institute of Radio Engineers and Sigma Xi.

HARRY F. OLSON received the B.S. degree in 1924, the M.S. degree in 1925, the Ph.D. degree in 1928 and the E.E. degree in 1932 from the University of Iowa. From 1928 to 1930 he was in the Research Department of Radio Corporation of America; from 1930 to 1932, in the Engineering Department of RCA Photophone; from 1932 to 1941, in the Research Division of RCA Manufacturing Company; since 1941, with RCA Laboratories Division. Dr. Olson is a member of Tau Beta Pi, Sigma Xi and the American Physical Society, a Fellow of the Institute of Radio Engineers and of the Acoustical Society of America.



JOHN PRESTON received his education in England, attended Manchester Scientific Institute taking courses in Mechanical Engineering. He then joined the engineering staff of the Bolton Power and Electrical Company. He became a member of Radio Corporation of America in 1929 and was associated with the Research Department of RCA Victor from 1930 to 1935; the Research Department of RCA Manufacturing Company from 1935 to 1941, and RCA Laboratories Division from 1941 to date. His work has been in the field of acoustics since joining Radio Corporation of America. Mr. Preston is a member of the Acoustical Society of America and of Sigma Xi.

OTTO H. SCHADE graduated from the Reform-Real-Gymnasium, Halle, Germany, in 1922. From 1922 to 1924 he was with the Telephonfabrik A. G. vorm. J. Berliner, Berlin and Dusseldorf; from 1924 to 1925, in charge of the laboratory in the radio manufacturing company "Ratag" in Berlin; and from 1926 to 1931, in the Engineering Department of the Atwater Kent Manufacturing Company. Since 1931 he has been with the Tube Department, RCA Victor Division at Harrison, N. J. He received a Modern Pioneer Award from the Radio Manufacturers Association in 1940. Mr. Schade is a Senior Member of the Institute of Radio Engineers, and was awarded the Morris Liebmann Memorial Prize in 1950.



JOHN L. SEIBERT received the B.S. degree in Electrical Engineering from Pennsylvania State College in 1927. From 1927 to 1935, he was with the Westinghouse Company at Chicopee Falls, Mass. in the Radio Transmitter Engineering Department, where he was engaged in the development and design of AM, TV, Police and Airways transmitters. He also assisted in the development and design of speech input equipment. In 1935, he joined the Radio and Allocations Engineering Group of the National Broadcasting Company in New York and has designed and built radio facilities for AM, FM, TV, and international broadcasting. At present, he is Staff Engineer for the Radio and Allocations Engineering Group. Mr. Seibert is an Associate Member of the Institute of Radio Engineers.



FREDERICK W. SMITH attended the RCA Institutes and the Polytechnic Institute of Brooklyn. In 1942, he joined the Engineering Department of the Radiomarine Corporation of America as a test engineer. In 1943, he held the position of Radio Engineer in the Department of Medicine, College of Physicians and Surgeons, Columbia University, where he was engaged in a research project on the bacteriological and biochemical applications of ultrasonics. From 1943 to 1946, as a member of the U.S. Army Signal Corps, he served as transmitter engineer for the Armed Forces Radio Network Station

VU2ZU in Calcutta, India, as well as for the theatre radio teletype transmitter installation there. In 1946, he joined the staff of RCA Institutes as an instructor. In 1948, he transferred to the Engineering Department of the National Broadcasting Company and is at present an engineer in the Radio and Allocations Engineering Group. Mr. Smith is a member of the Institute of Radio Engineers, the Acoustical Society of America and the American Association for the Advancement of Science.

